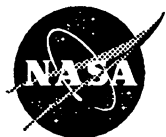# Quiet High-Speed Fan

Lysbeth Lieber, Russ Repp, and Donald S. Weir
AlliedSignal Engines
Phoenix, Arizona

November, 1996

National Aeronautics and
Space Administration

TABLE OF CONTENTS

i

LIST OF FIGURES

LIST OF FIGURES (Cont)

LIST OF FIGURES (Cont)

LIST OF FIGURES (Cont)

LIST OF FIGURES (Cont)

LIST OF FIGURES (Cont)

LIST OF FIGURES (Cont)

LIST OF TABLES

NAS3-27483, NASA-TASK 5
QUIET HIGH-SPEED FAN
FINAL REPORT

1.0 INTRODUCTION

The primary objective of the Quiet High-Speed Fan program is to develop an advanced high-speed fan design that will achieve a 3 dB reduction in overall fan noise over the baseline configuration. The program applies and validates acoustic, aerodynamic, and mechanical design tools developed by NASA, US industry, and academia. The successful fan design will be used in an AlliedSignal Engines (AE) advanced regional engine to be marketed in the year 2000 and beyond. This technology is needed to maintain US industry leadership in the regional turbofan engine market.

This program specifically addresses two level-three milestones to support "Model Tests for Code Validation/Concept Evaluation" in the Noise Reduction element of the NASA Advanced Subsonic Technology (AST) Program:

- Select second-generation, low-noise concepts for model tests (4Q, FY 1997)
- Complete second-generation model tests for low noise designs (4Q, FY 1999)

A 2-year effort was originally proposed for this task. During the first year, a calibration of the acoustic and aerodynamic prediction methods was performed and a baseline fan definition was established and evaluated. The second year activities were to include evaluation of several candidate noise reduction concepts using combinations of rotor and stator lean and sweep. The program scope has since been expanded. The program roadmap is illustrated in Figure 1. Four fan designs are planned to be used in the program. The existing NASA-Lewis QF-12 fan and the AE TFE731-60 fan will serve as baseline configurations. Data from these fans will aid in design tool validation. Two new advanced fans will be designed, one each by AE and NASA-Lewis. The program will lead to a model scale test using the Ultra High Bypass (UHB) Propulsion Simulator in the NASA-Lewis 9 x 15-foot wind tunnel. This report summarizes the results of the first year of the effort.

The quiet high-speed fan will be an advanced single-stage fan designed for a 5K to 20K pound thrust turbofan regional airline application. Advanced aerodynamic, mechanical, aeroelastic, and computational fluid dynamic (CFD) tools will be used to meet aggressive performance goals while achieving at least a 3 dB reduction in fan noise at a critical takeoff noise condition. Three fans will be built for evaluation at NASA; a baseline TFE731-60, an advanced NASA design, and an advanced AE design. A 22-in. diameter fan nacelle for the UHB Propulsion Simulator in the NASA-Lewis 9 x 15 foot wind tunnel will integrate NASA and AE aerodynamic designs and instrumentation to fulfill all aerodynamic, mechanical, distortion sensitivity, and acoustic test needs.

2.0 BACKGROUND

Since the early 1970s, AE has had extensive experience in design, development, and production of turbofan engines for commercial and military applications. Most of these applications have been in the medium bypass ratio range (BPR = 3 to 5), requiring single-stage transonic axial fans. Since the late 1970s, AE's aerodynamic and mechanical design approach has been to apply the best available 3-D CFD and mechanical design/analysis tools to turbomachinery design. The following paragraphs describe AE's fan experience, starting with our most recent and most advanced production fan, the TFE731-60.

TFE731-60 - The 5000-pound-thrust-class TFE731-60 engine is the latest derivative of the TFE731 product line. It received FAA certification on May 1, 1995, and has entered production for the Falcon 900EX aircraft. Relative to previous 731 engine models, the -60 engine incorporates a new fan module (rotor, stator, and front frame), new fan gearbox, and new high-pressure (HP) spool (HP compressor, combustor, HP turbine). The -60 also uses the 731-5 low-pressure (LP) turbine and -5A/5B forced mixer nozzle, both derived from the AE/NASA QCGAT program.

Aerodynamic and mechanical technologies and features incorporated in the TFE731-60 fan component are summarized in Figure 2. Key among the features contributing to the very high level of aerodynamic and acoustic performance of the -60 fan are the damperless, low-aspect-ratio, moderately swept rotor blades and the full-span swept composite stator vanes. The geared fan configuration common with all TFE731's allows the fan to run at a tip speed optimized for best performance, stall margin, and noise. Demonstrated -60 design point (typical climb/cruise condition) fan aerodynamic performance parameters are also noted in Figure 2. The -60 fan's polytropic efficiency (over 90 percent) is state of the art, especially for the relatively small size class of the -60 fan.

The TFE731-60 fan was the subject of considerable acoustic evaluation early in the design phase. Blade and vane counts, rotor/stator spacing, and stator vane sweep were selected to minimize the noise signature within the fan design constraints. Fan rig spinning-mode measurements were made to verify the design constraints and provide acoustic treatment design criteria. The acoustic effort was concluded with a full-scale engine acoustic test which verified that the acoustic design goals, including the acoustic treatment, were satisfied.

Installed performance of the TFE731-60 fan was a critical issue. Measuring fan component performance accurately during flight was required. The engine nacelle and inlet section of the flight test engine were custom tailored and instrumented for flow measurement. The engine front frame was also instrumented so fan performance could be measured without impacting fan or engine performance. The fan performance measured in flight at appropriate Reynolds numbers during the extensive flight test program agreed very well with rig and engine data acquired on the ground using conventional fluid metering techniques. The experience gained on these programs will be used on the Quiet High-Speed Fan program.

2

Fan	1995	1996	1997	1998	1999
QF-12	Calibration of Dawes CFD Code				
TFE731-60	Calibration of Dawes CFD & UTRC/ Eversman Acoustic Code		Fabricate Fan	Baseline for Rig Test	Data Reduction / Data Analysis / Reporting Results
AlliedSignal Advanced Design	Optimum Stator Aerodynamic Design	Optimum Rotor Design / Final Fan Aero Design	Mechanical and Aeroelastic Analysis	Fabricate Fan / Rig Test	
NASA Lewis Advanced Design	NASA Inhouse Design Effort			Rig Test 10/98	

Figure 1. The Quiet High-Speed Fan Program Roadmap Targets a Wind Tunnel Test in October of 1998.
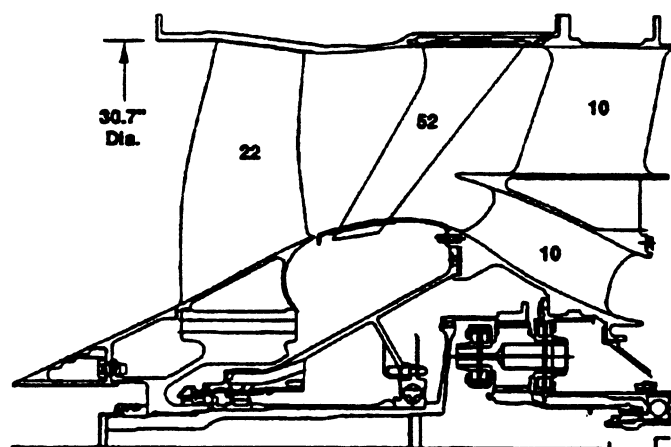
Fan Design Parameters

Corrected Flow	194.5 lb/sec
Specific Flow	43.1 lb/sec/ft^2 (annular)
Inlet hub/tip Ratio	0.35
Corrected Tip Speed	1474 ft/sec
Inlet Tip Relative Mach Number	1.45
Bypass Ratio	3.8
Pressure Ratio, stage	1.78

Fan Technologies:
- Damperless rotor
  - Proven on TFE1042 fan
- Moderate rotor sweep
  - Proven on USAF 1500 fan
- High flow / frontal area
  - Proven on CFE738 fan
- Composite full span stator
  - Proven on CFE738 fan (composite)
  - Proven on TFE731-5 (full span)
- One-piece cast Al frame
  - Proven on CFE738
- Geared fan configuration
  - Proven on all TFE731's
  - Optimum fan speed
  - High fan pressure ratio
  - High fan efficiency
  - Good fan stall margin

Figure 2. Demonstrated Fan Technologies Were Combined in the Successful TFE731-60 Fan.

3

Other Fans - Most of AE's commercial and military axial fan experience is summarized in Figure 3, spanning from the early 1970s at the bottom to the near future (late 1990s) at the top. Key features and technologies in each fan are shown on the left; basic aerodynamic fan design/analysis methods used are shown on the right. Applications for these fans range from business jets (most TFE731s, CFE738) and military trainers (some 731s, F109) to supersonic fighters (TFE1042/F124 3-stage fan). Design point corrected tip speeds and relative Mach numbers range from 1330 to 1500 ft/sec and 1.3 to 1.5 respectively, while stage pressure ratios range from 1.6 to 1.8 for the existing fans shown. These basic fan design parameters are likely to encompass design requirements for AE's future regional airline and business jet applications as well.

NASA QF-12 Fan - The presence of a shock at the inlet of the fan rotor in a turbofan engine can result in acoustic phenomena that represent substantial noise sources. Multiple Pure Tone (MPT) noise, for example, results when the pressure disturbances from the inlet shock move upstream out of the rotor blade passage. One approach to reducing these shock-related noise sources is to eliminate the formation of the inlet shock in the fan by tailoring the rotor blade shape. The introduction of sweep in the fan rotor blade can reduce the relative velocity component normal to the blade to subsonic values, much as a swept wing on an aircraft can produce subsonic velocities normal to the wing leading edge, even when the resultant velocity is supersonic.
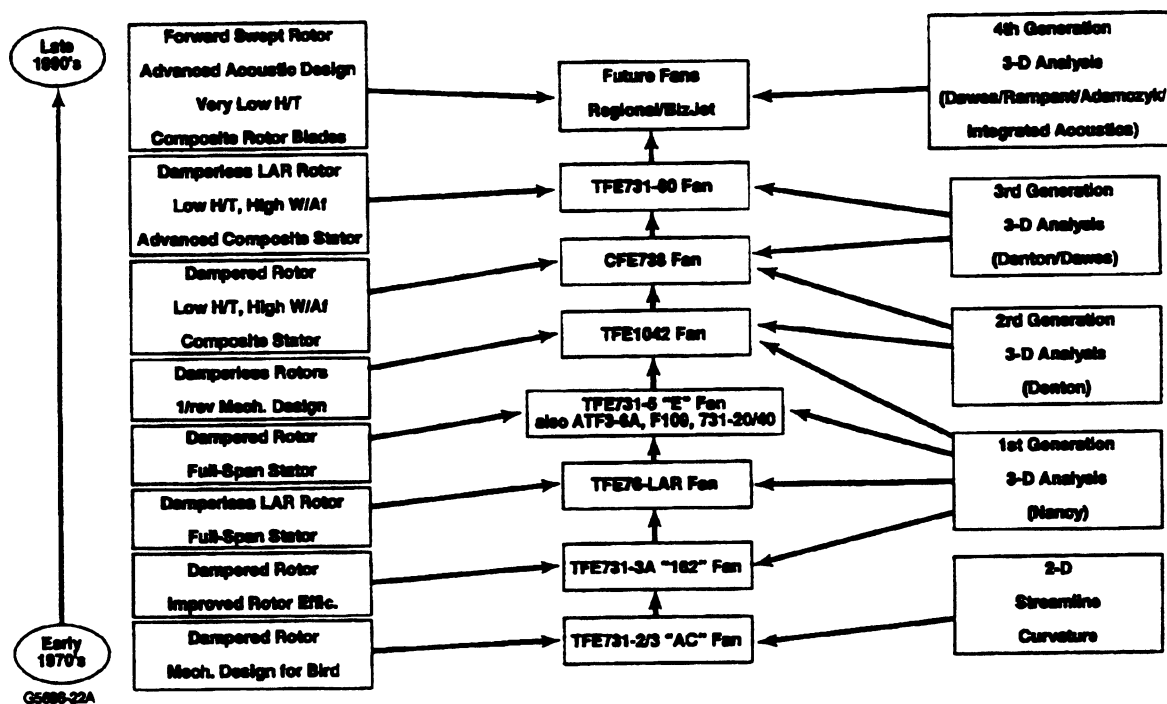
Figure 3. AE's Future Fan Technology Is Built on Advanced Analysis and Past Experience.

This noise minimization technique was applied by AlliedSignal Engines (formerly AVCO Lycoming) and Bolt, Beranek and Newman, Inc. (BBN) to the design of the QF-12 quiet high-speed fan, as part of a NASA-sponsored program performed between 1974 and 1977 (Reference 1). The fan rotor featured a compound forward-and-aft sweep to eliminate the leading edge shock. However, although shock-induced MPT noise was reduced, the aerodynamic performance of the fan did not meet design goals. The reasons for the performance deficiencies were not determined, but the source was found to be localized in the rotor. Figure 4 shows a summary of the results of the acoustic evaluation of the QF-12.

The ability to accurately predict, during the fan rotor design, the speed range over which the MPT noise will occur can provide a valuable tool for acoustically tailoring the design of the rotor to minimize the effect of this noise source.
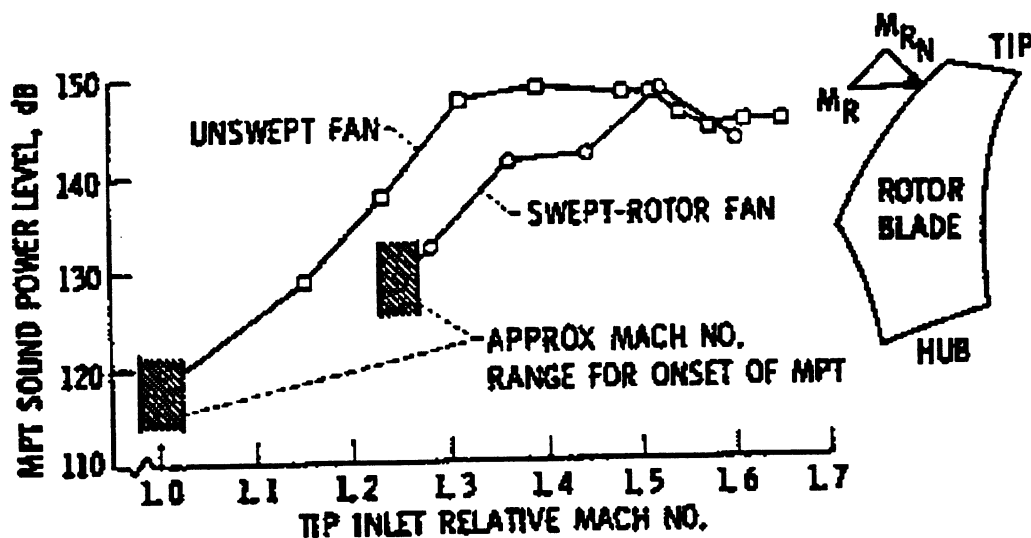
Figure 4. The QF-12 Fan Demonstrated the Feasibility of Using Blade Leading
Edge Sweep to Reduce Fan Noise.

3.0 QF-12 SWEPT ROTOR FAN ANALYSIS

3.1. Approach

The objective of this effort was to perform a CFD analysis of the QF-12 Fan rotor, using the DAWES flow simulation program, in order to demonstrate and verify the causes of the relatively poor aerodynamic performance observed during the fan test. In addition, the rotor flowfield characteristics were qualitatively compared to the acoustic measurements to identify the key acoustic characteristics of the flow.

The QF-12 Fan rotor geometry was not available in coordinate form, and therefore had to be reconstructed from various sources of documentation. An axisymmetric streamline curvature program was then applied to the geometry, in order to obtain initial estimates of performance, and to provide approximate exit static pressure boundary conditions for use in the DAWES 3-D viscous analyses. Next, the blade and flowpath geometry was analyzed over a range of speeds along the operating line, using the DAWES program. A comprehensive study of these flow simulations was then performed, in order to obtain aerodynamic performance predictions and details of the sources of the performance deficiencies. In addition, contour plots of relative Mach number were utilized to establish the presence or absence of inlet shocks, in order to verify how well the design functioned from an acoustic standpoint.

3.2. QF-12 Fan Rotor Geometry

The QF-12 Fan rotor, shown in Figure 5, is a dampered rotor consisting of 28 blades defined by DCA blade sections. The rotor leading edge has forward sweep from the hub to approximately 40 percent span, and backward sweep in the outer span region. The transition between the inner and outer regions consists of a sharp slope discontinuity, or "beak," on the leading edge of the blades. The midspan damper is also swept.

The QF-12 rotor geometry is described in the NASA Contractor Report (Reference 1). Additional information was obtained from drawings of the blade produced by BBN's subcontractor AVCO Lycoming, and coordinate measurement machine (CMM) inspection data supplied by NASA Lewis.

The QF-12 rotor blade and flowpath geometry were modeled using AE's axisymmetric streamline curvature program, AXCAPS. This program provides a discrete-point definition of the blade geometry along specified sections intersected with the blade surface. Endwall definition is also provided in terms of radial and axial coordinates at discrete points. The AXCAPS model of the flowpath is shown in Figure 6.
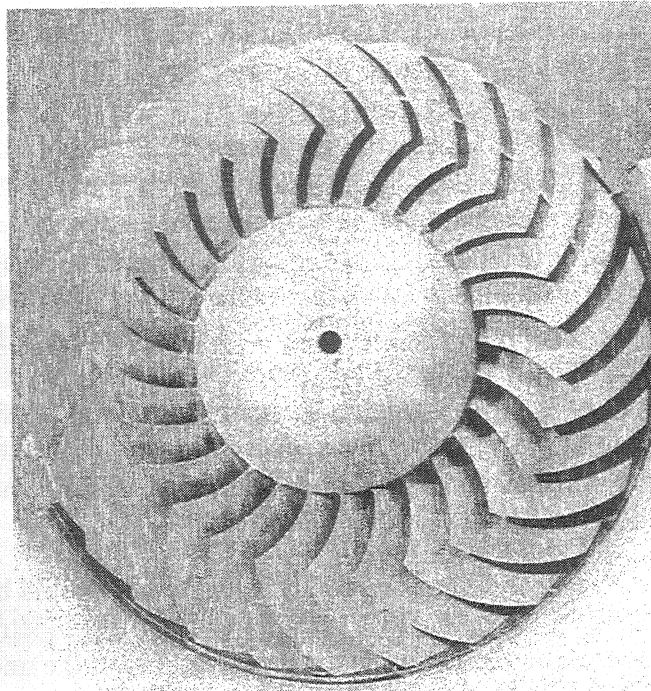
Figure 5. The QF-12 Was an Early Attempt at Using Sweep to Reduce Fan Noise.
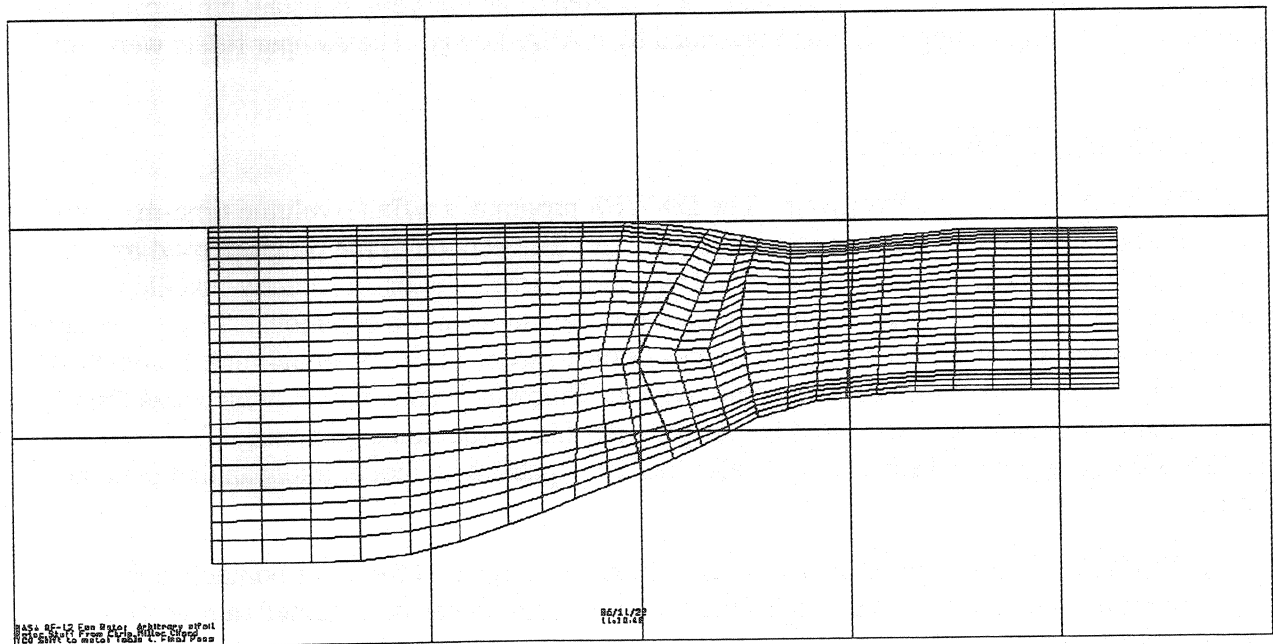
Figure 6. The AXCAPS Flowpath Model Defines the Fan Mean Streamline Characteristics.

Several iterations were made in an attempt to accurately model the QF-12 blade. First, the inlet and exit metal angles from the report were used and DCA airfoil coordinates on stream-surfaces of revolution were applied to produce the blade geometry. The key to a proper stacking of the blade in this manner was to define the center-of-gravity (CG) position properly. Small differences in the CG position in the tangential direction significantly affected planar section airfoil contours, producing trailing edge irregularities. A comparison of the AE and NASA-Lewis interpretation of the blade geometry showed that the leading edge and center-of-gravity coordinates in the report are not consistent and that the leading edge coordinates are correct. A second AE blade model was defined to be consistent with the leading edge coordinates. However, the blade shape generated by this process was also unsatisfactory. Finally, a blade shape was implemented based directly on the CMM data. Figure 7 shows the results of the chord and stagger angle comparisons of the CMM and design intent data. Angle differences of one degree at the tip to 8 degrees at the hub are observed. The chord length and stagger angles were calculated based on planar section cuts and a specified cone angle. They do not reflect the calculation of a conical section wrapped in space.

The Contractor Report implies that deflections for the QF-12 rotor would be minimal, and therefore no allowances were made in the hardware for deflections in geometry due to rotation. As a result, the geometry analyzed in the DAWES program was that of the undeflected hardware. However, if the deflections actually were significant, then the blade geometry that was analyzed may not have represented the true deflected shape.

To accommodate the gridding limitations of the AXCAPS and DAWES programs, the fillets on the rotor hub were not modeled, and the blade tip was modeled as tapered, rather than squared-off. Also, the swept damper had to be modeled as an unswept, constant elliptical cross-section airfoil, using an approximation provided by NASA-Lewis. The damper fillets were not modeled.

3.3 QF-12 Rotor Flow Analysis

DAWES Flow Analysis Program - The DAWES program is a finite-volume time-marching solver for the 3-D thin-layer Navier-Stokes equations. The version of the program used by AE uses the full energy equation (including the dissipation terms), and has a recently-installed correction of the viscous stress tensor formulation for the momentum equations. Two turbulence models are available in the program, a Baldwin-Lomax model and a one-equation k-l model. All rotor analyses performed for this study employed the Baldwin-Lomax model, which was found to be preferable for rotor analyses based on our previous fan calibration experience. The version of the DAWES program used for this study also has the capability to model midspan dampers on fan rotors.

The DAWES program currently serves as a standard design tool for all turbomachinery components at AE. Considerable experience with the program has been gained during its use over the last 6 years.

8
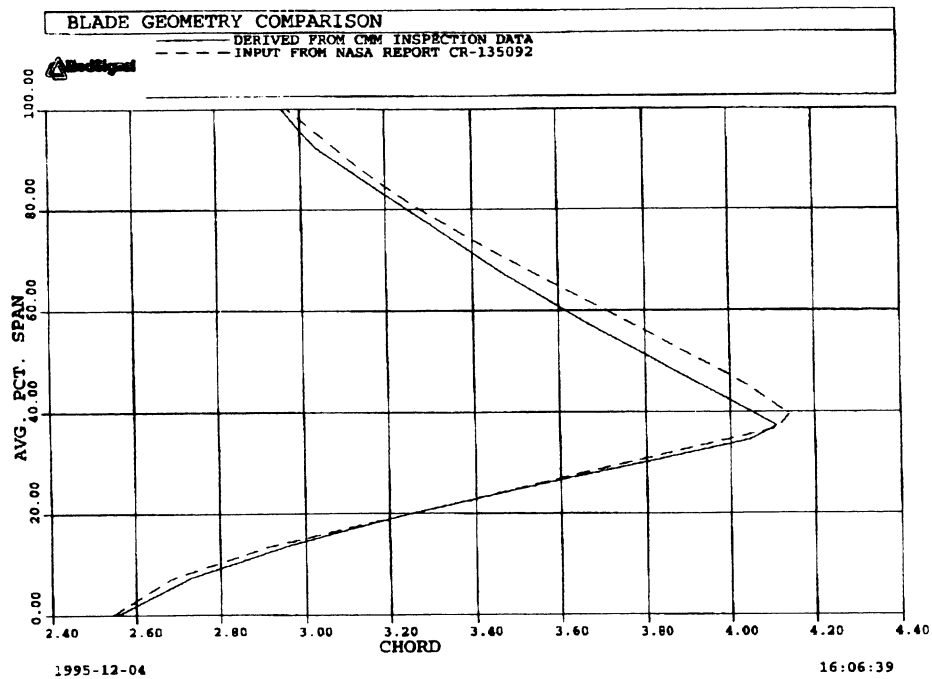
(a) chord
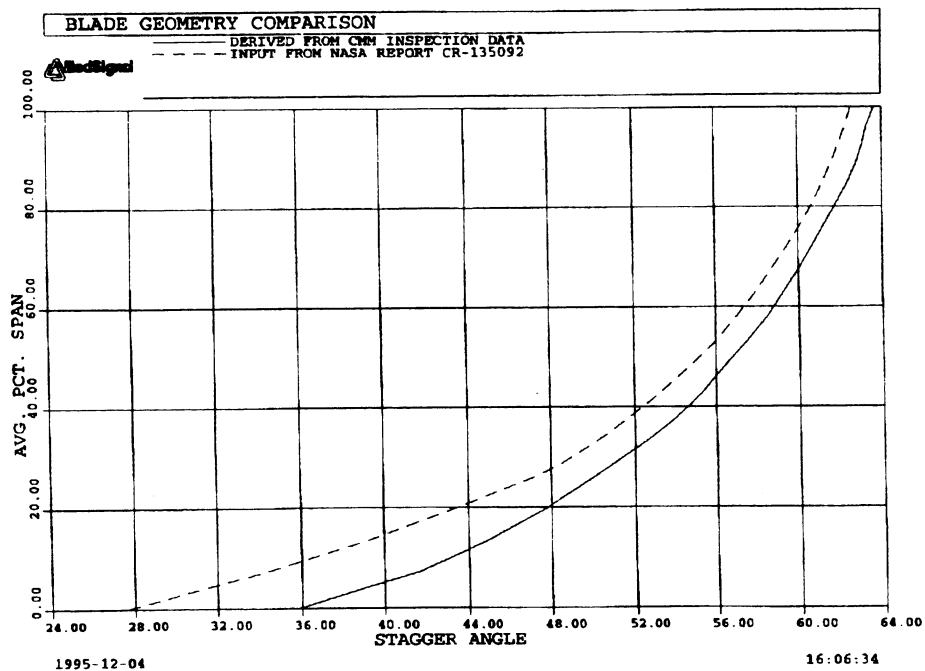
(b) stagger angle

Figure 7. Comparisons of the CMM Data With the Design Intent in the QF-12 Final
Report Show Geometry Inconsistencies.

9

Computational Grid - The computational domain for the QF-12 rotor consisted of a single rotor blade passage, with the suction surface of one blade forming one pitchwise boundary, and the pressure surface of the adjacent blade forming the other pitchwise boundary. The inlet to the computational grid was positioned approximately 120 percent of the hub axial chord upstream of the leading edge to minimize any boundary impact on the development of the upstream shock structure. The exit of the computational domain was located approximately 110 percent of the hub axial chord downstream of the blade trailing edge.

The computational grid for the DAWES program is a structured single-block skewed H-grid. The grid size employed for the rotor analyses was specified as:

Pitchwise:	41 Nodes
Spanwise:	81 Nodes (with eight cells in the clearance gap)
Streamwise:	145 Nodes (52 nodes on blade)

The total grid size was 481,545 nodes. The eight cells within the tip clearance gap were equally spaced. Grid spacing was nonlinearly expanded from the remaining walls using a hyperbolic tangent-based algorithm, with the grid node closest to the blade surface located at approximately 0.15 percent pitch away from the surface.

The grid spacing around the midspan damper was also expanded, using a hyperbolic tangent scheme. However, this near-damper spacing was transitioned to a typical undampered spanwise spacing in the upstream and downstream regions.

Typical sections of the computational grid are presented in Figure 8. A detail of the tip clearance region, illustrating the tapered blade tip, is shown in Figure 9. Details of the midspan damper grid clustering are shown in Figure 10.

Boundary Conditions - Boundary conditions for the DAWES computational domain consist of wall, periodic, and inlet/exit conditions. The wall conditions are equivalent to a no-slip condition on all solid walls, with a fully-rotating hub. Because the solution is performed in the relative frame of reference, the shroud endwall is modeled as rotating opposite in direction to the rotor.

Periodic boundaries are defined upstream and downstream of the rotor suction and pressure surfaces and also in the tip clearance region. Inlet conditions are based on the AXCAPS rotor solution, with radial distributions of total pressure, total temperature, and tangential velocity being specified. Wall boundary layers were not modeled at the upstream inflow position. At the exit, static pressure on the shroud is held fixed to establish the mass flow. The boundary conditions are summarized in Figure 11.

10
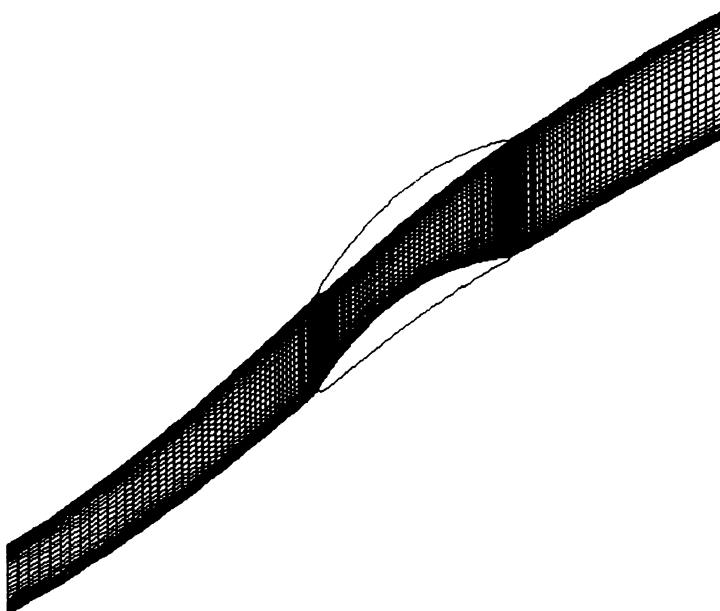
(a) tangential section at hub
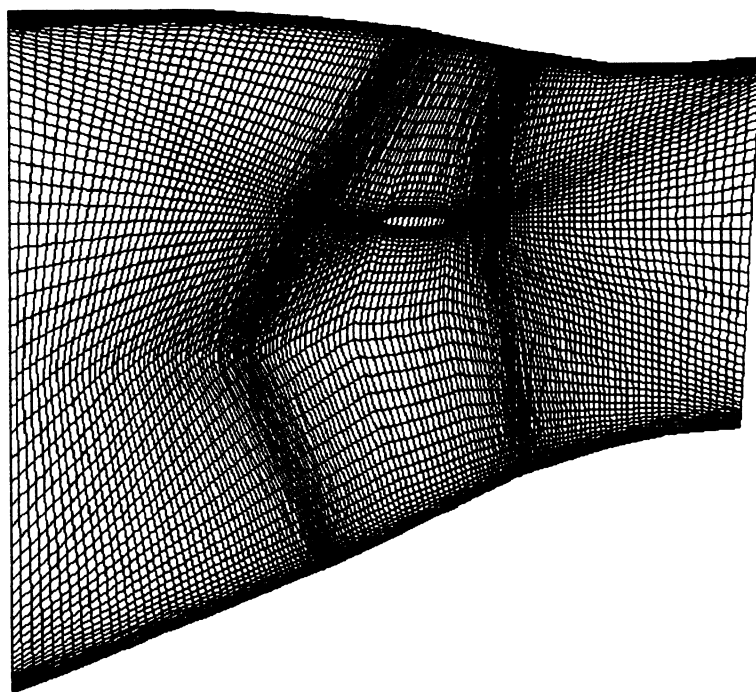
(b) meridional section
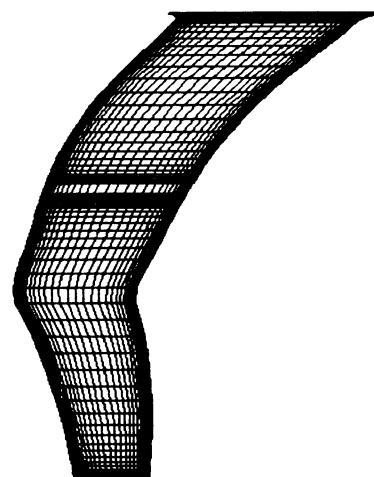
(c) cross section at mid-chord

Figure 8. **Typical Sections of the Computational Domain Show the Characteristics of the Rotor Passage H-Grid.**
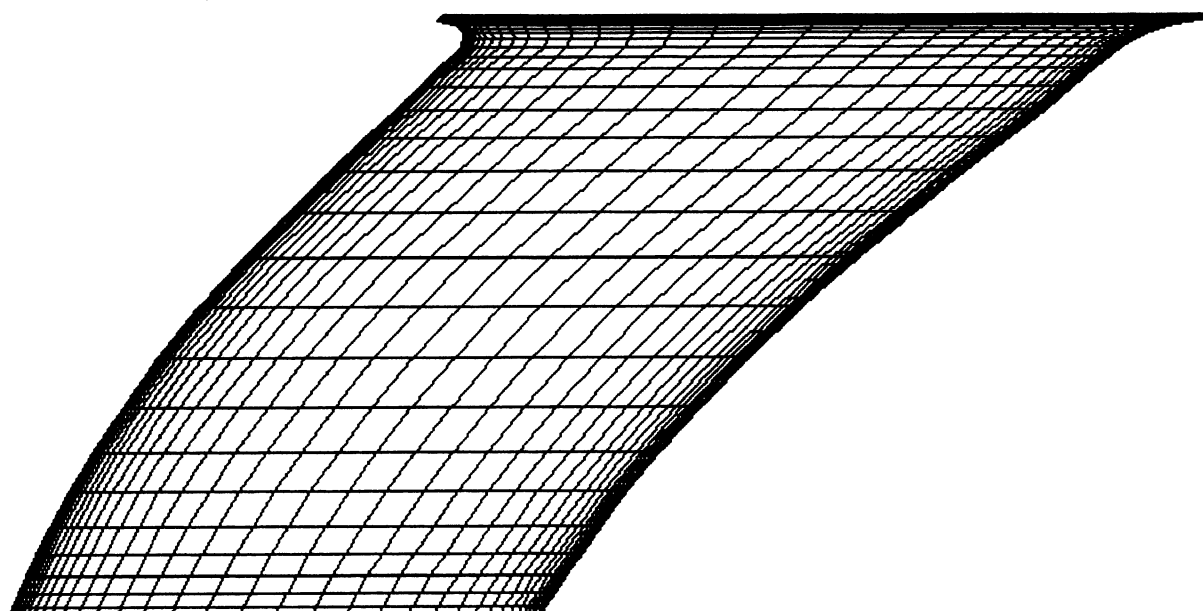
Figure 9. Enlarged View of Tip Section of DAWES Computational Grid Shows Artificial Blade Tapering.
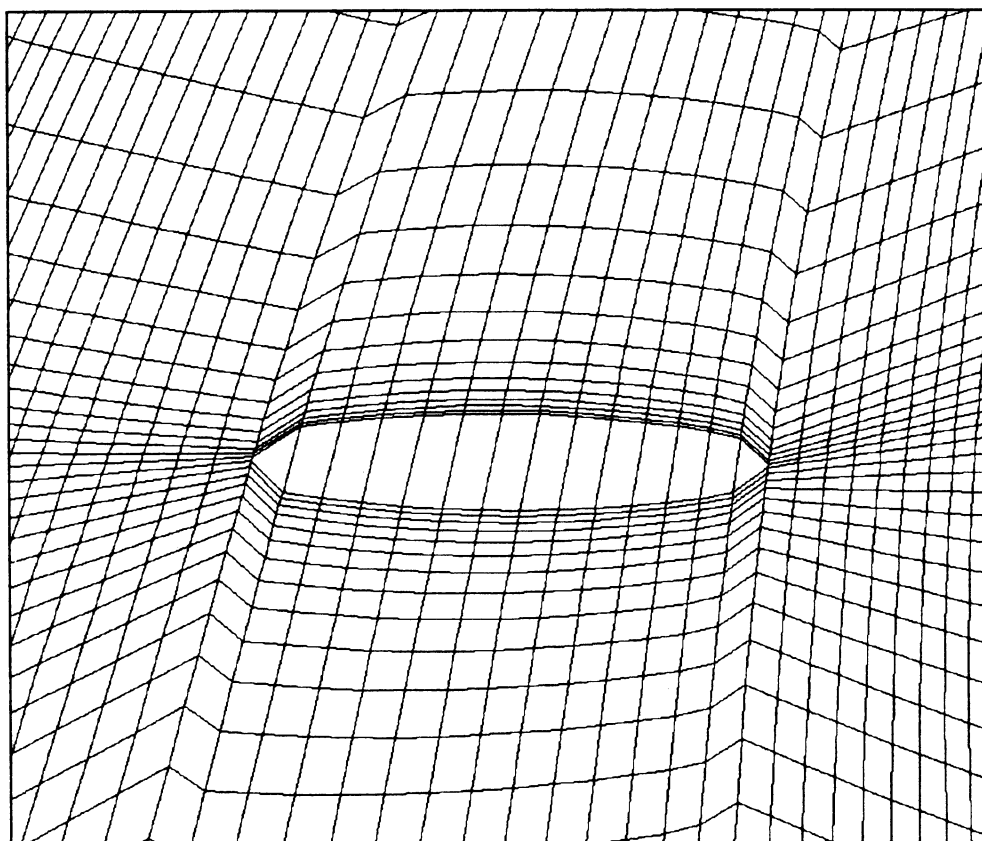
Figure 10. The Grid for the Mid-Span Damper Shows the Grid Clustering Approach.
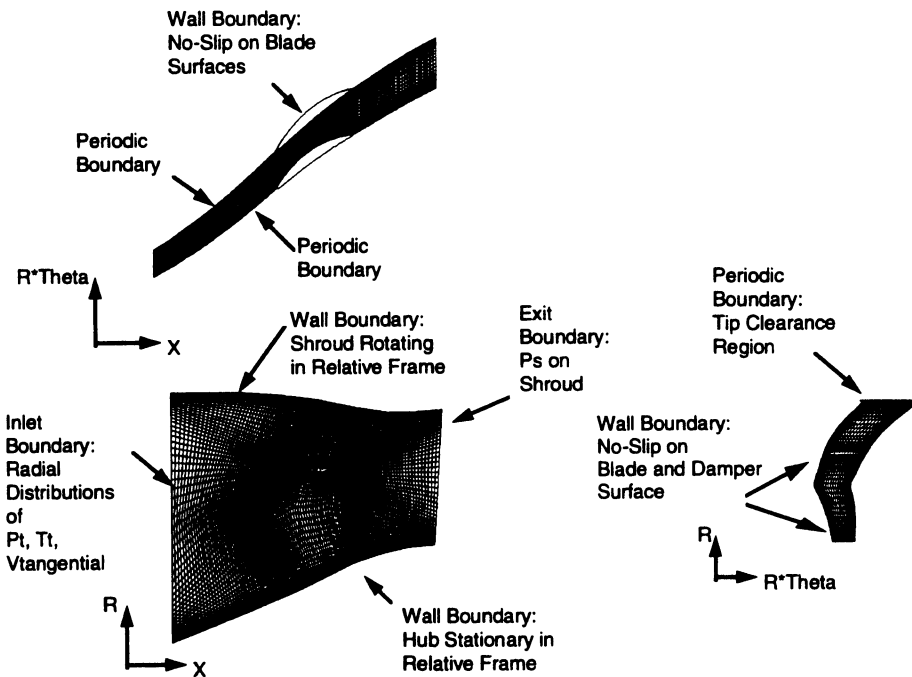
Figure 11. Summary of the Boundary Conditions Used in the QF-12 DAWES Analysis.

Convergence - The DAWES program displays a set of six quantities for monitoring convergence. Root-mean-square and maximum residuals of the governing equations are computed, along with inlet mass flow, mass flow error (expressed as a ratio of the maximum mass flow excursion in the computational domain relative to the inlet mass flow), the minimum static pressure in the system, and the overall total pressure ratio. Convergence is assumed to have been reached when the inlet mass flow, minimum static pressure, and overall total pressure ratio stabilize, the mass flow error remains below 1 percent, and the residuals continue to decrease.

Analyses - DAWES analyses of the QF-12 Fan rotor were performed on the operating line at four speeds, which were selected to match acoustic test points having published MPT noise measurements (Reference 2). The speeds, identified in terms of the design fan speed, were as follows: 100, 90, 80, and 70 percent. The resulting performance map is shown in Figure 12.

3.4. Results

Comparison With Aerodynamic Performance Data - The DAWES analyses were consistent with the test results, in that performance failed to meet the design goals. As shown in Figure 13, the tested performance at 100 percent design speed was low in flow, total pressure ratio, and efficiency. A comparison of predicted and measured total pressure ratio versus flow at four speeds along the operating line, presented in Figure 12, shows that the predicted

13
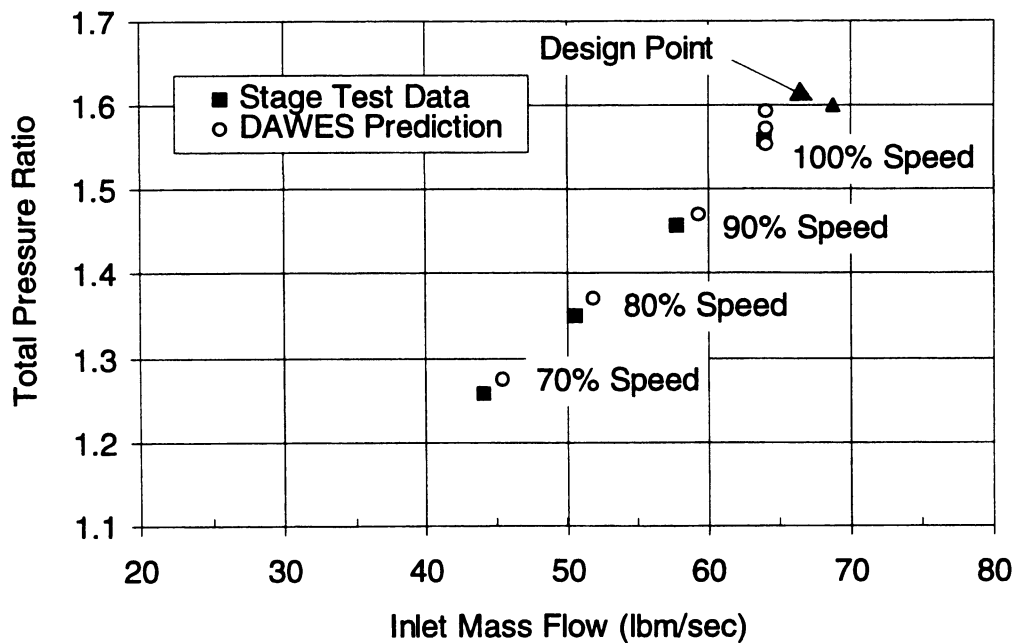
**Figure 12.   The DAWES Program Predicts Performance for the QF-12 Fan Rotor
That Matches Test Data.**

performance closely matches the test results, including the failure to meet the design goal. Because the DAWES analyses were performed for the rotor alone, the predicted total pressure ratio is higher than the data, which represents the stage total pressure ratio. The DAWES predictions are also slightly higher in flow than the data, for the part-speed cases.

More detailed examination of the 100 percent speed case shows that the DAWES prediction of the spanwise distribution of pitch-averaged total pressure ratio follows the trend of the data quite well, as presented in Figure 14. The predicted profile of pitch-averaged efficiency is higher in level than the measured data, but the profile shape is similar, as shown in Figure 15. Once again, the comparisons are between stage measurements and rotor-only predictions. The DAWES analysis presents a very pronounced midspan damper wake, which appears to have been missed entirely by the instrumentation, due to the radial positioning of the five probes on each of the four rakes. The DAWES distributions were obtained at a location approximately 30 percent axial chord downstream from the rotor trailing edge. The rake data used for comparison was taken behind the stator, at the fan discharge, and therefore some distortion of the rotor exit profiles may have occurred, due to mixing through the stator.

As discussed in Reference 2, one test was performed with the stators removed and the exit rakes realigned to the rotor exit flow. The results of this test showed that essentially the same radial distributions of total pressure ratio and efficiency were present for the rotor-only measurements as were seen for the fan stage. Because these measured radial profiles were deficient in performance, relative to the design intent, it was concluded that the performance problem was isolated in the rotor. Thus, because the DAWES results match the trends of the stage radial distributions (and therefore, the rotor-only distributions), it may be concluded that

14
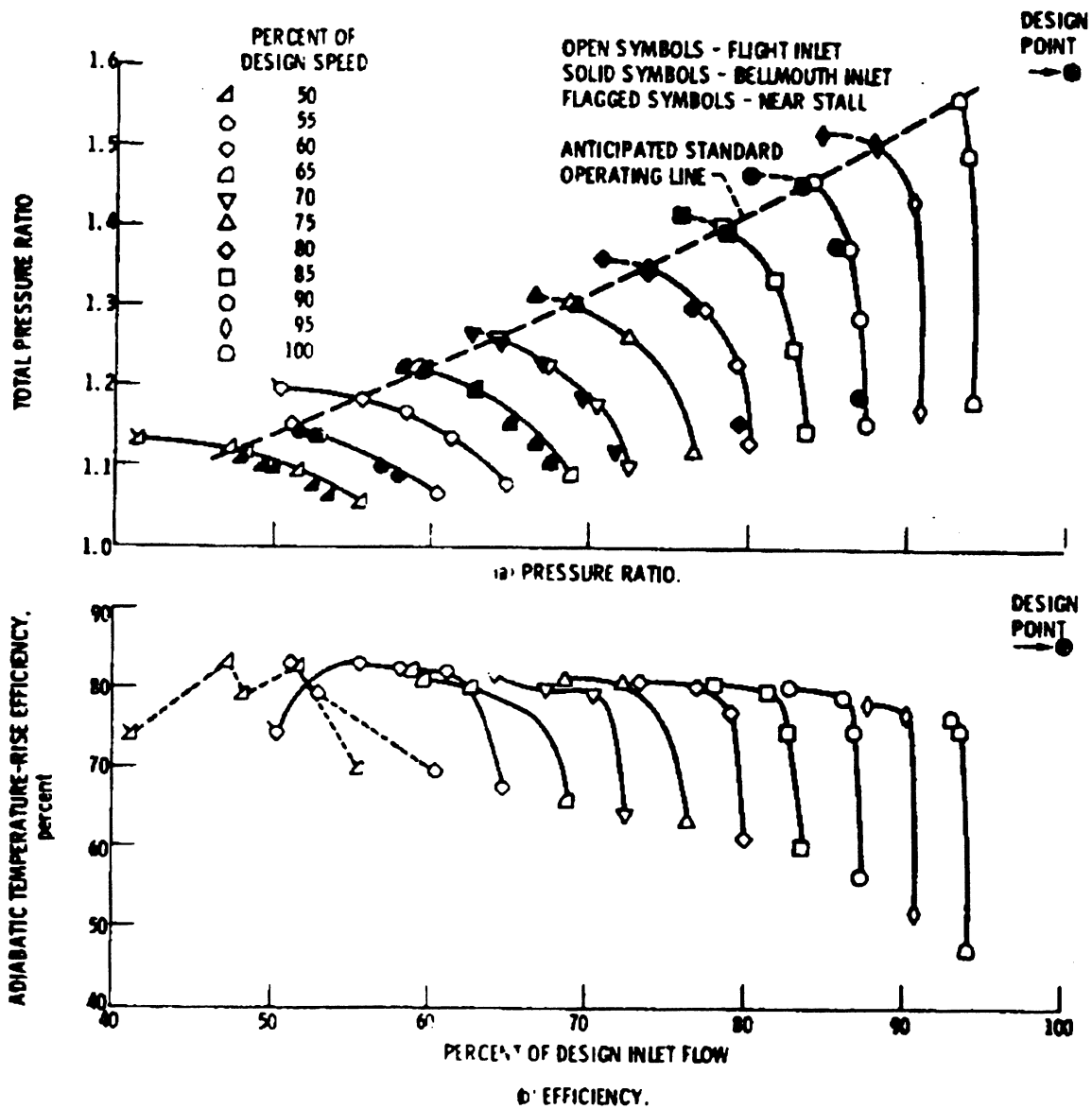
Figure 13. Tested Aerodynamic Performance for the QF-12 Fan Failed to Meet the Design Goals.

15
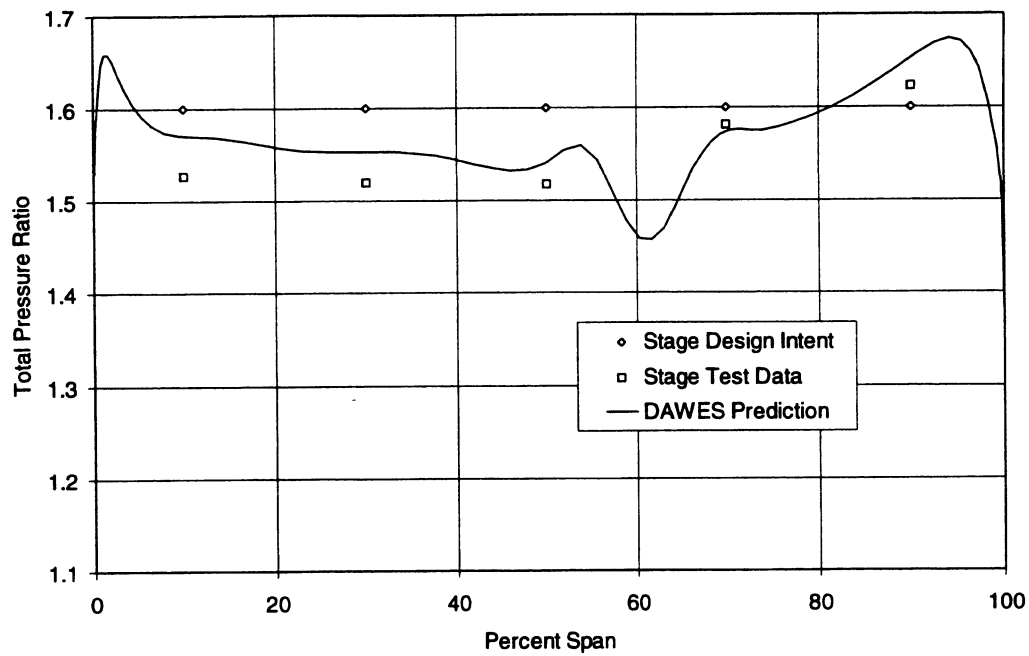
Figure 14. The Predicted Radial Profile of Rotor Total Pressure Ratio Exhibits the Same Trend as the Stage Data.
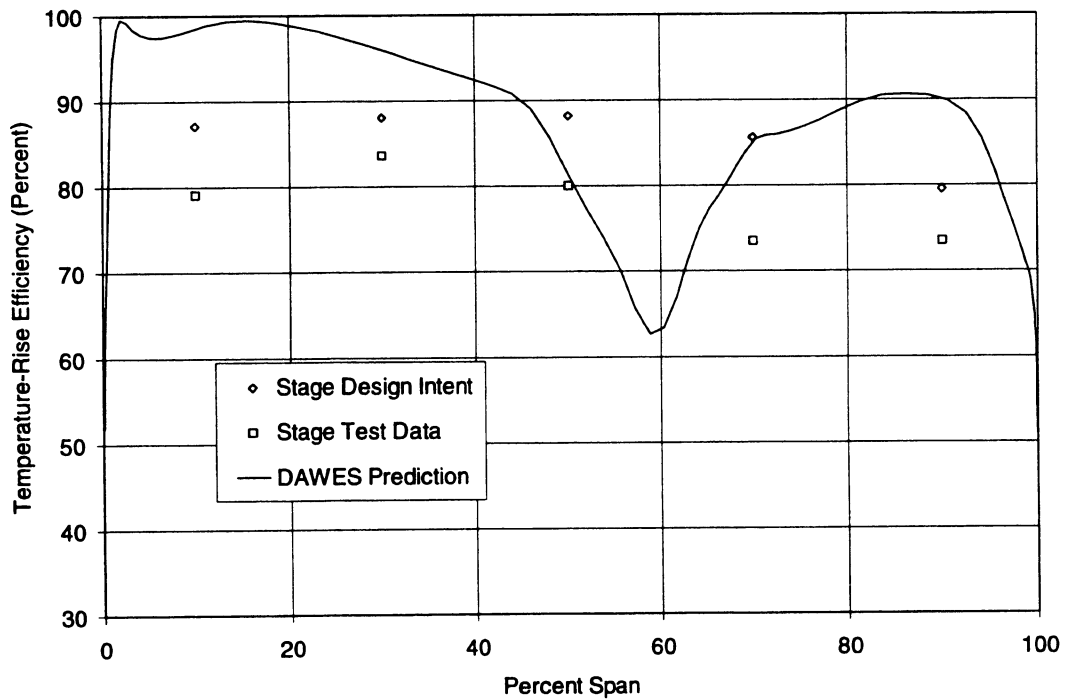
Figure 15. The Predicted Radial Profile of Rotor Efficiency Shows Trends Similar to the Stage Test Data, but at a Higher Level.

16

the CFD simulation is reasonably accurate, and may be employed to identify the possible cause(s) of the performance deficit seen in the tested QF-12 fan stage.

Source(s) of the Aerodynamic Performance Deficit - According to Reference 2, the design point values of mass flow, pressure ratio, and efficiency were established prior to the addition of the midspan damper on the rotor. Therefore, the effects of the damper were not accounted for in the determination of design point performance. However, the authors noted that, after accounting for the estimated blockage and loss effects of the damper, the measured performance was still low. This additional deficit could be explained by the presence of separated flow around the damper, as seen in the DAWES simulation.

As shown in the Mach contour and velocity vector plots of Figure 16, a shock-induced separation occurs near the pressure surface of the rotor, on both the upper and lower surfaces of the midspan damper, at 100 percent speed. This flow separation results in a significant blockage, and the associated losses may be tracked downstream, as presented in the relative total pressure contours of Figure 17.

With the wheel speed lowered to 90 percent design speed, the shock strength is reduced, and the extent of the separation diminishes, as seen in Figures 18 and 19. At 80 percent speed, the shock is much weaker, and the separated region is no longer evident, with no disruption to the flow, as illustrated in Figures 20 and 21.

Reference 2 suggests that the aerodynamic performance of the rotor could possibly be impacted by an unexpected shock near the blade tip in the rotor passage entrance region. However, the only evidence of such a shock structure in the CFD flow simulation is confined to a region in the outer 3 percent span, and would be expected to have only a localized effect. Based on the relative agreement between the measured performance and that predicted by the DAWES program, the most likely cause for the aerodynamic performance deficiency is the presence of the flow separation around the midspan damper at design wheel speed, rather than the rotor inflow aerodynamics.

Prediction of MPT Noise Onset - Because the existence of MPT noise is dependent upon the presence of shock waves in the inlet region of the rotor flowpath, CFD simulations may be used to determine under what conditions a rotor inlet shock will be present.

Contour plots of relative Mach number were used to determine the variation of predicted shock position with wheel speed, and to ascertain the presence or absence of an inlet shock for the QF-12 rotor. Mach contours from the DAWES simulation at 100 percent design speed are shown in Figure 22, for surfaces near the suction surface and near the blade tip. A prominent passage shock is visible both above and below the midspan damper on the suction surface. However, this shock is entirely contained within the blade passage and does not extend upstream into the inlet region where it would generate MPT noise. Another weaker shock is also present at the leading edge of the midspan damper. This shock is swept back along the outer span of the rotor, running essentially parallel to the leading edge of the blade, and almost coalescing with the stronger damper shock near the blade tip.
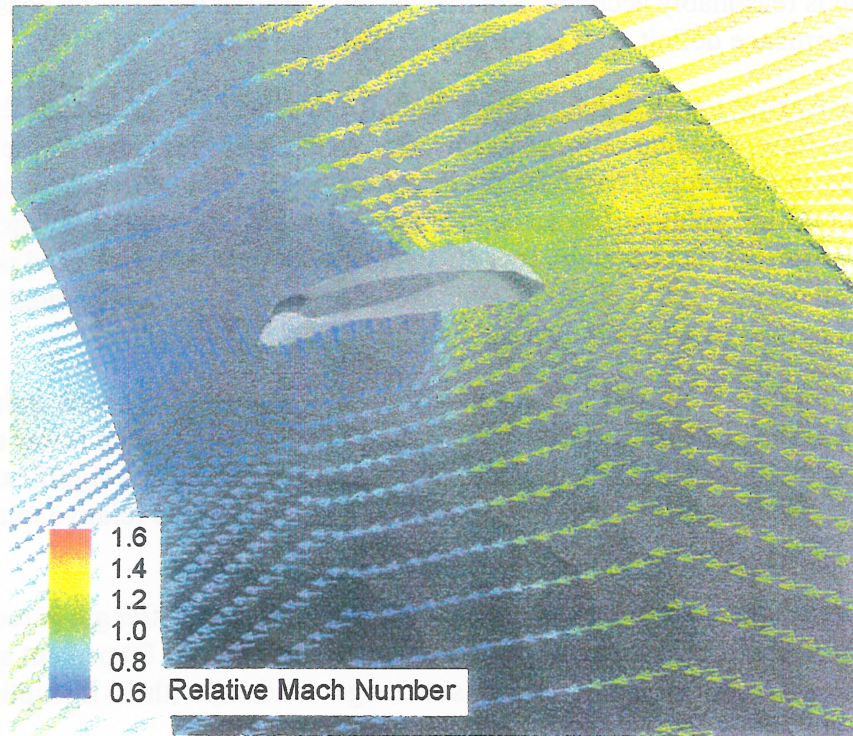
(a) relative Mach vectors
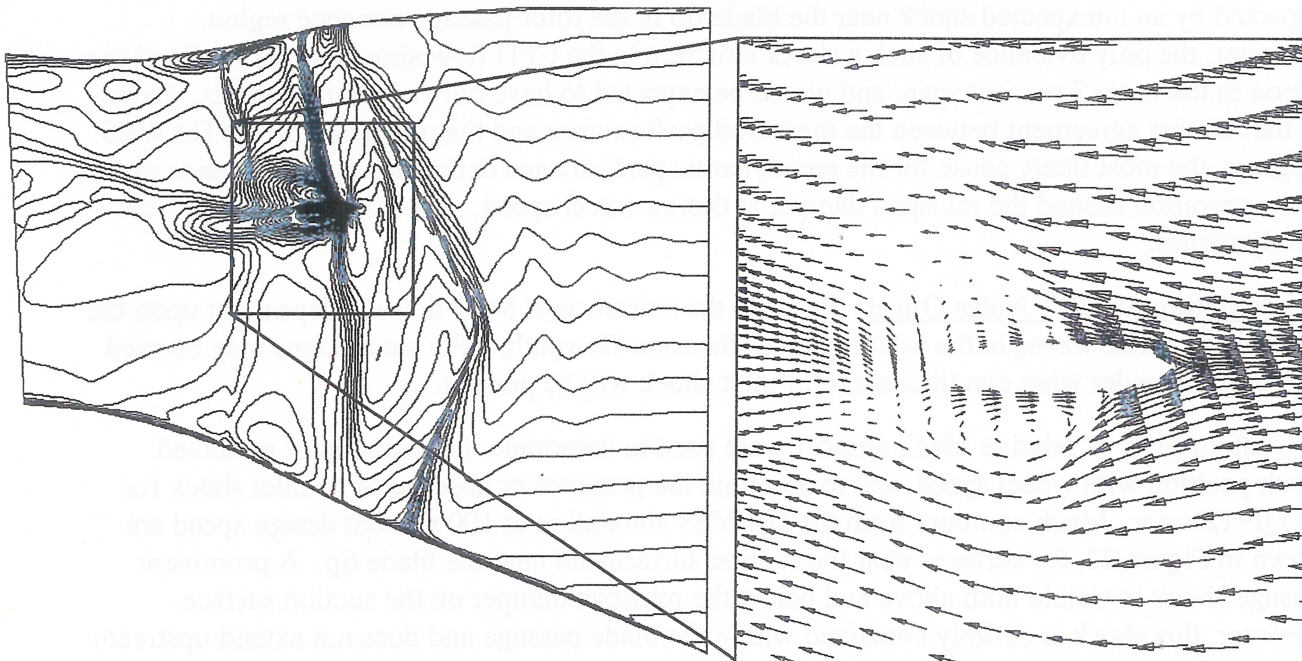
(b) relative Mach number contours

(c) velocity vectors

Figure 16.   Contours of Relative Mach Number and Velocity Vectors Depict the Shock-Induced Flow Separation at the Midspan Damper at 5 Percent Pitch Away From the Pressure Surface of the Rotor for 100 Percent Design Speed.

18

(a) total pressure (psi)

suction
surface

midspan damper
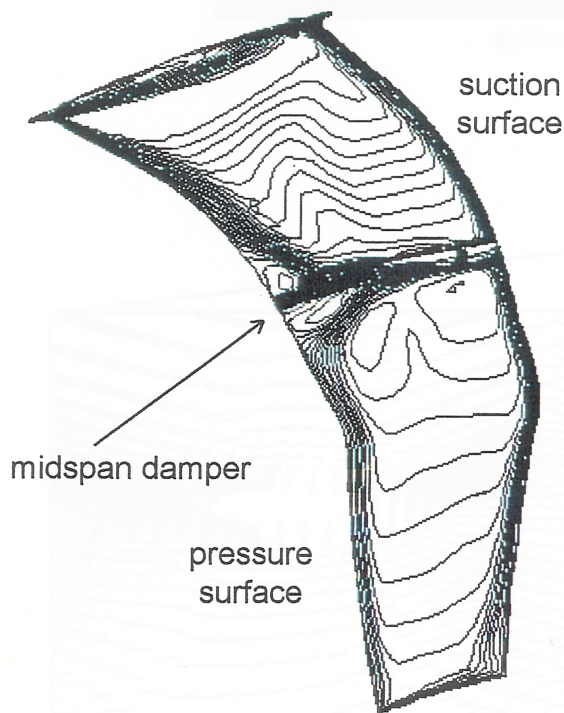
pressure
surface

(b) 70% axial chord

(c) trailing edge

Figure 17.   Relative Total Pressure Contours Show the Effect of the Flow Separation on the Pressure Side of the Passage Around the Midspan Damper at 100 Percent Speed.
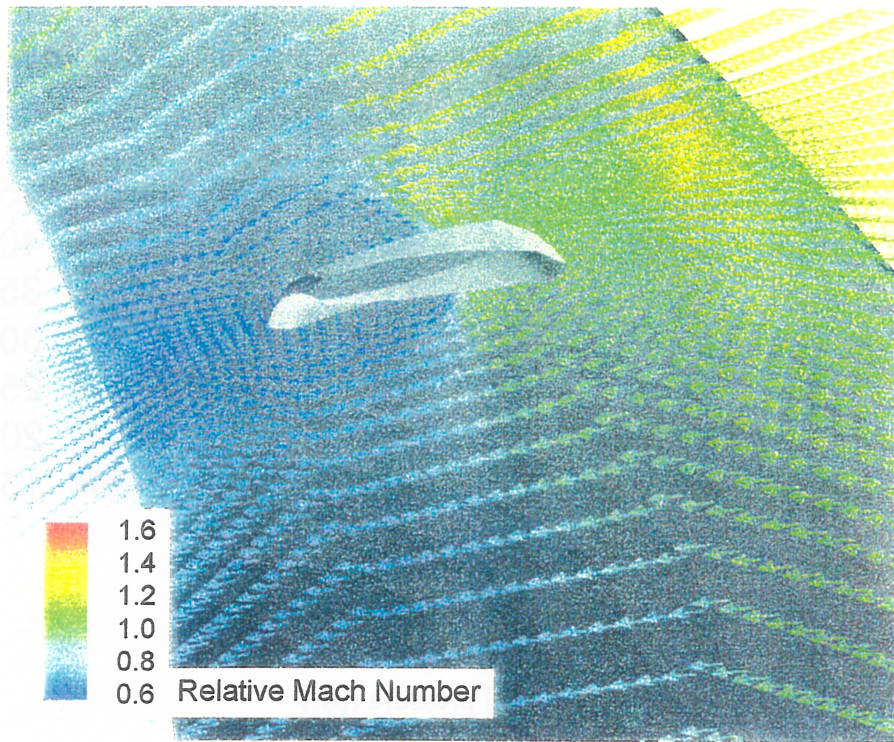
(a) relative Mach vectors
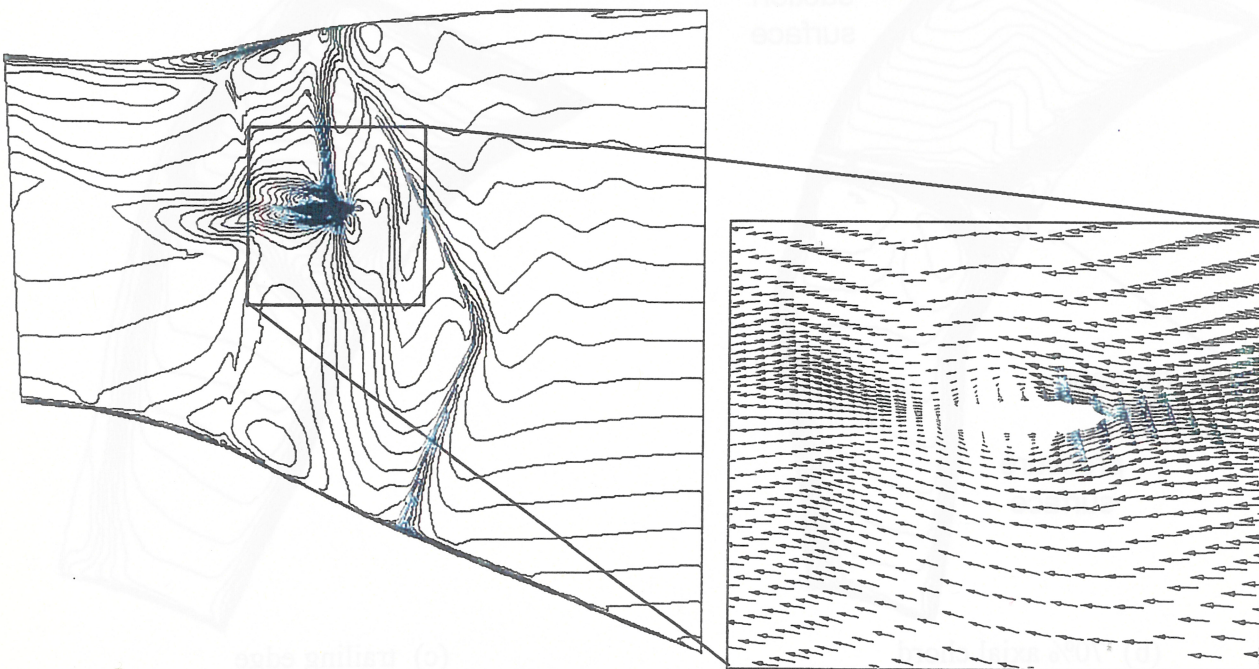
(b) relative Mach number contours

(c) velocity vectors

Figure 18. **The Shock-Induced Flow Separation Zone Is Significantly Reduced in Size at 90 Percent Speed (5 Percent Pitch Away From Pressure Surface).**

(a) total pressure (psi)

suction
surface

midspan damper
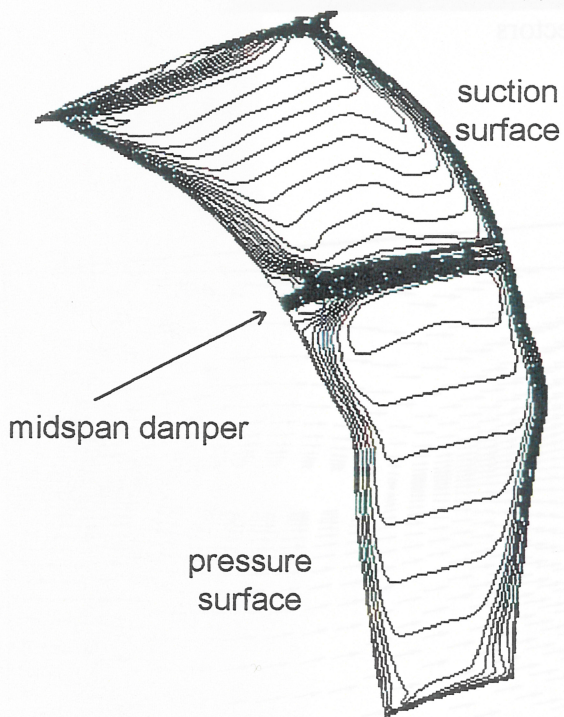
pressure
surface

(b) 70% axial chord

(c) trailing edge

**Figure 19.   Relative Total Pressure Contours Show the Effect of the Flow
Separation on the Pressure Side of the Passage Around the Midspan
Damper at 90 Percent Speed.**
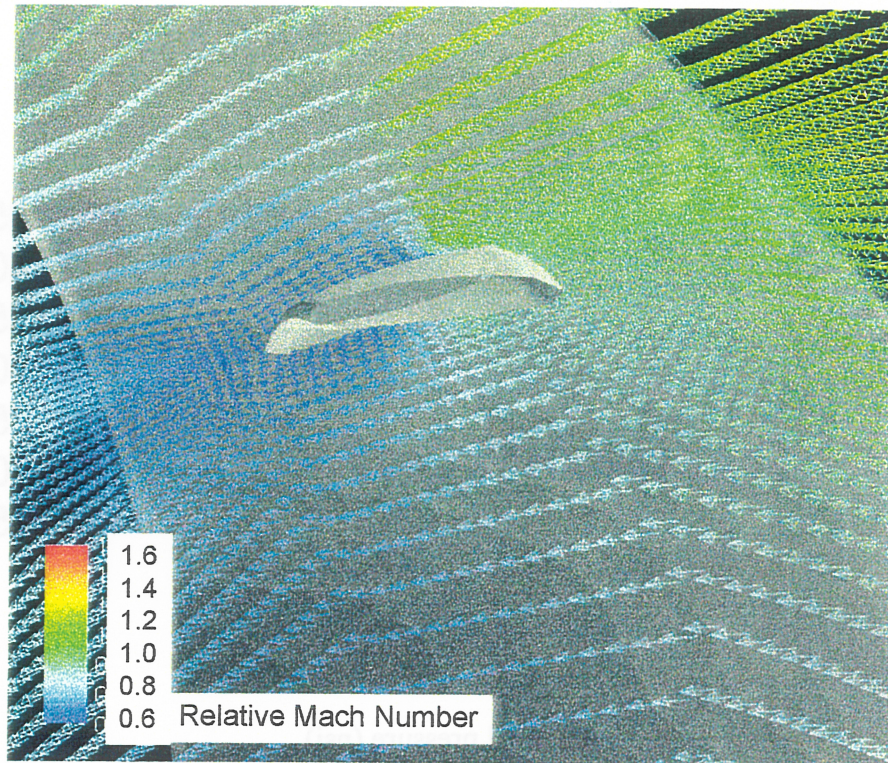
(a) relative Mach vectors
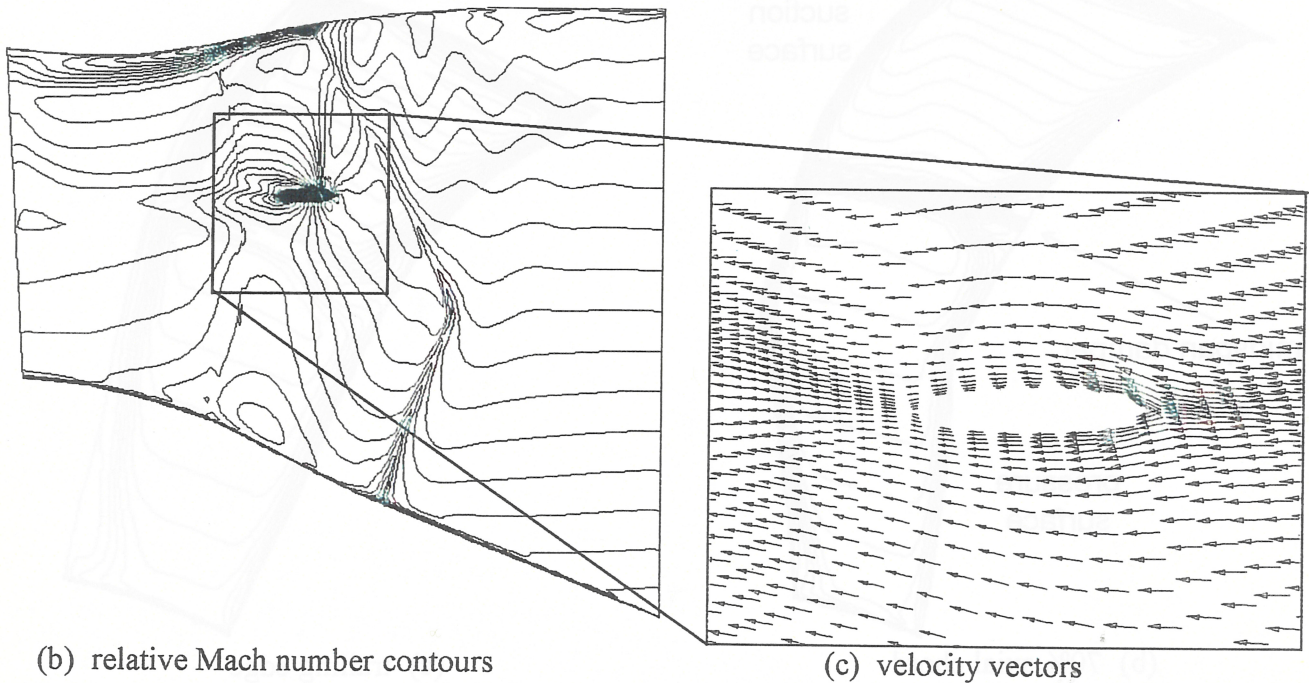
(b) relative Mach number contours

(c) velocity vectors

Figure 20.   Flow Separation Around the Damper Is No Longer Evident at 80 Percent Speed (5 Percent Pitch Away From Pressure Surface).
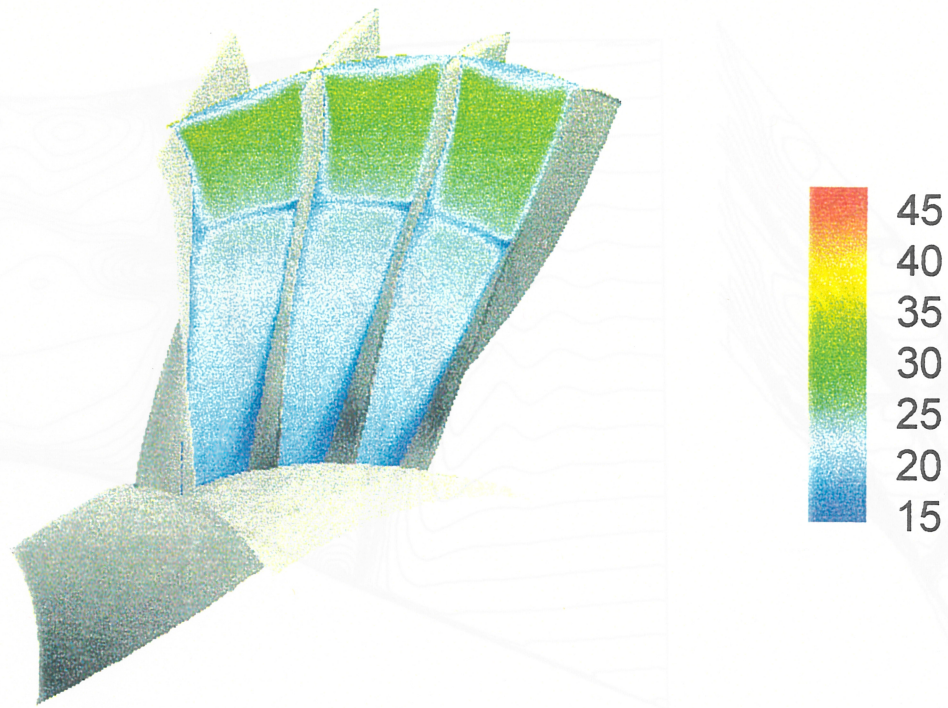
(a) total pressure (psi)
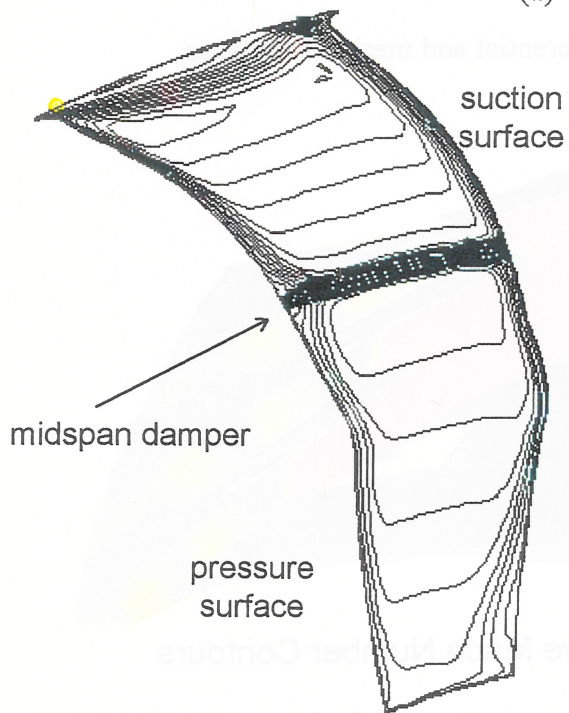
(b) 70% axial chord
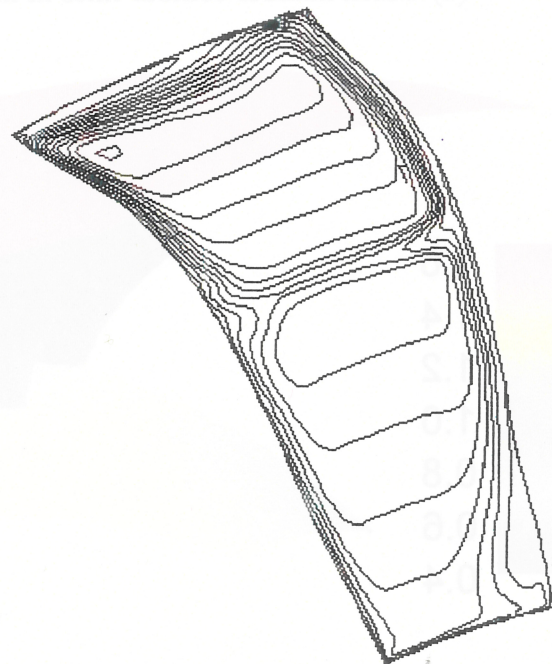
(c) trailing edge

Figure 21.   Relative Total Pressure Contours Show No Effect of Flow Separation on the Pressure Side of the Passage Around the Midspan Damper at 80 Percent Speed.
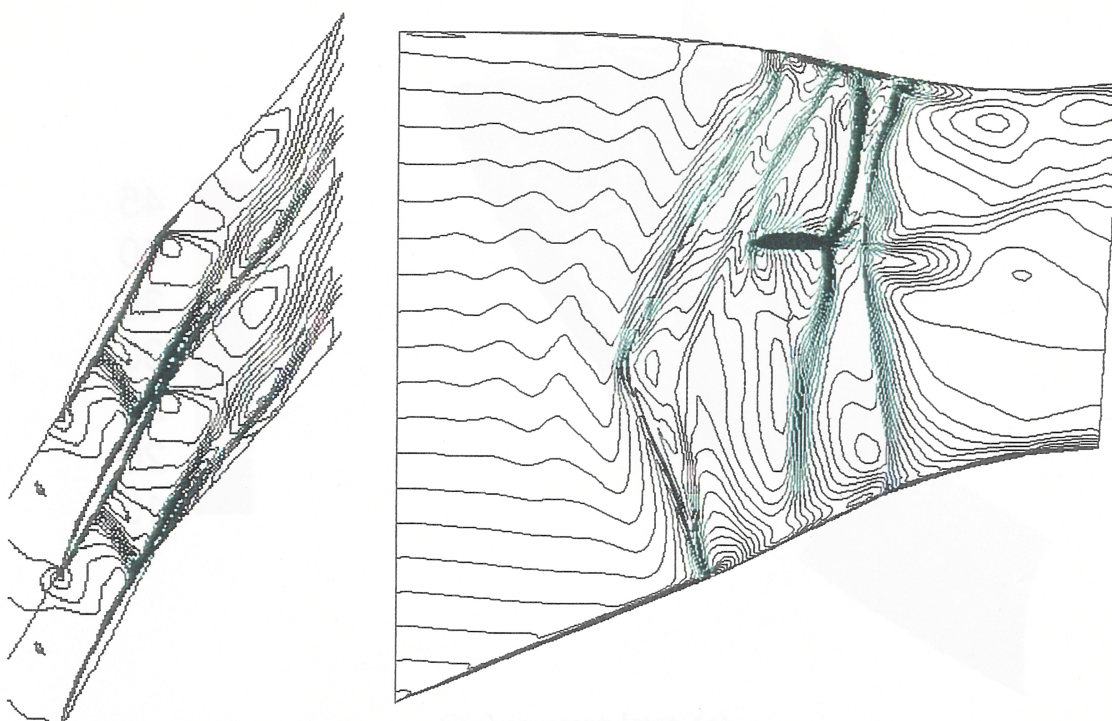
(a) Mach number contour lines in the circumferential and meridional planes
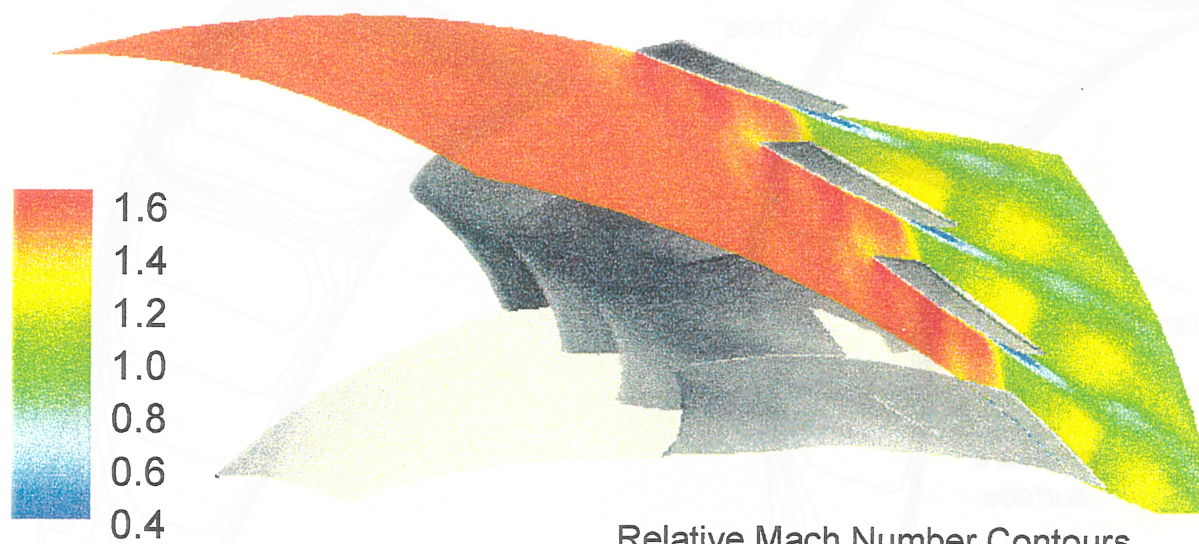
Relative Mach Number Contours

(b) Mach number color contours in a circumferential plane at 90% span

Figure 22.   DAWES Calculations Show a Strong Shock in the Blade Passage at 100 Percent Speed.
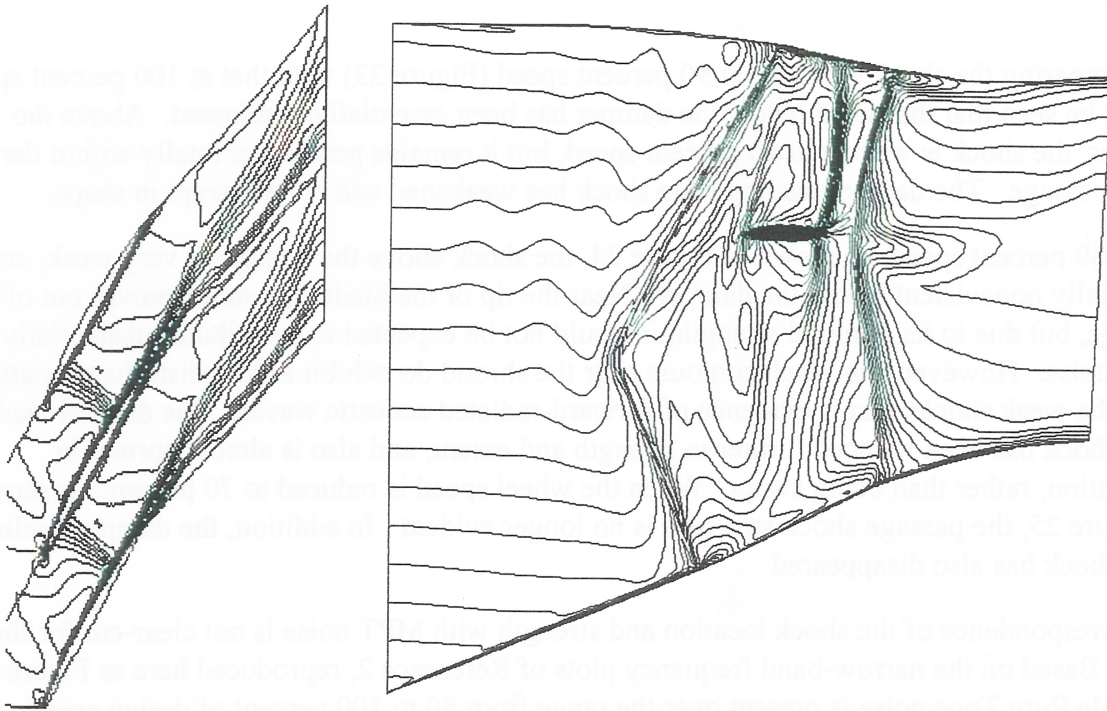
(a) Mach number contour lines in the circumferential and meridional planes
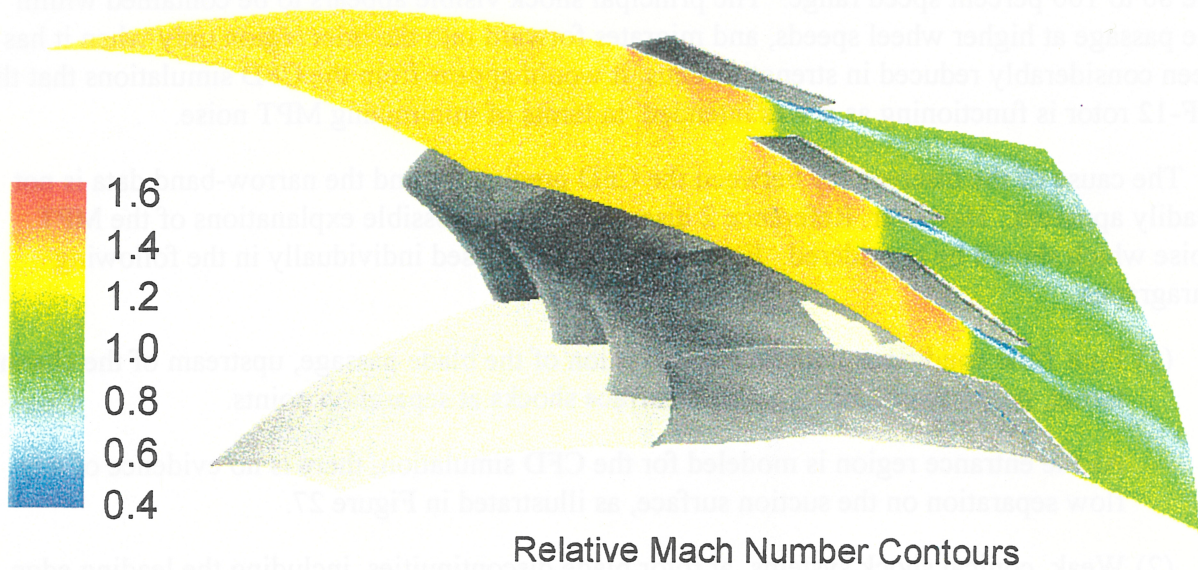
Relative Mach Number Contours

(b) Mach number color contours in a circumferential plane at 90% span

Figure 23. **At 90 Percent Speed, the Contours of Relative Mach Number Indicate a Weakening of the Shock, Particularly Below the Midspan Damper.**

Comparing the shock structure at 90 percent speed (Figure 23) with that at 100 percent speed, it may be seen that the shock below the damper has been essentially eliminated. Above the damper, the shock is weaker at 90 percent speed, but it remains positioned totally within the blade passage. The damper leading edge shock has weakened and is less swept in shape.

At 80 percent speed, as shown in Figure 24, the shock above the damper is very weak, and is essentially nonexistent below the damper. Near the tip of the blade, the shock moves out of the passage, but due to its minimal strength, it would not be expected to contribute substantially to MPT noise. However, the Mach contours near the shroud do exhibit a flow disturbance pattern from the weak shocks that is evidence of forward-radiated acoustic waves. The damper leading edge shock has been reduced further in strength and extent, and also is almost normal in orientation, rather than being swept. When the wheel speed is reduced to 70 percent, as shown in Figure 25, the passage shock structure is no longer evident. In addition, the damper leading edge shock has also disappeared.

Correspondence of the shock location and strength with MPT noise is not clear-cut for this rotor. Based on the narrow-band frequency plots of Reference 2, reproduced here as Figure 26, Multiple Pure Tone noise is present over the range from 80 to 100 percent of design speed. The onset of MPT noise occurs between 70 and 80 percent speed. Based on the Mach contour plots from the DAWES simulations, MPT noise would not have been expected to be a factor within the 80 to 100 percent speed range. The principal shock visible appears to be contained within the passage at higher wheel speeds, and migrates forward into the inlet region only when it has been considerably reduced in strength. Thus, it would appear from the CFD simulations that the QF-12 rotor is functioning as it was intended, in terms of minimizing MPT noise.

The cause of the discrepancy between the CFD predictions and the narrow-band data is not readily apparent. However, Reference 2 discusses several possible explanations of the MPT noise which should be considered. Each of these is discussed individually in the following paragraphs.

(1) Poor flow conditions in the entrance region of the blade passage, upstream of the channel throat, possibly producing suction-surface shocks at separation points.

As the entrance region is modeled for the CFD simulation, there is no evidence of any flow separation on the suction surface, as illustrated in Figure 27.

(2) Weak, conical shock systems, at rotor blade discontinuities, including the leading edge sweep reversal point, the leading edge of the blade tip, and the midspan damper leading edge.

The impact of these weak shock systems with respect to MPT noise was expected to be minimal, when compared to the reduction in MPT noise resulting from the elimination of the strong rotor inlet shock system, typical of conventional high-speed fans.
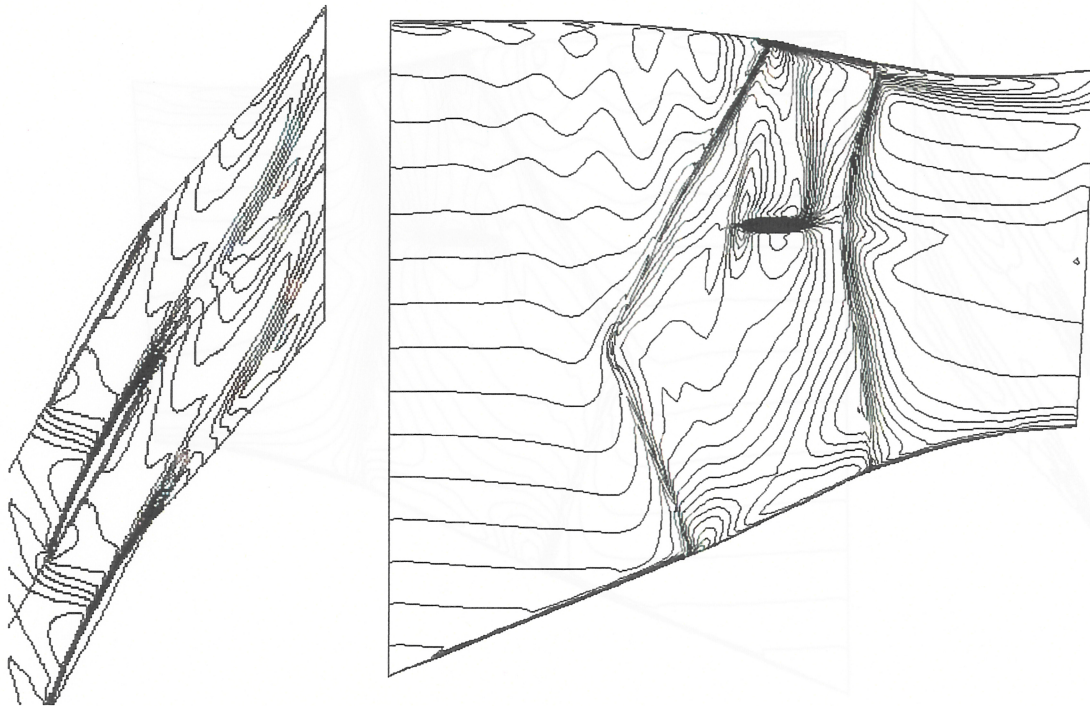
(a) Mach number contour lines in the circumferential and meridional planes

Relative Mach Number Contours
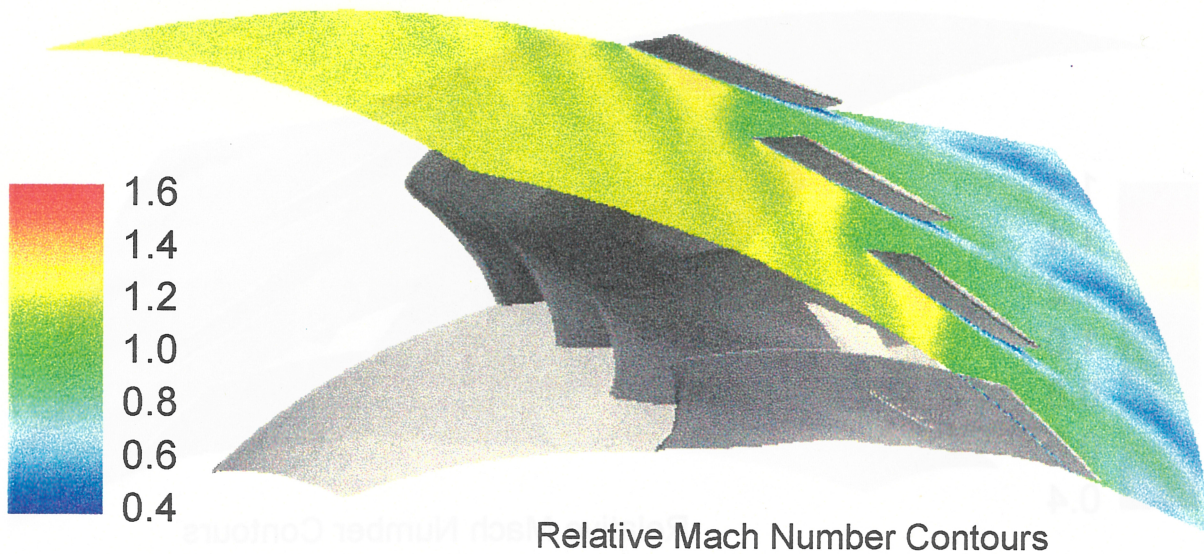
(b) Mach number color contours in a circumferential plane at 90% span

Figure 24.   Mach Contours Indicate Further Weakening of the Shock Structure at 80 Percent Speed.
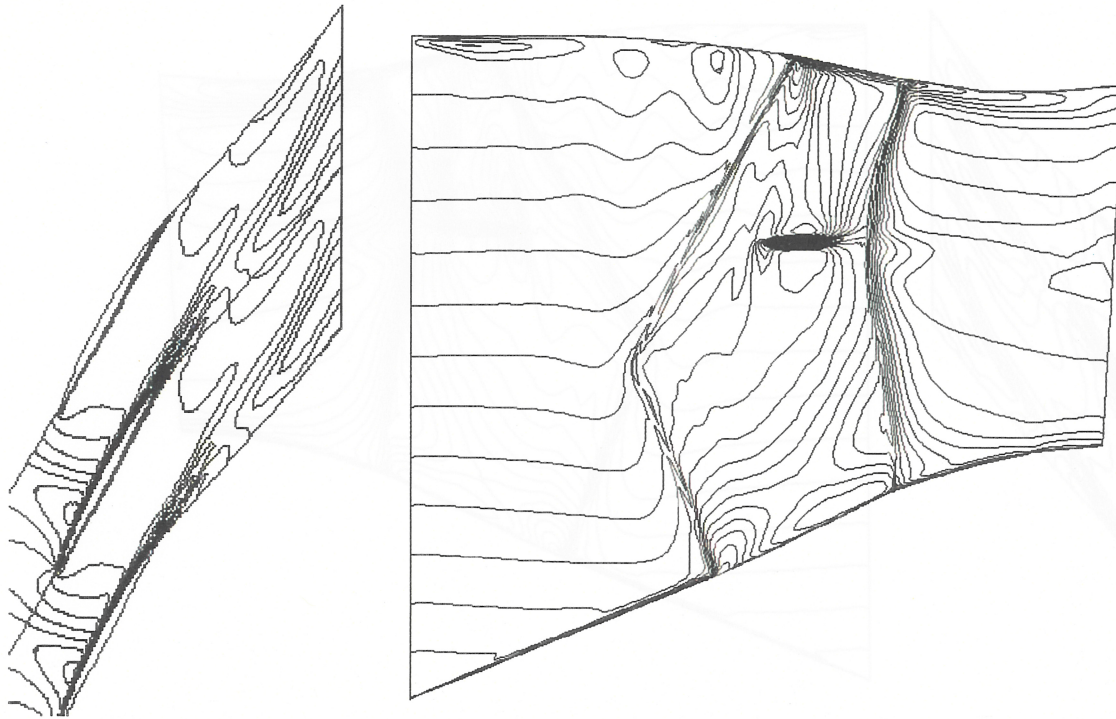
(a) Mach number contour lines in the circumferential and meridional planes

1.6
1.4
1.2
1.0
0.8
0.6
0.4

Relative Mach Number Contours
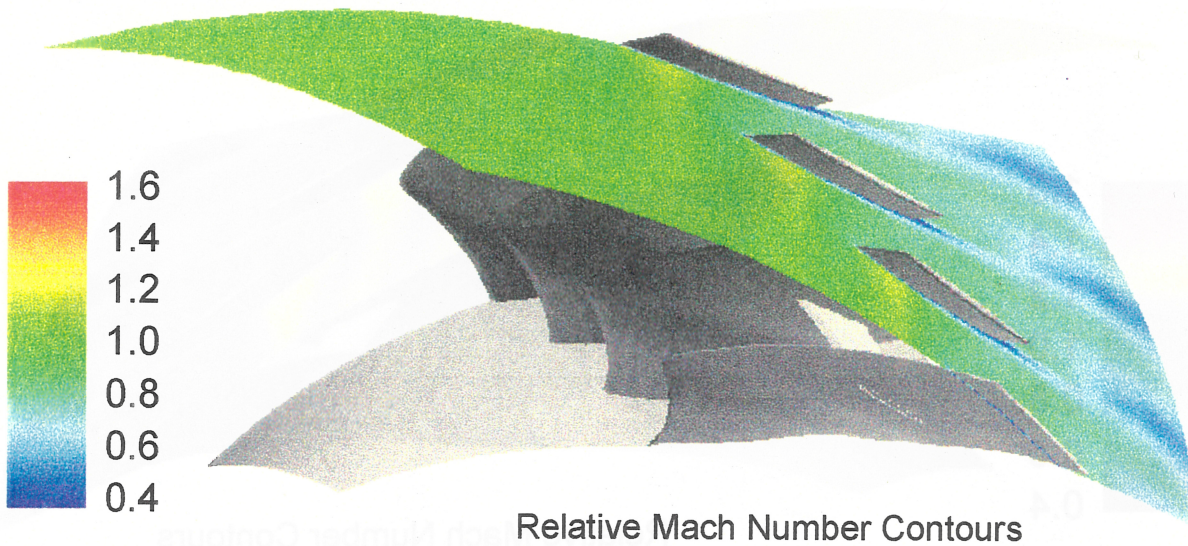
(b) Mach number color contours in a circumferential plane at 90% span

Figure 25.   The Passage Shock Structure Is No Longer Evident at 70 Percent Speed.

(a) 100 percent SPEED.

(b) 90 percent SPEED.

10 dB

(c) 80 percent SPEED.

FREQUENCY, kHz

(d) 70 percent SPEED.
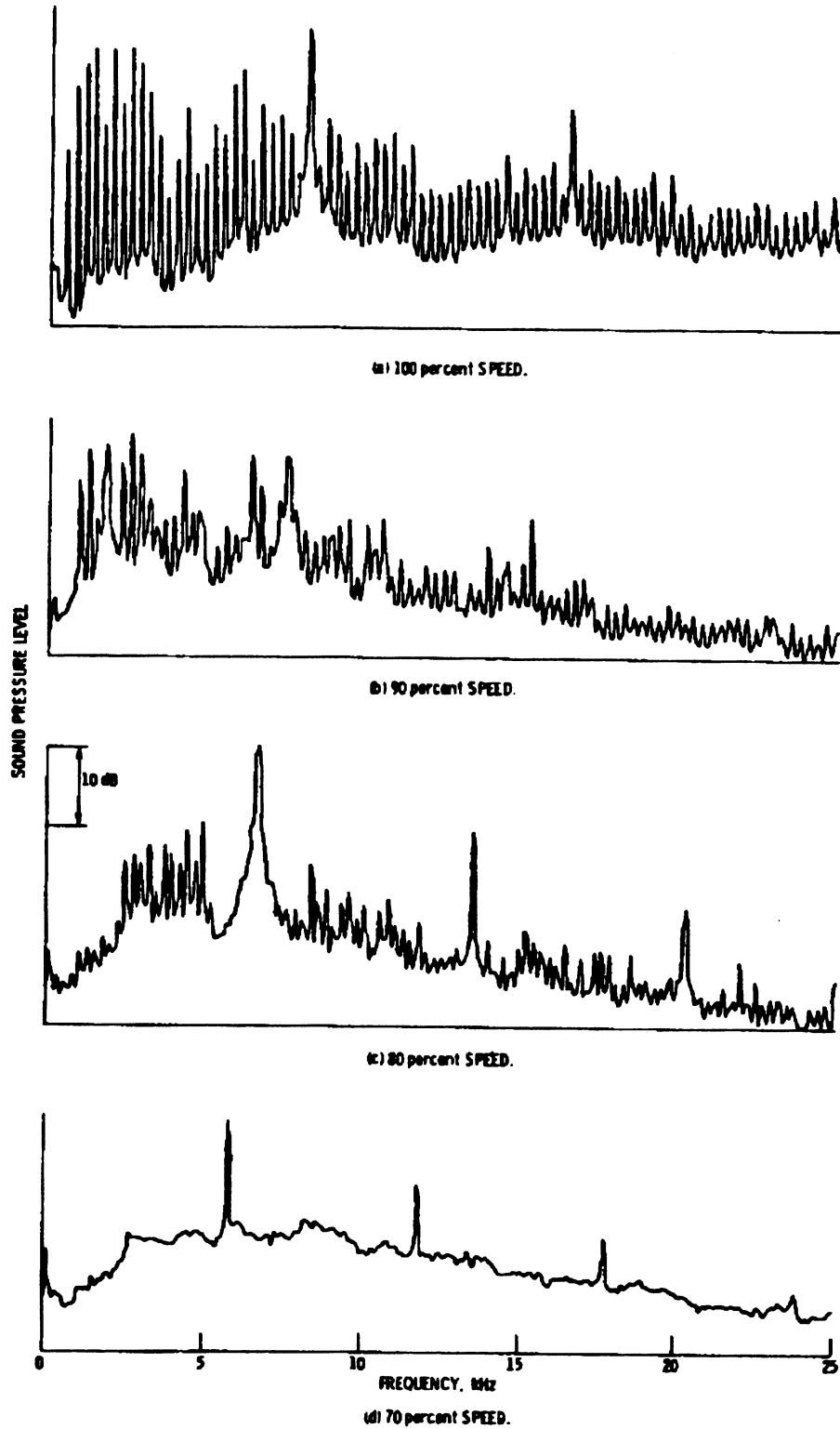
Figure 26. The Narrow Band Spectra of the QF-12 on the Standard Operating Line at 70 Degrees From Fan Inlet Axis Show Multiple Pure Tone Noise.

29
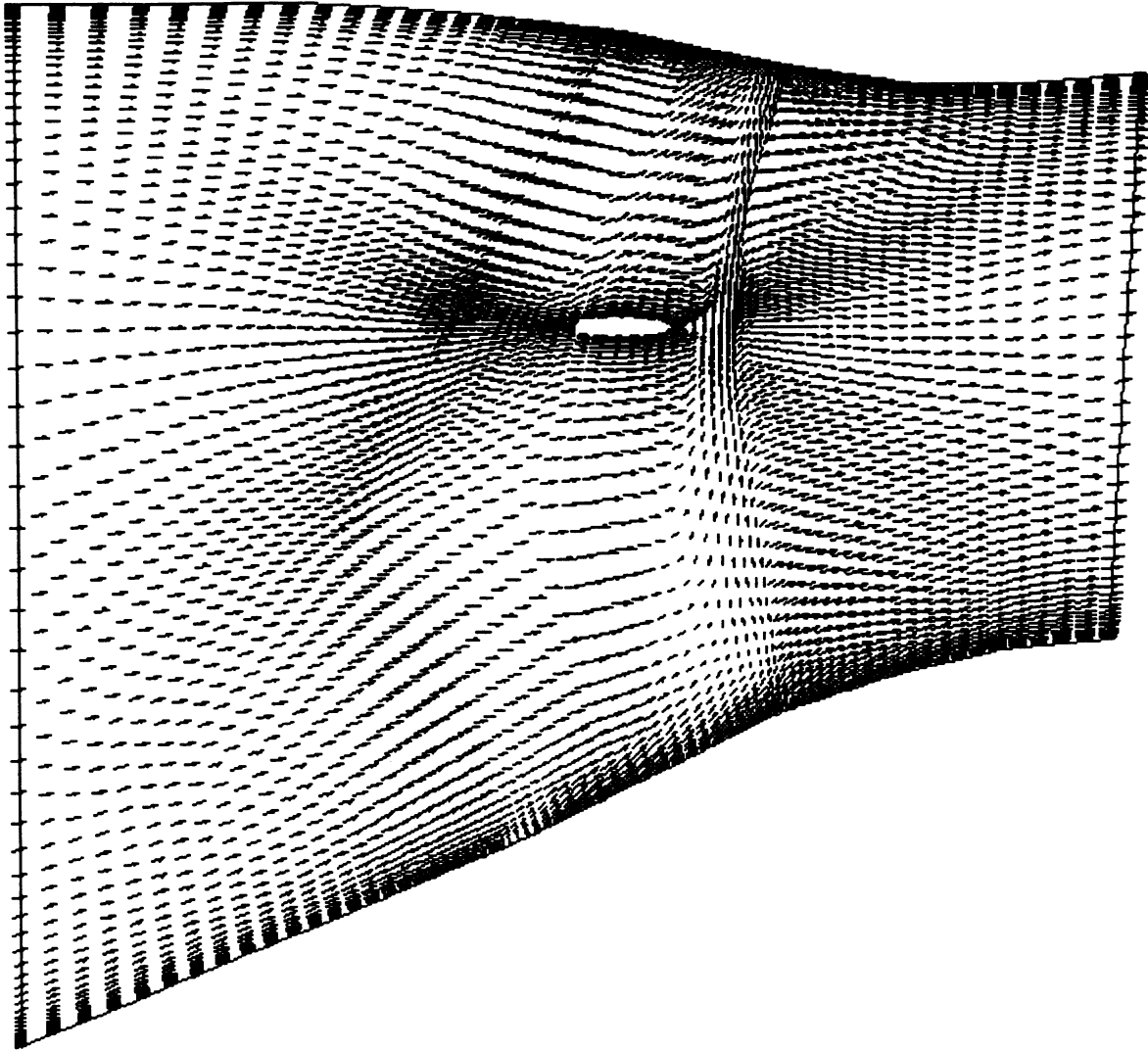
Figure 27.   No Separation Points Associated With Shocks Are Evident in the Entrance Region of the Passage at 100 Percent Speed.

In particular, the shock associated with the midspan damper leading edge was not considered to be of consequence, because the damper was positioned far enough back in the rotor passage that any leading-edge shock waves would be contained within the passage, and would not contribute any forward-radiated noise. This behavior has been confirmed through the Mach contour plots of Figures 22 through 25. Additionally, a weak leading edge shock was seen very near the rotor tip, but it does not appear to have significant strength to generate MPT noise.

(3) Possible radial diversion of streamlines, due to the presence of the midspan damper, which could have decreased the effective sweep angle on one side of the blade, producing local leading edge shocks.

30

The midspan damper itself does not appear to have much influence on deflection of streamlines near the leading edge; however, there is a very localized radial diversion of streamlines along most of the leading edge, which should have a favorable effect on the sweep angle. As shown in Figure 28, the streamlines are deflected radially outward in the outer span region and radially inward nearer the hub, which tends to reduce the velocity component normal to the leading edge.

(4) Adverse effect on sweep angle at some radii due to tapered rotor blade platform, which has its effective sweep angle at the quarter-chord line rather than at the leading edge.

There is no direct evidence that the effective sweep angle due to the tapered platform results in shock creation.
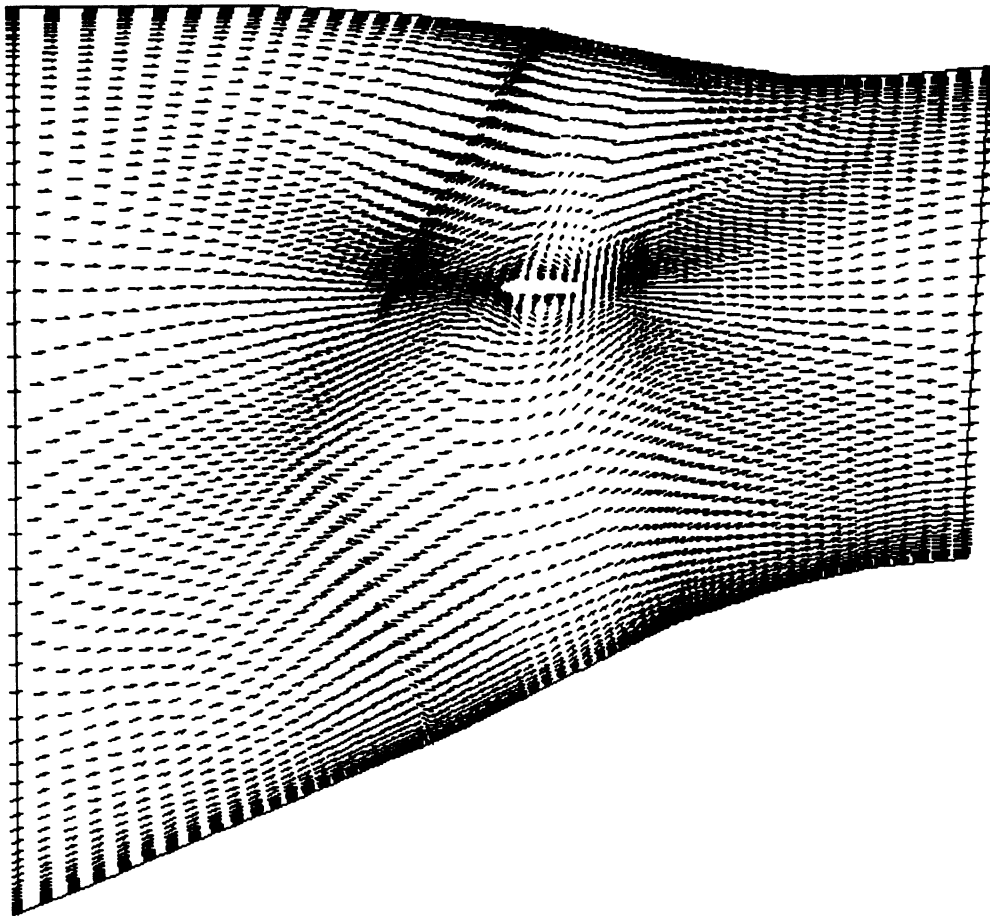
Figure 28. Radial Diversion of Streamlines Is Not Substantially Influenced by the Midspan Damper (100 Percent Speed).

(5) Decreased effectiveness of leading edge sweep. The swept-edge concept on an aircraft wing requires freedom for some spanwise adjustment of the streamlines. The fan rotor streamlines cannot adjust spanwise near the endwalls, and possibly near the damper.

Near the rotor tip, upstream of the leading edge, the streamlines follow the shroud, which tapers inward. Thus, in this localized region, the streamlines are directed more normally, relative to the leading edge sweep, as shown in Figure 29. It is in this region that evidence of a weak shock is seen. Thus, the shroud endwall contour may have some influence on the presence of MPT noise.

Consideration must also be given to the question of geometric consistency, relative to the actual tested blade geometry and the modeled geometry. The CMM data was used to model the rotor coordinates for the CFD flow simulation. However, more recent investigation has revealed that the original TL coordinates were different from the CMM data. Errors could be present in either set of coordinates. Differences in stagger angle and chord at the rotor tip could explain the presence of the MPT noise signature in the narrow-band test data, but not in the simulation produced with a blade having geometry corresponding to the CMM data. In addition, rotational deflections of the blade tip have not been modeled. The CMM-based geometry represents the undeflected blade shape. If, in fact, the blade deflections were substantial, the tested blade would have a different shape than that which was analyzed. Validity of the rotor geometry model is still not completely determined, and may be the cause of the discrepancy.
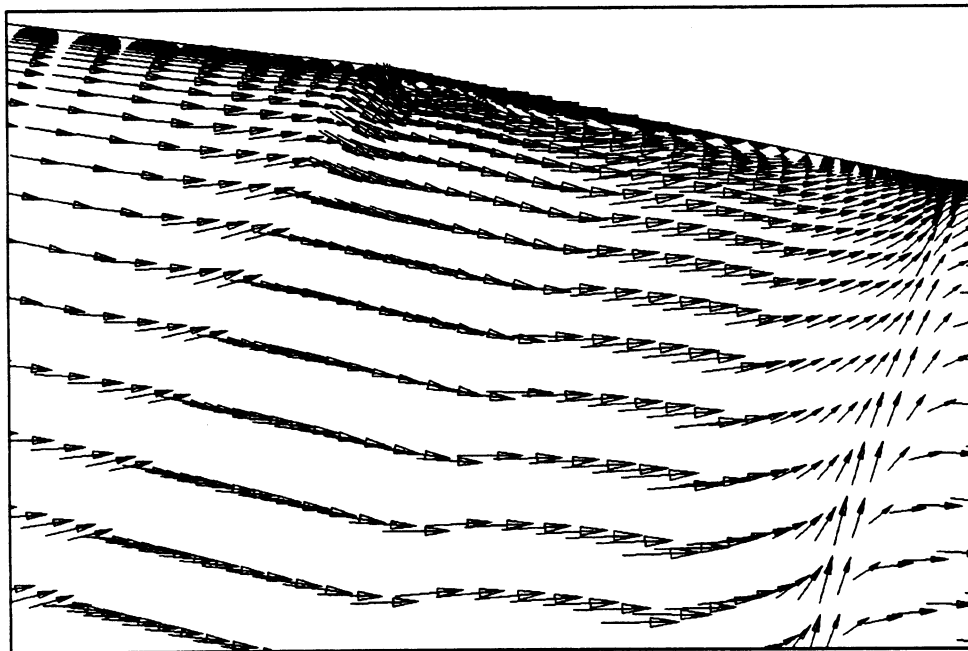
Figure 29.   The Inward-Tapering Shroud Directs the Flow More Normal to the Swept Leading Edge in the Near-Tip Region.

4.0 ACOUSTIC CODE CALIBRATION

4.1 V072 (BBN/PW) Turbofan Source Noise Prediction Code

The BBN/PW (Bolt, Beranek, & Newman/Pratt & Whitney) or V072 turbofan source noise prediction code was used to generate noise predictions for the TFE731-60 fan at three operating conditions and to create input files for use in the Acoustic Radiation Code (ARC) developed by Walter Eversman. Streamline data from the AE AXCAPS mean streamline analysis program was used to provide the necessary aerodynamic performance information needed for the V072 program.

The V072 code calculates the noise generated by the interaction of a rotor wake and stator vanes. Semi-empirical information concerning the wake characteristics is used in conjunction with aerodynamic performance data to predict the noise produced by such an interaction within an engine duct. The V072 code calculates the inlet and aft sound power levels for the blade pass tones and the higher harmonics, and also outputs the complex radial mode amplitudes of the propagating modes. These radial mode amplitudes are later used as inputs to the Eversman code to predict the radiation out of the engine nacelle. V072 provides several models to describe the rotor wake characteristics and can handle rotor wake/stator, fan wake/fan exit guide vane, and fan wake/core stator interactions. For the present case, the interaction between the 22-bladed fan and 52-bladed swept stator is examined using V072.

Software Installation - The V072 system code was compiled to run on a Hewlett-Packard (HP) Workstation using the IRIS Makefiles. A small modification to two of the Makefiles was necessary in order for the code to be compiled successfully. In addition, the code did not run to completion until a modification was made to subroutine SRCHV. Changes were also made to the output portion of the code so that the input files to the ARC were generated automatically. Once these modifications were made, the code ran to completion using the TEST 3 input data. The output was successfully compared to the results generated by Pratt & Whitney. Detailed information regarding V072 operation, capabilities, and input configuration is available in References 3 and 4.

Acoustic Predictions - Several AXCAPS runs were produced for the TFE731-60 at speed points where acoustic data is available. Figure 30 shows the fan geometry being used for the predictions. An input file for the speed points has been created by extracting the pertinent data from the AXCAPS runs. Geometry and performance along 24 streamlines is used. For the three speed points, the noise from the rotor wake/stator interaction was calculated using the default values for the V072 options. In particular, the loaded fan wake option was used along with the loaded rotor 67-wake profile.

Table 1 summarizes the V072 results for the 75.3 percent speed condition. The fundamental blade passage tone is near cutoff with a single radial mode, and a large number of radial modes exist for the twice blade passage frequency tone. The complex incident modal amplitudes are available for input into the Eversman code.

Figure 30. Rotor/Stator Geometry of the TFE731-60 Fan Used for the V072 Calculations.

Table 1. Sample Results of the V072 Code for the TFE731-60 Fan.

Scalar Geometry & Performance for the 75.3% Speed Case	
N1=8288 RPM	Uncorrected Rotor Speed
NBLADE=22	Number of Rotor Blades
NVANES=52	Number of Stator Vanes
DDUCT=30.698 in	Rotor Leading Edge Tip Diameter
MAS=0.481	Mass Averaged Axial Mach No. at the Stator Leading Edge
TS=535.90 R	Mass Averaged Static Temperature, Rotor Trailing Edge
RHOS=0.07850 lbm/ft^3	Mass Averaged Static Density, Rotor Trailing Edge

Inlet Noise Results for the Rotor/Stator Interaction at 75.3% Speed			
	Circumferential Mode Number	Radial Mode Number	Radial Mode Power Level (dB)
Blade passage frequency:	22	0	134.9
Twice blade passage	-8	0	104.3
		1	106.3
		2	104.0
		3	97.3
		4	103.6
		5	91.0
		6	105.8
		7	100.3
		8	102.7
		9	102.3
	44	0	106.4

<u>Acoustic test description</u> - Acoustic data are available for comparison with the V072 predictions. The AE acoustic test arena is located at the San Tan test site located southeast of Phoenix, Arizona. It is at an elevation of 1395 feet above sea level at the test stand and is a flat desert area free of any structures or other obstacles on the acoustic test arena. Since it is located at a remote site, the acoustic test arena has very low ambient noise levels.

The engine support structure for the acoustic test facility is of J-stand design to minimize the interference effects with both the acoustic propagation paths and the engine flowfield. A photograph of the stand is shown in Figure 31. The support for the stand is located on one side of the engine away from the microphone positions and is not in the direct propagation path. The support is also well out of the way of the engine inlet and exhaust to eliminate inflow distortion or exhaust impingement effects.
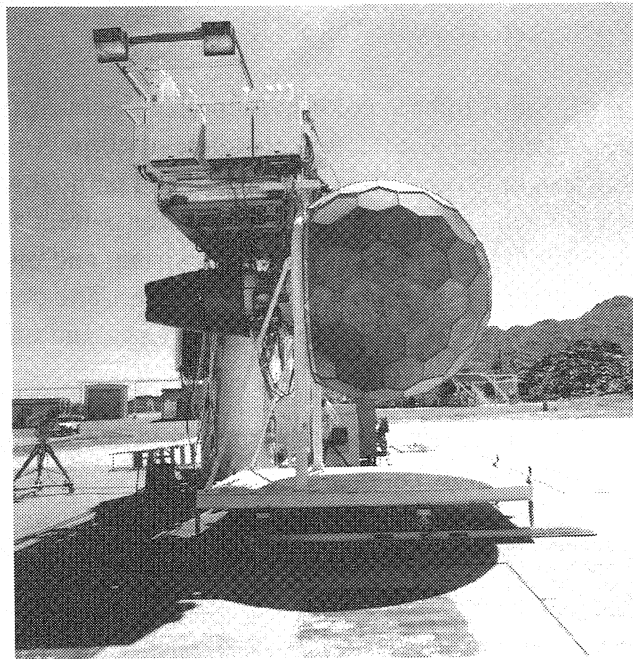
Figure 31. Photograph of an Engine at the San Tan Acoustic Test Facility Shows the Test Configuration.

The engine is mounted on the stand such that the engine centerline is 10 feet above the ground. At this engine centerline height and with the use of the Inflow Control Device (ICD), there are no inflow distortion or exhaust impingement effects caused by the ground.

The Acoustic Test Facility was designed to meet all of the standards of SAE ARP 1846 (Reference 5). A schematic diagram of the facility is presented in Figure 32. The acoustic arena extends from beneath the engine to a distance that is at least 3 meters beyond all microphones. The engine support structure sits on a 58 by 58 ft. concrete pad. The concrete is uniformly
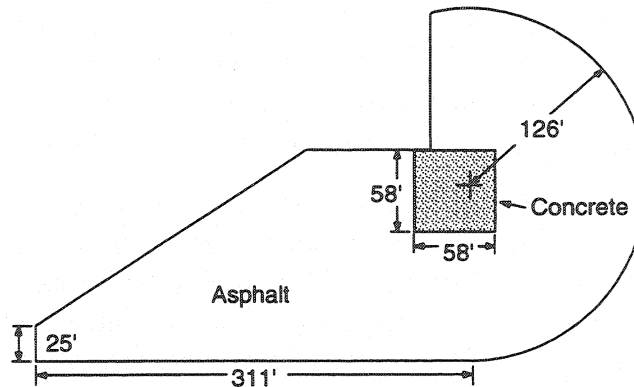
Figure 32. Layout of San Tan Acoustic Test Facility Shows Suitability for 100 ft. Polar Arc Acoustic Data.

smooth and hard, troweled level, and is light in color to minimize thermal gradients. The pad is surrounded by asphalt sloping downward at a 0.5 percent slope to allow for proper drainage. The asphalt is hard packed and uniform in texture. It is well sealed and painted white to minimize thermal gradients. Thus, the entire acoustic arena surface is a near perfect sound reflector with no structures or natural obstacles. The engine fuel lines, control wiring, and microphone cables are run through underground conduits to prevent acoustic interference. The control room is located outside of the test arena at a distance of over 200 feet from the test stand on the opposite side from the microphones.

Results - Total acoustic power comparisons with the measured engine data show a general trend towards underprediction as shown in Table 2.

Table 2. Comparison of Total Measured and Predicted Acoustic Power for the TFE731-60 Engine.

75.3% Speed	Inlet PWL			Exit PWL		
	1*BPF	2*BPF	3*BPF	1*BPF	2*BPF	3*BPF
Predicted	146.7	133.9	116.5	151.2	135.7	124.0
Measured	117.8	112.3	102.0	117.7	112.2	104.3
81.1% Speed	Inlet PWL			Exit PWL		
	1*BPF	2*BPF	3*BPF	1*BPF	2*BPF	3*BPF
Predicted	133.8	131.8	123.0	147.6	137.0	127.0
Measured	125.2	115.2	104.4	123.8	114.9	107.1
86.5% Speed	Inlet PWL			Exit PWL		
	1*BPF	2*BPF	3*BPF	1*BPF	2*BPF	3*BPF
Predicted	137.1	129.7	120.2	148.6	136.7	127.3
Measured	119.2	106.2	95.8	119.8	107.0	100.1

4.2 Acoustic Radiation (Eversman) Code

The Acoustic Radiation Code (ARC) was used to generate noise radiation results for the TFE731-60 nacelle at three speed points for the blade passage tone. Also, results for two circumferential modes at twice the blade passage frequency were generated at the 75.3 percent speed point. The complex modal amplitudes for the various modes were generated using the V072 program. A detailed description of the ARC is presented in References 6 and 7.

Software Installation - The Eversman radiation code consists of five FORTRAN modules: a spline interpolation program, a mesh/duct eigenvalue generator, a potential flow solver, a mean flow superposition program, and an acoustic radiation program. The code received by AE was designed to run on Sun and Silicon Graphics Iris workstations. A test case was included with the code to verify program implementation. Considerable difficulty was encountered in getting this code to run properly on HP workstations. Certain compiler options were required in order for the code to run to completion. Eventually the test case was run through all modules successfully.

However, more difficulty was encountered when other meshes (which were dimensioned well within the size constraints) were introduced. After some investigation, we found that the code was very sensitive not only to which compiler options were used but also to the type of machine it was compiled on (i.e., a HP 735 with UNIX version A.09.05 versus a HP 770 with UNIX version B.10.01). For example, in one of the output files (FTN20) generated by the mesh program, a portion of the output describing the nodal connectivity was not always properly generated, even though an internal connectivity check reported no errors. In these cases the radiation portion of the code would not run successfully, and usually no output was generated. (This same difficulty was encountered by Paul Bent running the code on an HP platform- see Reference 8). The source of these peculiar errors is not known, but it may be a result of inconsistent data typing that was leftover from the original IBM mainframe version of the code.

An updated version of the ARC, which uses an in-core matrix inverter, was also obtained by AE. This version consists of four FORTRAN modules similar to the above modules but with the flow and radiation programs linked with LAPACK subroutines. The first module (PRATPREH) of the original code is used along with these to generate the interpolated nacelle geometry. This revised code was compiled on an HP 770 running UNIX version B.10.01. Certain compiler options (most importantly the static memory allocation option -K) were necessary for the radiation code to run successfully. Fortunately, the mesh sensitivity problems displayed by the original version were not encountered with this version. In general, the code works very well. One difficulty that has been encountered is the inability to put more than 20 nodes on the fan face (the code appears to be dimensioned for 30) or more than 40 nodes on the upper surface of the nacelle (the code appears to be dimensioned for 100). Because of this problem it was sometimes difficult to satisfy the 4 to 5 nodes per wavelength criterion, and so the higher blade passage results might not be very accurate. This updated version of the code was used to generate the results in this report.

Computational Grid - A finite-element mesh for the TFE731-60 nacelle was created with the ARC. The nacelle geometry was taken from a combination of data describing the nacelle surfaces

and AXCAPS flowpath output. The coordinate information was fed into the PRATPREH and INLMESH modules to generate the mesh. The ARC mesh generation routines provide for quite a bit of freedom in tailoring various aspects of the mesh. In particular, one can vary the:

- Number and location of elements on the upper nacelle surface
- Number and location of elements on the lower nacelle surface
- Number and location of elements on the fan face
- Number of radial elements in the exterior finite element domain
- Number and location of wave envelope layers
- Origin of the coordinate mesh
- Location of the baffle
- Radial extent of the exterior finite element domain
- Radial extent of the wave envelope domain

The quality of the results obtained from the radiation module depends in part on the selection of the above parameters. The supporting documentation for the ARC provides recommendations in determining some of the parameters. Because the position of the mesh elements are determined by percentages, the mesh generation process is usually an iterative one -- creating a mesh, viewing the POSTSCRIPT output to see how to adjust the mesh spacing, and regenerating the mesh.

The main limitation encountered in using the code was the constraint on the number of grid points along various surfaces. Even though the "5000 elements or less" and the "21000 nodes or less" constraints were satisfied, the maximum number of elements that were successfully used on the upper surface and on the fan face were 40 and 20 respectively. Exceeding this caused problems in the radiation portion of the code.

Figures 33 through 35 show the mesh geometry, which consists of 4820 elements and 14,823 nodes, used for the fundamental blade passage tone (circumferential mode number m=22, radial mode number n=0). This mesh provides 4 to 5 nodes per wavelength in the interior and exterior finite-element domain in the main direction of propagation. The duct extends back to the leading edge of the stator, where the complex modal amplitudes are input.

The TFE731-60 nacelle has a hard-walled inlet 30.7 inches in diameter at the fan leading edge. No axial mean flow is modeled outside the nacelle, corresponding to a static engine test condition. The ambient sound speed and air density are 1117 ft/sec and 0.00238 slugs/ft^3 respectively. The fan face Mach numbers used in the 75.3, 81.1, and 86.5 percent speed cases are 0.414, 0.4634, and 0.5175 respectively. The potential flow solution output and the mean flow superposition output are shown in Figures 36 and 37 for the 75.3 percent case.

Acoustic Results - Figures 38 through 40 show the predicted radiation results for the 75.3 percent case. Note that the Eversman code solves for each circumferential mode individually (for any number of radial modes), so the code must be rerun for each desired mode. The results of the m=22 blade passage tone are presented. Figure 40 also shows the comparison with the measured TFE731-60 data. It is clear that the engine has additional lower order modes that result in noise radiation at smaller directivity angles.
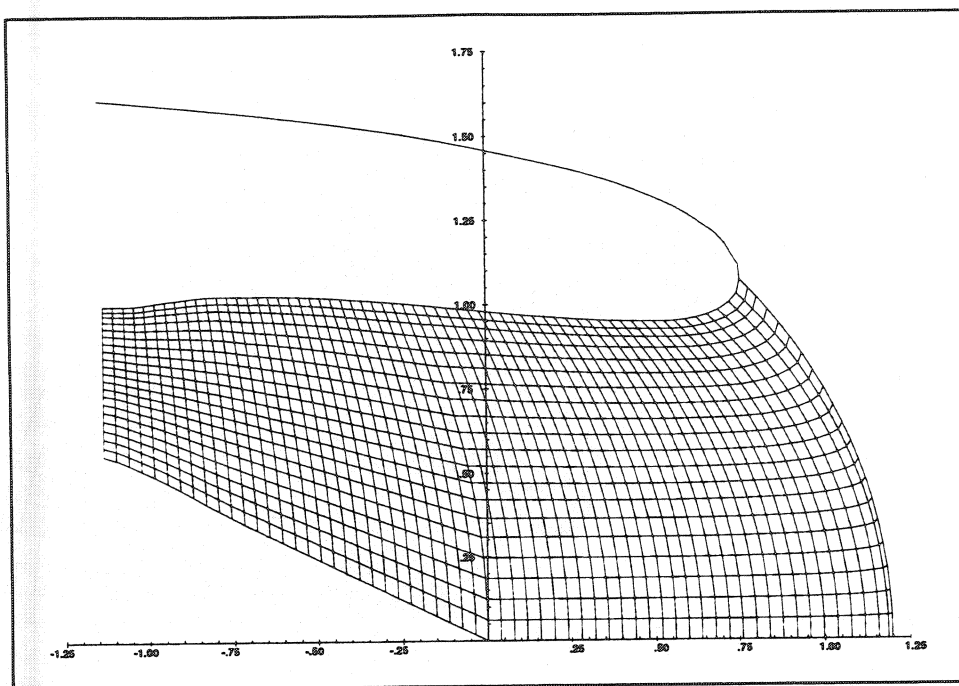
Figure 33.   Finite-Element Mesh Inside the Nacelle (Region 1) for the TFE731-60 Inlet.
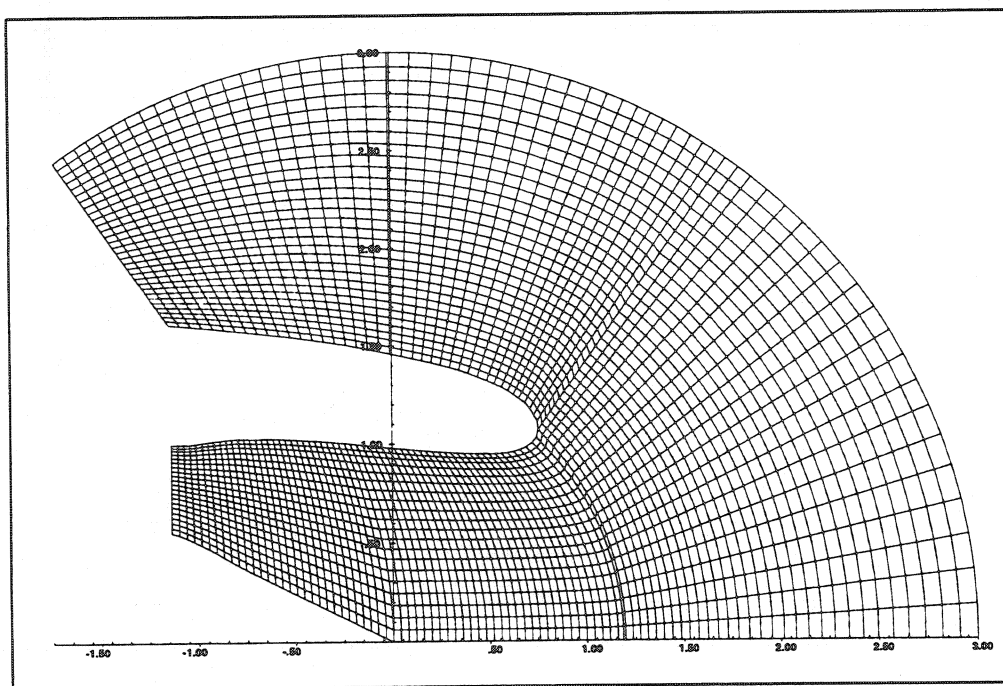
Figure 34.   Finite-Element Mesh Inside (Region 1) and Outside (Region 2) the Nacelle for the TFE731-60 Inlet.

39
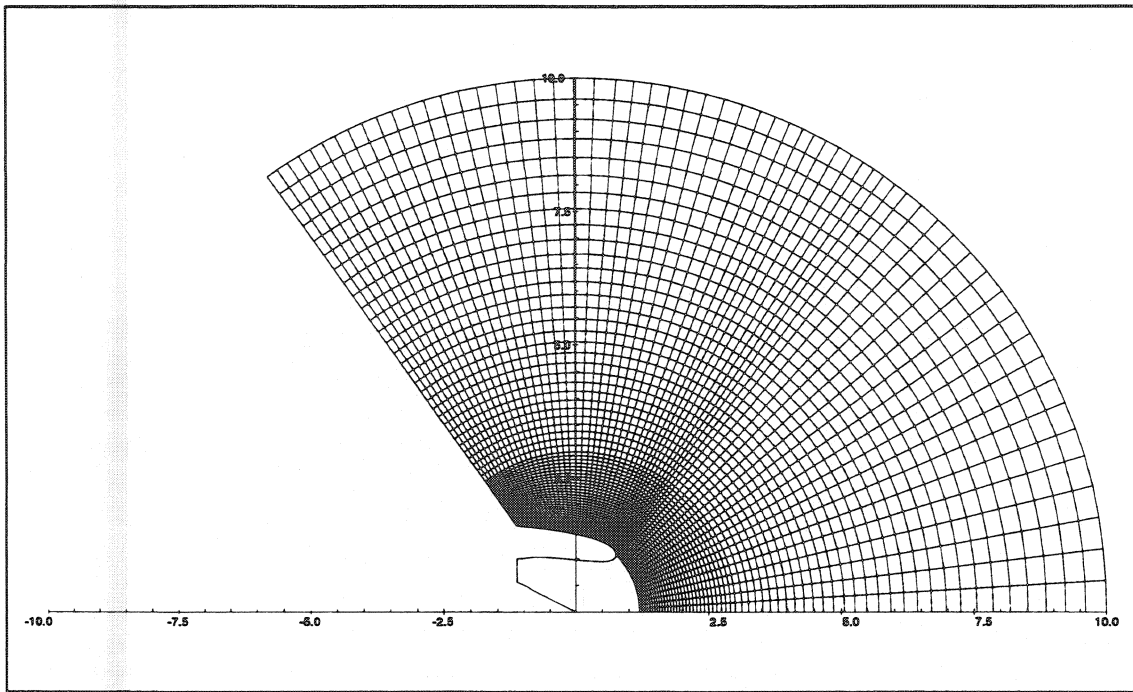
Figure 35. Exterior Finite-Element Mesh (Region 2) and Wave Envelope Layers (Region 3) for the TFE731-60 Inlet.
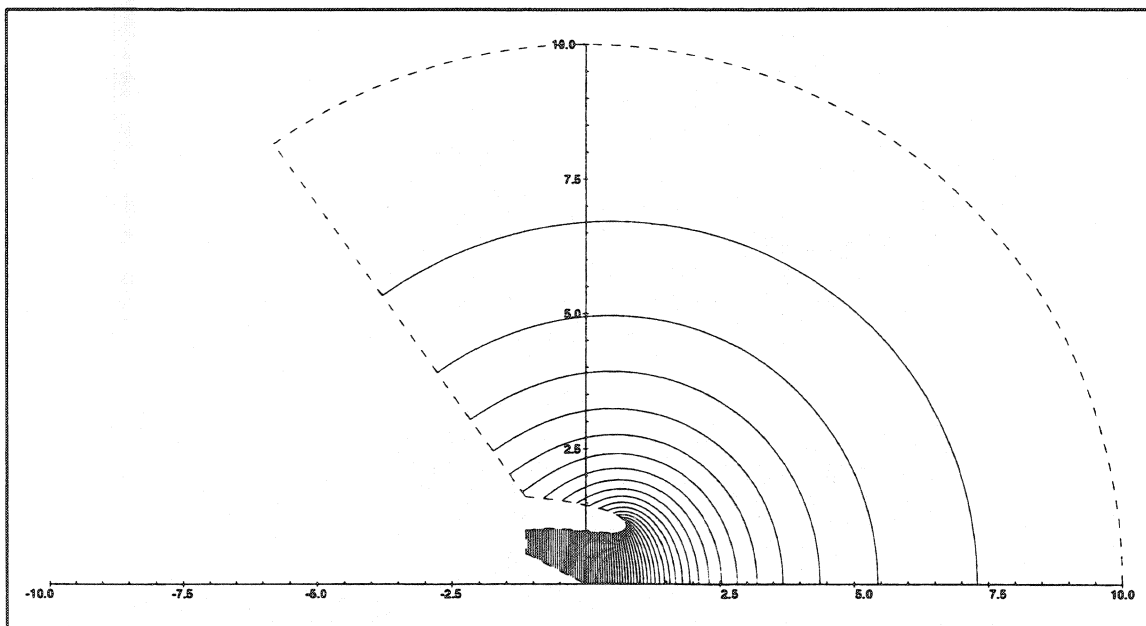
Figure 36. Contours of Constant Velocity Potential for the TFE731-60 Inlet at 75.3 Percent Speed.
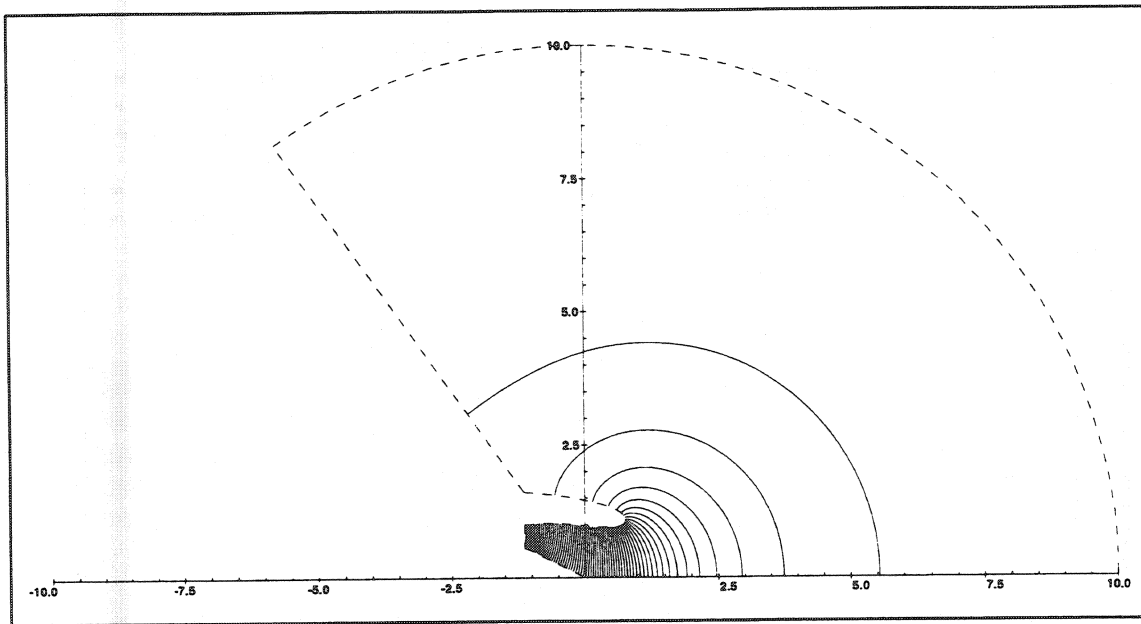
Figure 37. Contours of Constant Superimposed Velocity Potential for the TFE731-60 Inlet at 75.3 Percent Speed.

Figure 38. Acoustic Potential Plot for the M=22 Mode for the TFE731-60 Inlet at 75.3 Percent Speed (Dimensions Normalized by Inlet Radius, A).

41
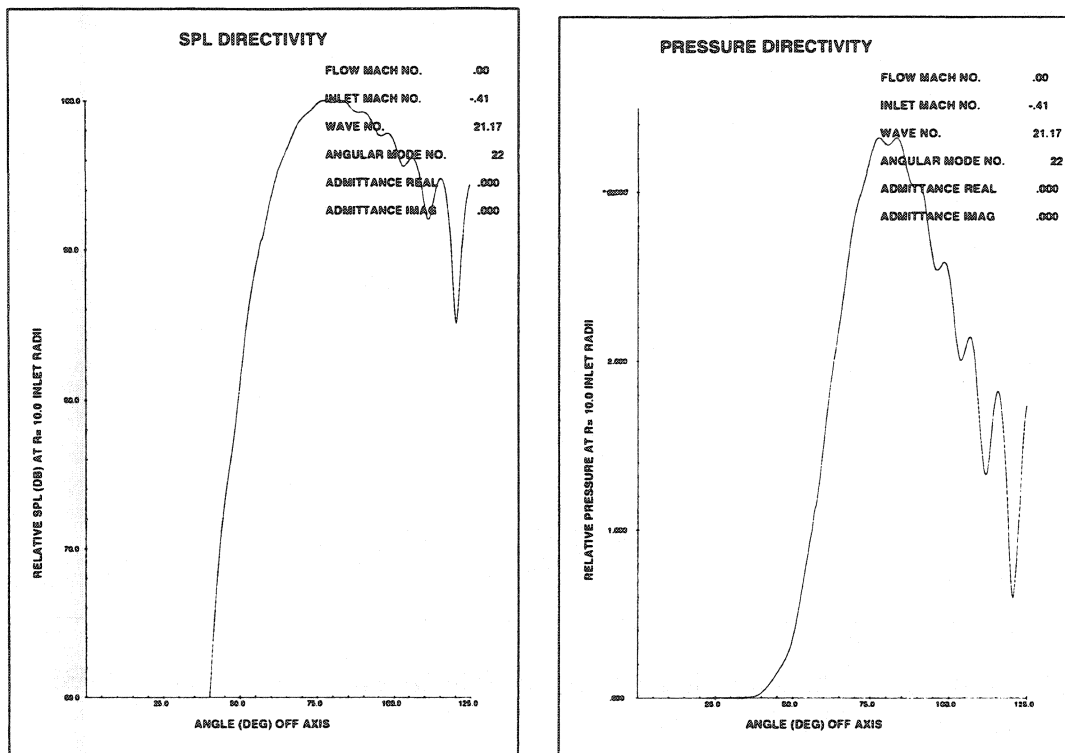
Figure 39. Sound Pressure Level and Pressure Directivities for the M=22 Mode for the TFE731-60 Inlet at 75.3 Percent Speed.
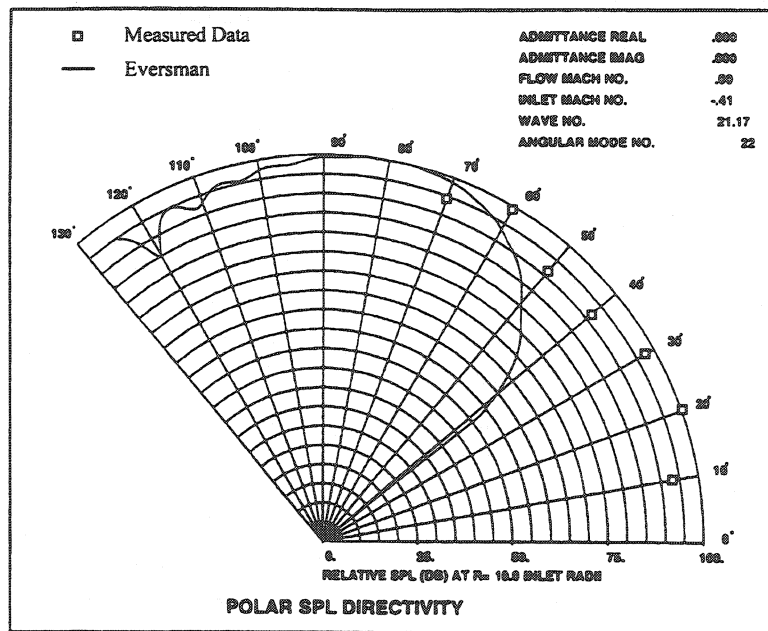
Figure 40. Polar Sound Pressure Level Directivity for the M=22 Mode for the TFE731-60 Inlet at 75.3 Percent Speed.

For the higher speed points, the mesh for the 75.3 percent speed case was used in the blade passage tone noise predictions. Note that for a given mesh, the number of nodes per wavelength decreases as the velocity at the fan face increases. In the present case, the mesh already has 4820 nodes (close to the 5000 maximum), so it was decided to leave the mesh unchanged, even though the number of nodes per wavelength dropped below four. However, it appears that the results are still quite good. Figures 41 and 42 show the polar sound pressure level and acoustic pressure at 81.1 percent speed for the (22,0) mode. Figures 43 and 44 display the results at 86.5 percent speed. Note that as the fan speed increases, the angle of peak radiation decreases as expected. The comparisons with the measured TFE731-60 results show similar trends as the 75.3 percent case.

For the higher harmonics, a finer mesh is necessary to resolve the wave features. The mesh used for twice blade passage frequency was refined, but because of the matrix size limitations within the code, the desired 5 nodes per wavelength could not be achieved (only about three nodes per wavelength were achieved in the interior). The mesh was refined somewhat in the interior and exterior finite-element domains (the number of wave envelope layers was reduced), and contains 4920 elements and 15153 nodes. The radiation portion of the code used about 190 Mb of RAM, just shy of the 200 Mb RAM computer capacity. Figures 45 to 47 show the mesh used in these higher harmonic cases. Figures 48 and 49 show the polar sound pressure level and the acoustic pressure plots for the m=44 circumferential mode, with only the n=0 radial mode contributing. Figure 50 shows the sound pressure level directivity for the m=-8 mode . There are ten radial modes contributing to the m=-8 mode. Curiously, the angular mode number is labeled as -7 in the plot, although the text output of the radiation code appears to handle it properly as the m=-8 mode. Also, the multi-lobed feature of the plot is characteristic of the ARC when more than one radial mode is contributing (see reference 8).

Figure 41. Polar Sound Pressure Level Directivity for the M=22 Mode for the TFE731-60 Inlet at 81.1 Percent Speed.
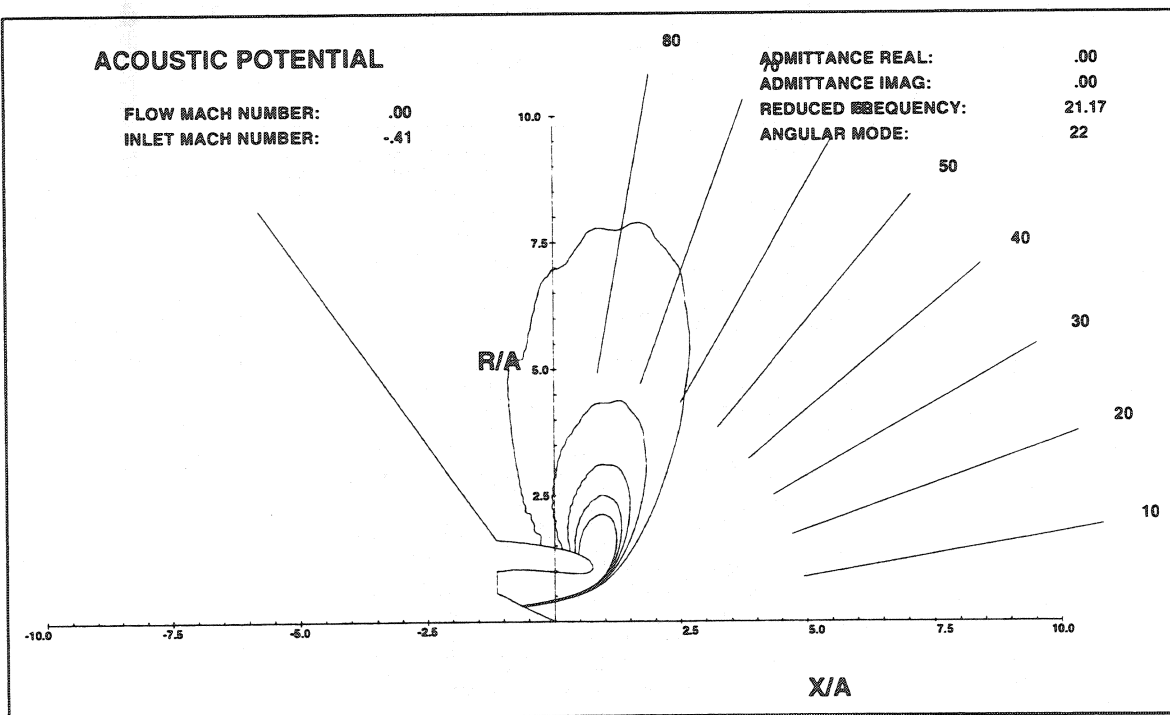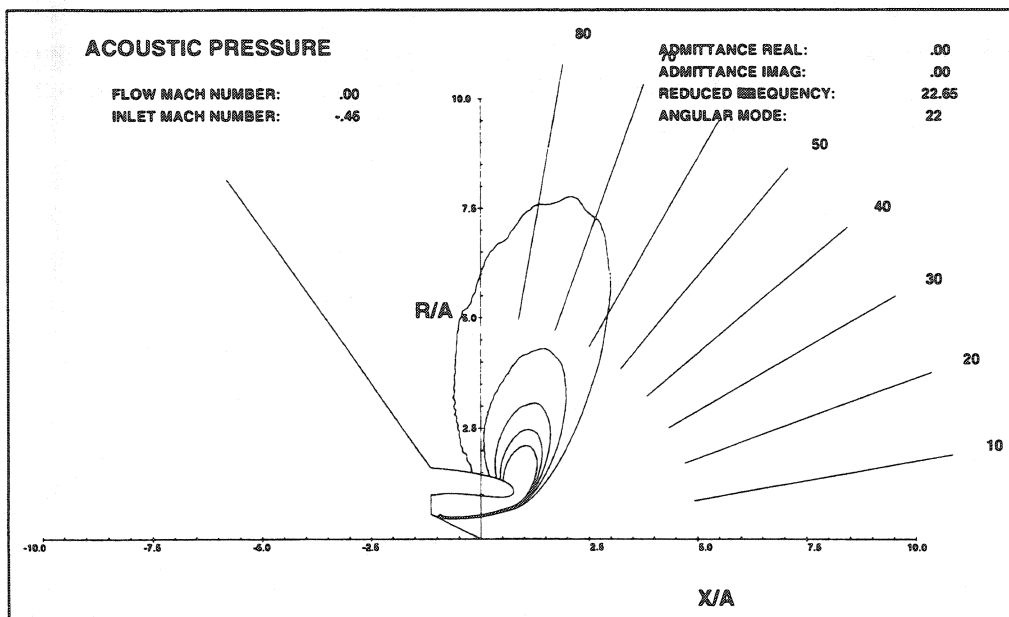

Figure 42. Acoustic Pressure for the M=22 Mode for the TFE731-60 Inlet at 81.1 Percent Speed (Dimensions Normalized by Inlet Radius, A).

44
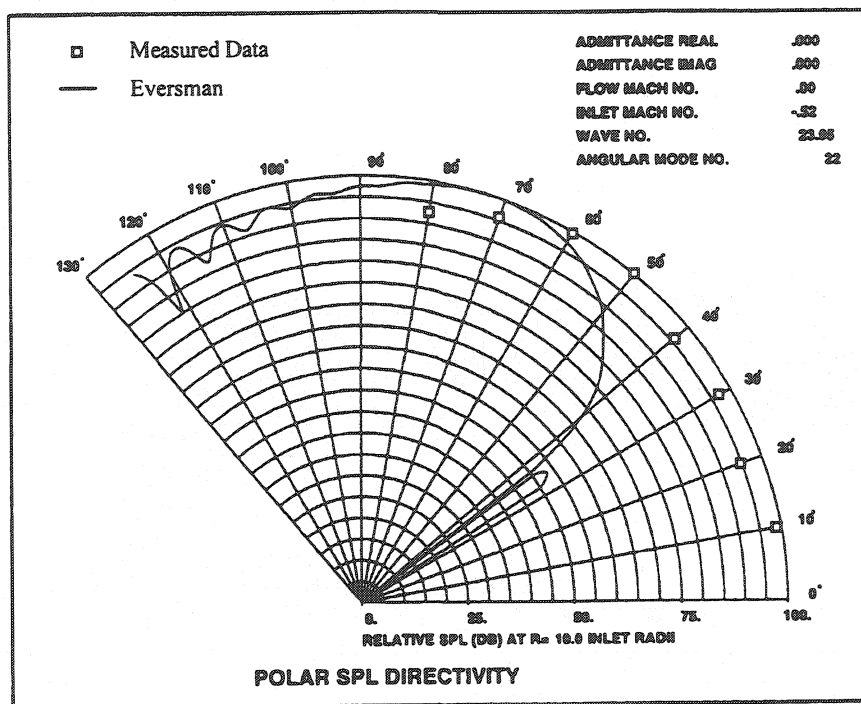
Figure 43. Polar Sound Pressure Level Directivity for the M=22 Mode for the TFE731-60 Inlet at 86.5 Percent Speed.
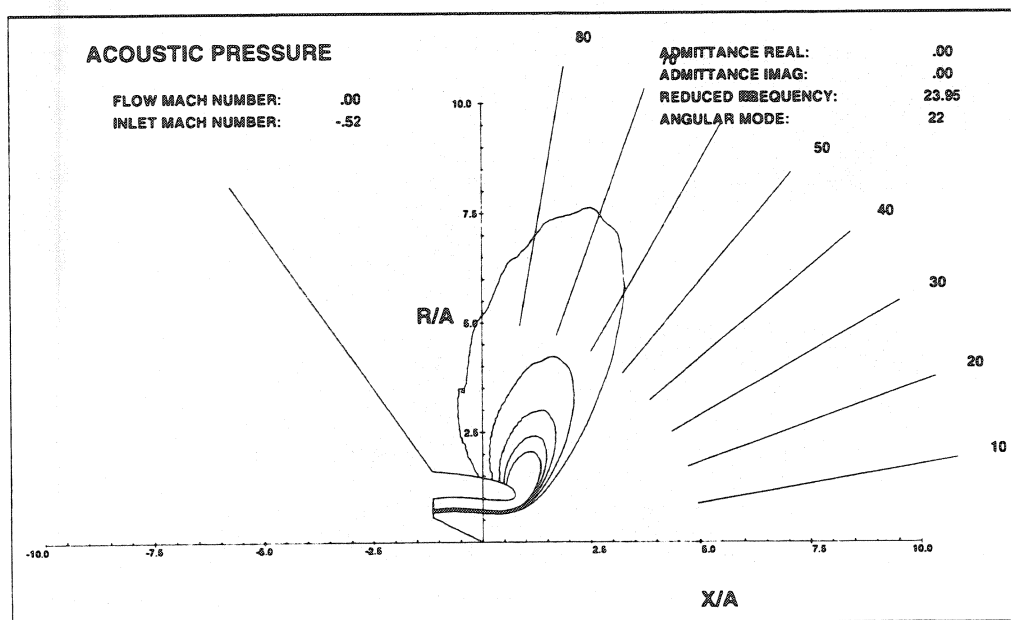
Figure 44. Acoustic Pressure for the M=22 Mode for the TFE731-60 Inlet at 86.5 Percent Speed (Dimensions Normalized by Inlet Radius, A).
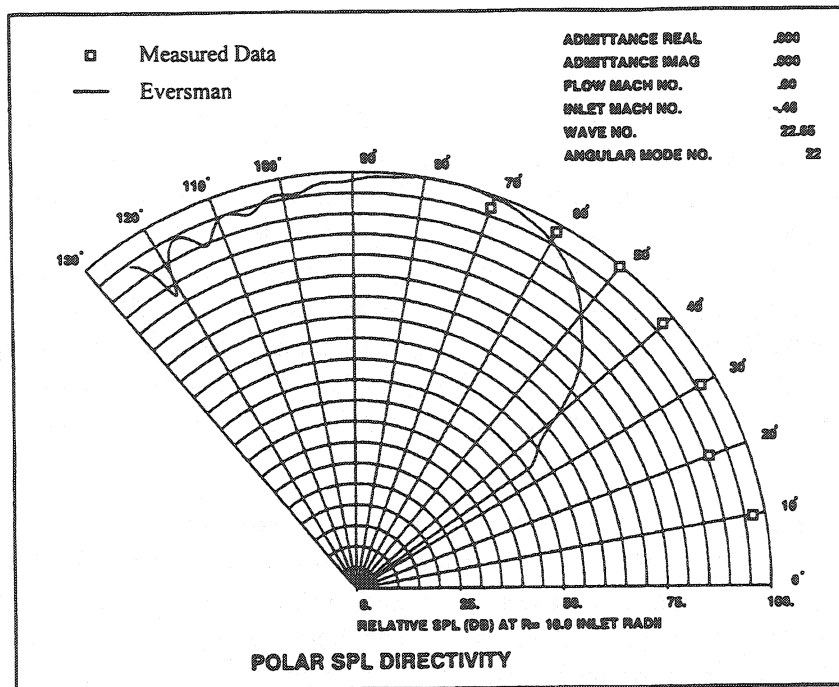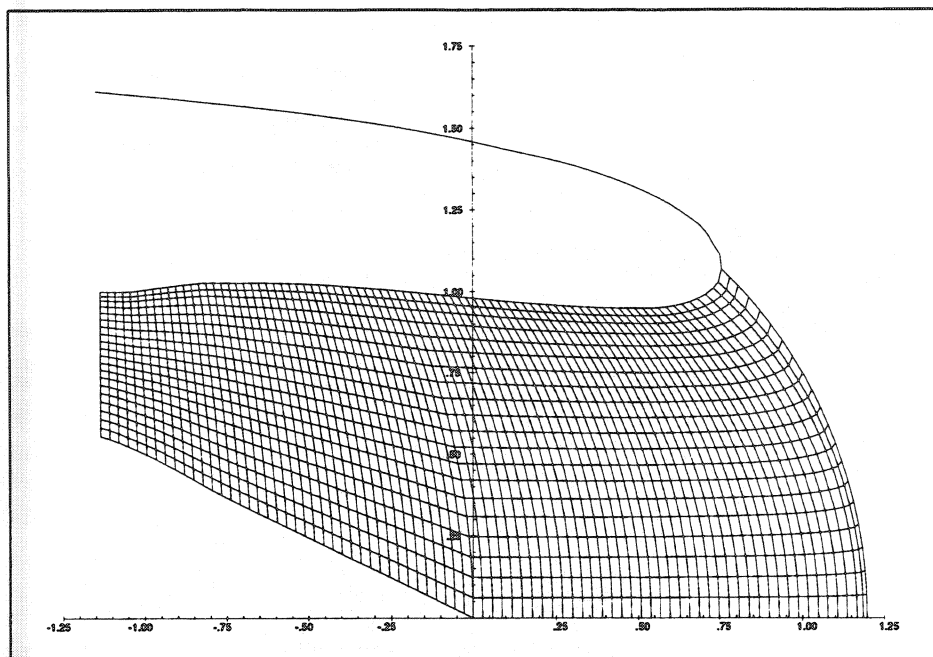
Figure 45.   Finite-Element Mesh Inside the Nacelle (Region 1) for the Higher
             Harmonics for the TFE731-60 Inlet.
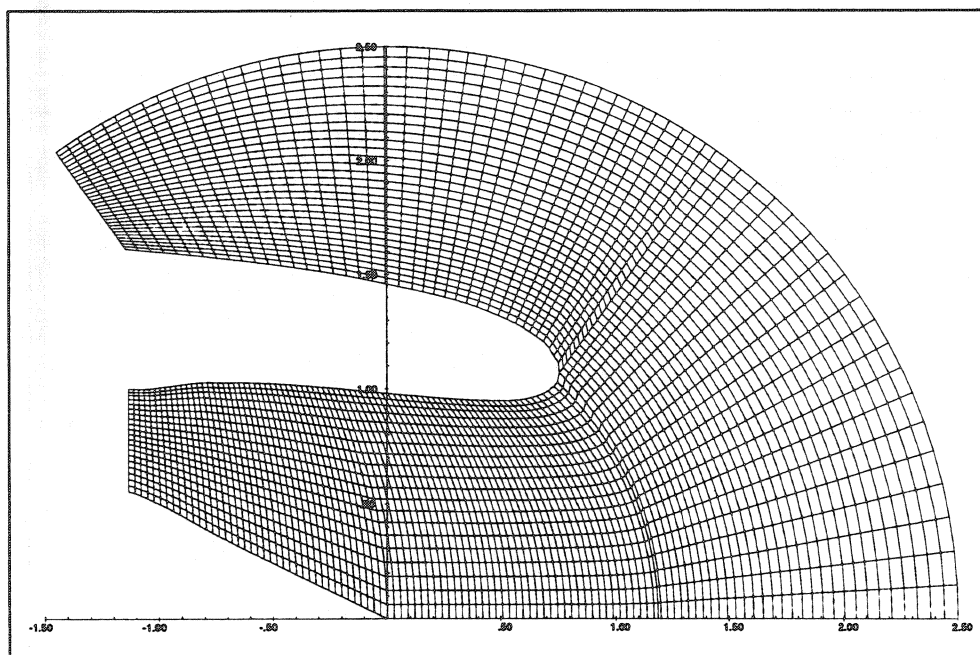
Figure 46.   Finite-Element Mesh Inside (Region 1) and Outside (Region 2) the Nacelle
             for the Higher Harmonics for the TFE731-60 Inlet.

46
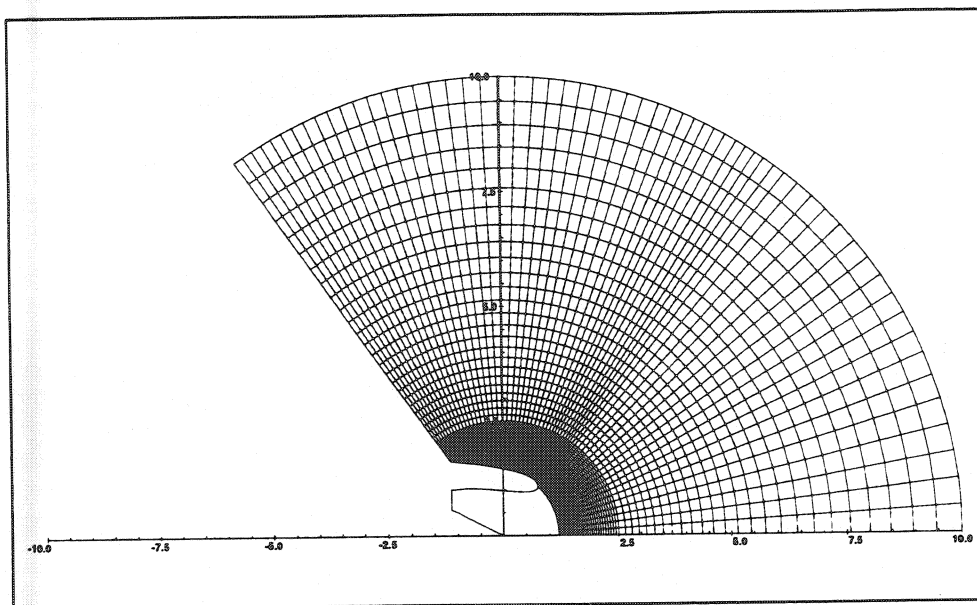
Figure 47. Exterior Finite-Element Mesh (Region 2) and Wave Envelope Layers (Region 3) for the Higher Harmonics for the TFE731-60 Inlet.
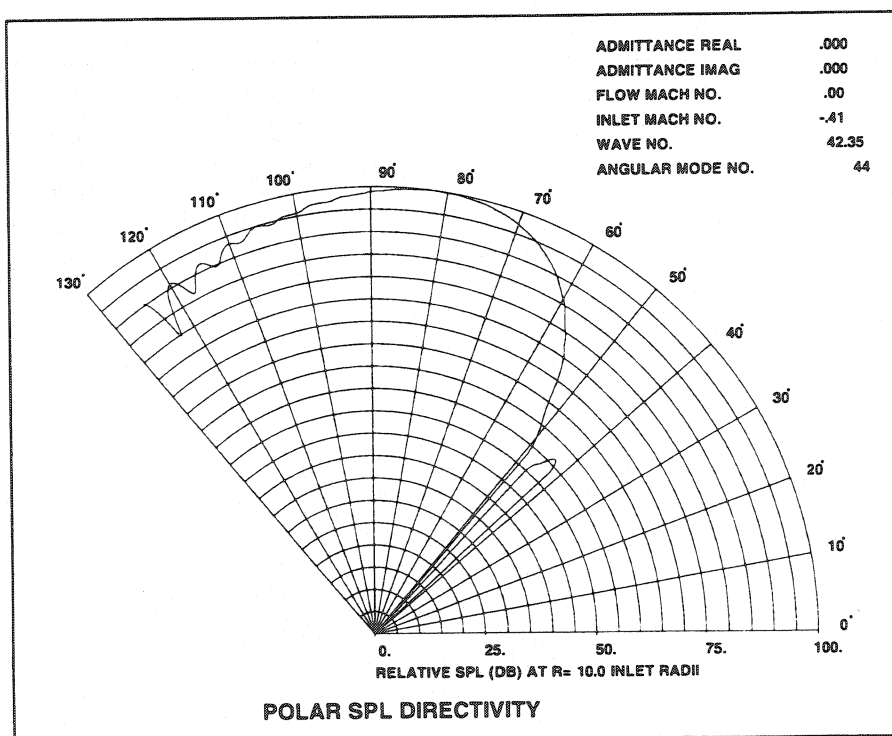
Figure 48. Polar Sound Pressure Level Directivity for the M=44 Mode for Twice Blade Passage Frequency for the TFE731-60 Inlet at 75.3 Percent Speed.

47

ACOUSTIC PRESSURE

| FLOW MACH NUMBER: | .00 |
| INLET MACH NUMBER: | -.41 |

ADMITTANCE REAL:	.00
ADMITTANCE IMAG:	.00
REDUCED FREQUENCY:	42.35
ANGULAR MODE:	44
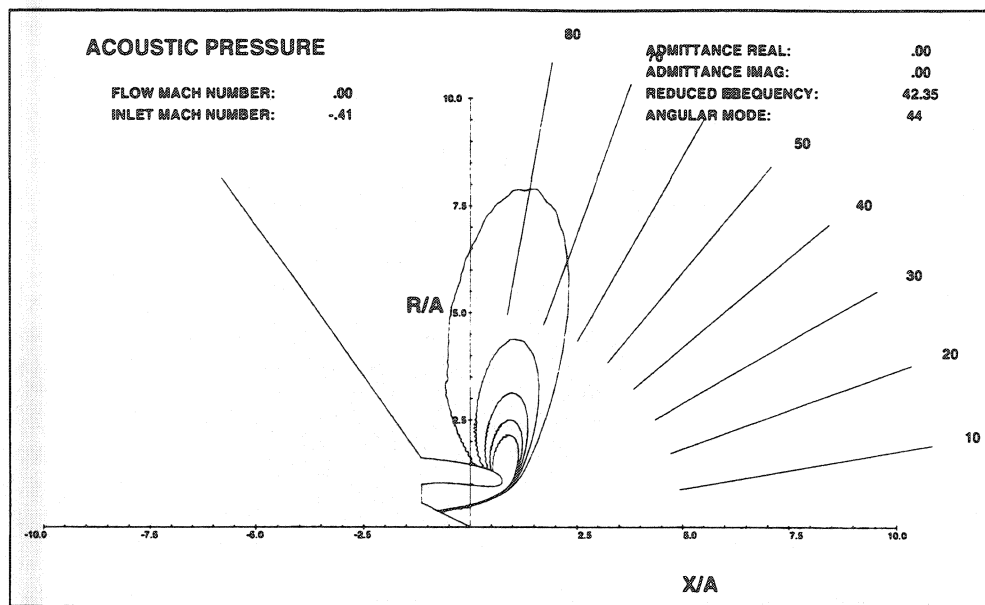
Figure 49. Acoustic Pressure Directivity for the M=44 Mode for Twice Blade Passage Frequency for the TFE731-60 Inlet at 75.3 Percent Speed (Dimensions Normalized by Inlet Radius, A).

ADMITTANCE REAL	.000
ADMITTANCE IMAG	.000
FLOW MACH NO.	.00
INLET MACH NO.	-.41
WAVE NO.	42.35
ANGULAR MODE NO.	-7

RELATIVE SPL (DB) AT R= 10.0 INLET RADII

POLAR SPL DIRECTIVITY
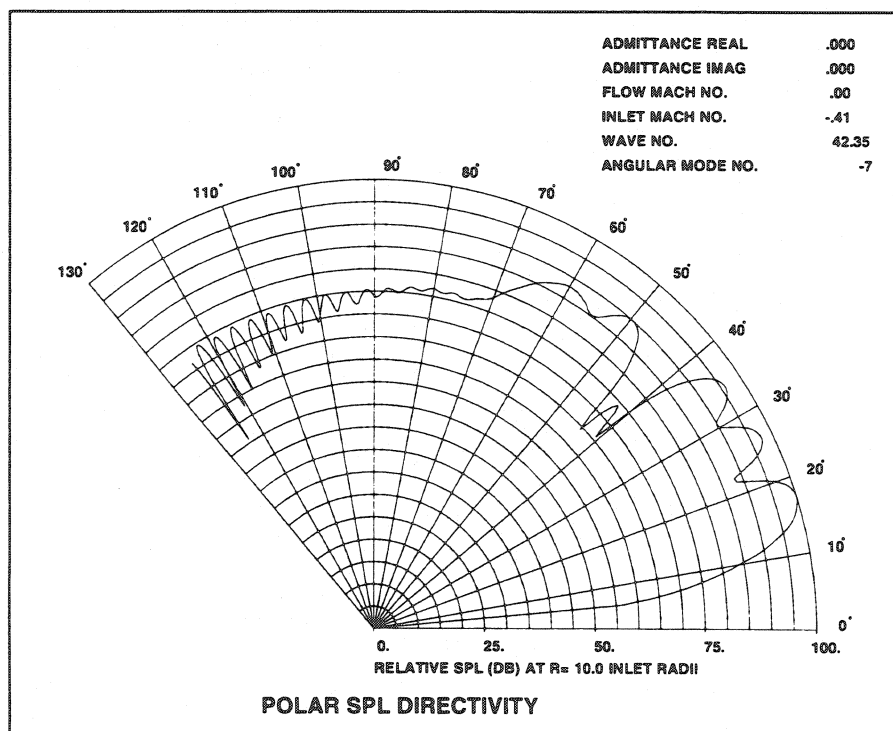
Figure 50. Polar Sound Pressure Level Directivity for the M=-8 Mode for Twice Blade Passage Frequency for the TFE731-60 Inlet at 75.3 Percent.

5.0 ROTOR INLET SHOCK PREDICTIONS

5.1 Approach

The objective of this effort was to perform a full 3-D viscous flow simulation of the current production TFE731-60 fan rotor, using the DAWES flow analysis program. The DAWES analyses would be used to estimate the onset of MPT noise, based on predictions of inlet shock position as a function of the rotor tip speed. The results of this study would also serve as a baseline for the evaluation of advanced rotor design concepts, which include noise minimization design features.

Inlet shock location was qualitatively determined from a DAWES analysis by producing contour plots of relative Mach number on blade-to-blade surfaces. By analyzing the flow at a range of rotor tip speeds, it was possible to graphically determine at what speed the inlet shock forms upstream of the rotor passage, signifying the onset of MPT noise. These predictions were then compared with acoustic measurements to determine the validity of the prediction method.

5.2 TFE731-60 Fan Rotor Geometry

The fan rotor used in this study is the production rotor of the AE TFE731-60 engine, and represents current fan technology for 5000-pound thrust-class engines. The rotor, shown in Figure 51, has wide-chord, moderately swept blades, and produces measurable MPT noise in the range of approximately 70 to 100 percent fan design speed. All CFD analyses for this rotor were performed at engine scale.
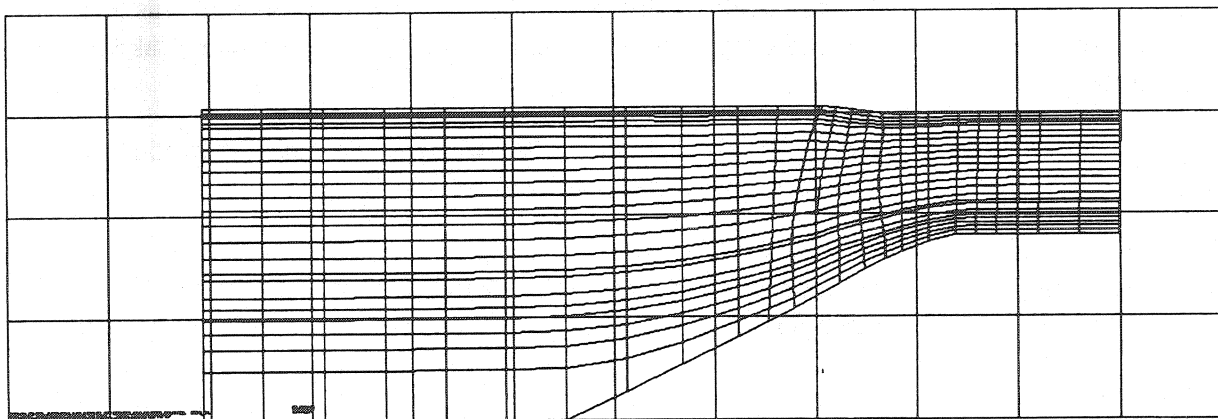
Figure 51. The AXCAPS Program Provides the Blade and Flowpath Definitions for the TFE731-60 Fan Rotor Geometry.

5.3 TFE731-60 Rotor Flow Analysis

DAWES Flow Analysis Program - The DAWES program is a finite-volume time-marching solver for the 3-D thin-layer Navier-Stokes equations. The version of the program used by AE utilizes the full energy equation (including the dissipation terms), and has a recently installed correction of the viscous stress tensor formulation for the momentum equations. Two turbulence models are available in the program, a Baldwin-Lomax model and a one-equation k-l model. All rotor analyses performed for this study employed the Baldwin-Lomax model, which was found to be preferable for rotor analyses based on our previous fan calibration experience.

The DAWES program currently serves as a standard design tool for all turbomachinery components at AE. Considerable experience with the program has been gained during its use over the last 6 years.

Geometry Model - The blade and flowpath geometry descriptions for the TFE731-60 fan rotor were obtained from AE's axisymmetric streamline curvature program, AXCAPS. This program provides a discrete-point definition of the blade geometry along specified stream surfaces intersected with the blade surface. Endwall definition is also provided in terms of radial and axial coordinates at discrete points. The AXCAPS model of the flowpath is shown in Figure 51.

The geometry represented in the AXCAPS model was the deflected aerodynamic blade shape at 100 percent wheel speed. Hub fillets were not modeled. The blade tip was modeled as tapered, rather than squared-off, which is required by a gridding limitation within the DAWES program.

Computational Grid - The computational domain consisted of a single rotor blade passage, with the suction surface of one blade forming one pitchwise boundary, and the pressure surface of the adjacent blade forming the other pitchwise boundary. The inlet to the computational domain was positioned approximately 1.40 axial chord lengths upstream to avoid impacting the development of the upstream shock structure. The exit of the computational domain was located far enough downstream to include the stator leading edge, for purposes of the Rotor Wake/Stator Interaction study.

The computational grid for the DAWES program is a structured single-block skewed H-grid. The grid size employed for the final set of rotor analyses was specified as:

Pitchwise:	41 Nodes
Spanwise:	81 Nodes (with 8 cells in the clearance gap)
Streamwise:	145 Nodes

The total grid size was 481,545 nodes. The eight cells within the tip clearance gap were equally spaced. Grid spacing was nonlinearly expanded from the remaining walls using a hyperbolic tangent-based algorithm, with the grid node closest to the blade surface located at approximately 0.15 percent pitch away from the surface.

50

Typical sections of the computational grid are presented in Figure 52. A detail of the tip clearance region, illustrating the tapered blade tip, is shown in Figure 53.

Boundary Conditions - Boundary conditions for the DAWES computational domain consist of wall, periodic, and inlet/exit conditions. The wall conditions are equivalent to a no-slip condition on all solid walls, with a fully-rotating hub. Because the solution is performed in the relative frame of reference, the shroud endwall is modeled as rotating opposite in direction to the rotor.

Periodic boundaries are defined upstream and downstream of the rotor suction and pressure surfaces and also in the tip clearance region. Inlet conditions are based on the AXCAPS rotor solution, with radial distributions of total pressure, total temperature, and tangential velocity being specified. Wall boundary layers were not modeled at the upstream inflow position. At the exit, static pressure on the shroud is held fixed to establish the mass flow. Boundary conditions are summarized in Figure 54.

Convergence - The DAWES program displays a set of six quantities for monitoring convergence. Root-mean-square and maximum residuals of the governing equations are computed, along with inlet mass flow, mass flow error (expressed as a ratio of the maximum mass flow excursion in the computational domain relative to the inlet mass flow), the minimum static pressure in the system, and the overall total pressure ratio. Convergence is assumed to have been reached when the inlet mass flow, minimum static pressure, and overall total pressure ratio stabilize, the mass flow error remains below 1 percent, and the residuals continue to decrease.

Analyses - Flow analyses of the TFE731-60 Fan rotor were performed on six speed lines, five of which were selected to match a subset of the acoustic test points, as shown in Figure 55. The speed lines, identified in terms of the design fan speed, were as follows: 100, 86.5, 81.1, 75.3, 68.9, and 55.9 percent. The 100 percent speed case did not have a corresponding acoustic test point.

On each of the six speed lines, a series of back pressures was analyzed, in order to establish the shape of the speed line and identify the intersection of the speed line with the operating line, on which the acoustic data was measured. The resulting performance map is shown in Figure 56. The speed lines predicted by the DAWES program represent rotor total pressure ratio, in contrast to the acoustic test data which represents stage total pressure ratio. The DAWES total pressure ratio is comparable to the measured stage pressure ratio; suggesting that the rotor loss is being slightly over-predicted. The DAWES speed lines are also shifted somewhat lower in flow than the data. A set of DAWES points was selected as being most representative of the actual operating line points, based on their position on the speed lines. These points, which are marked with an asterisk in Figure 56, were then used for the Rotor Inlet Shock Study.
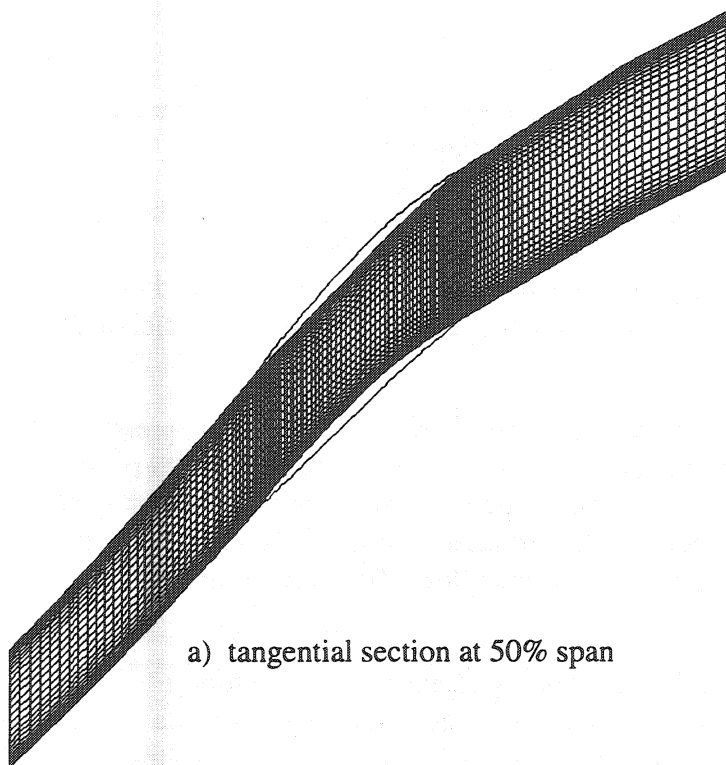
a) tangential section at 50% span
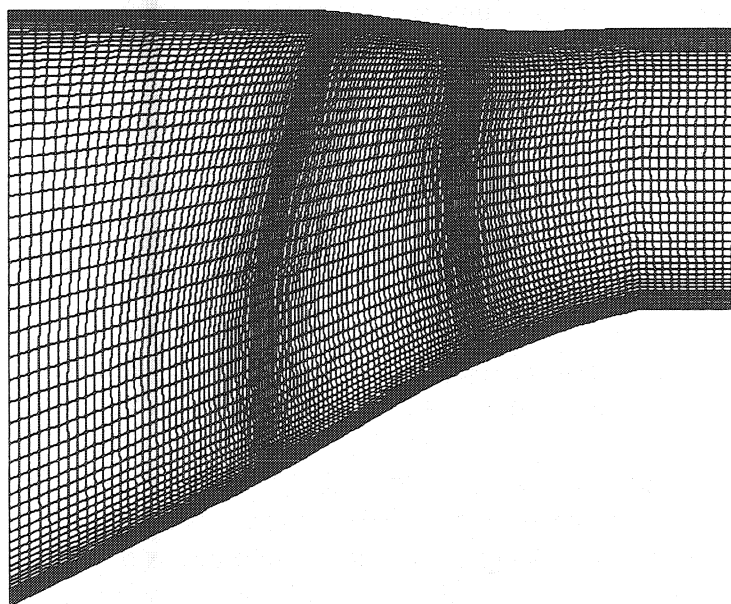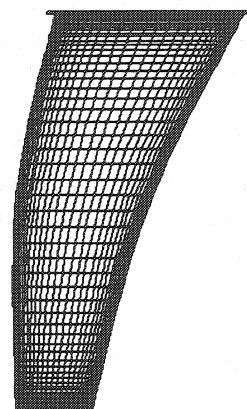
(b) meridional section   (c) cross section at mid-chord

Figure 52. **Typical Sections of the Computational Domain Show the Characteristics of the Rotor Passage H-Grid for the TFE731-60 Fan Rotor.**
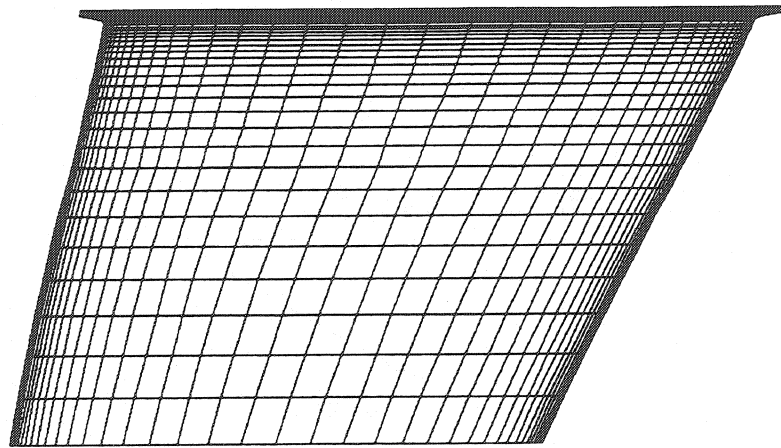
Figure 53. Enlarged View of Tip Section of DAWES Computational Grid Shows Artificial Blade Tapering.
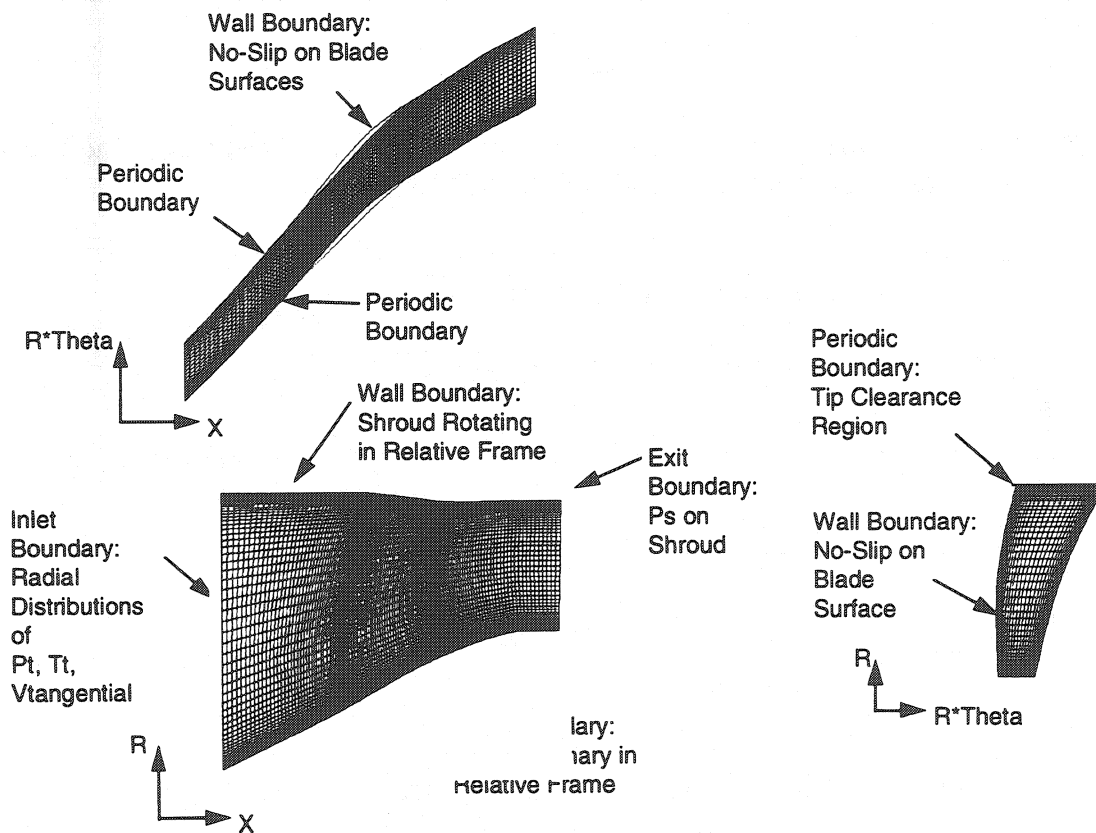
Figure 54. Boundary Condition Flow Properties for the DAWES Computational Domain Are Established from the AXCAPS Mean Streamline Analysis.
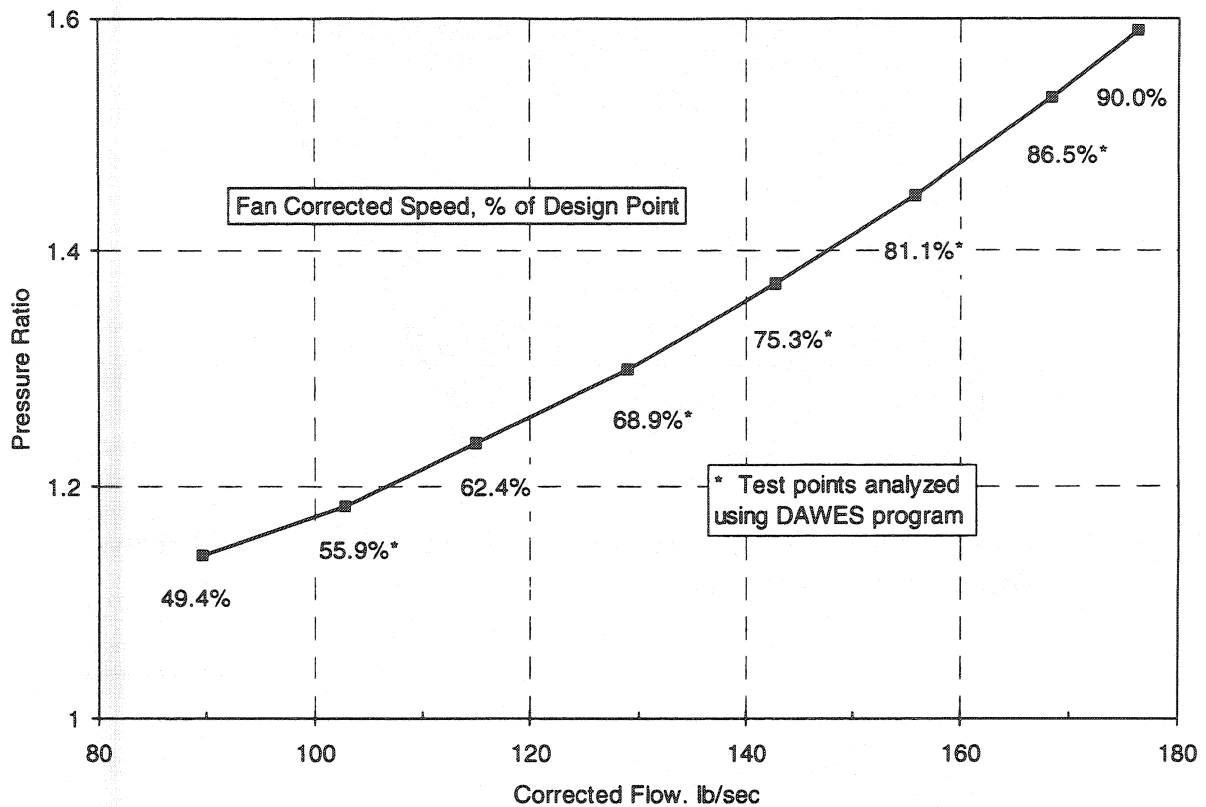
Figure 55. DAWES Analysis Points Were Selected to Match the Operating Line Where Acoustic Data Were Available for the TFE731-60.
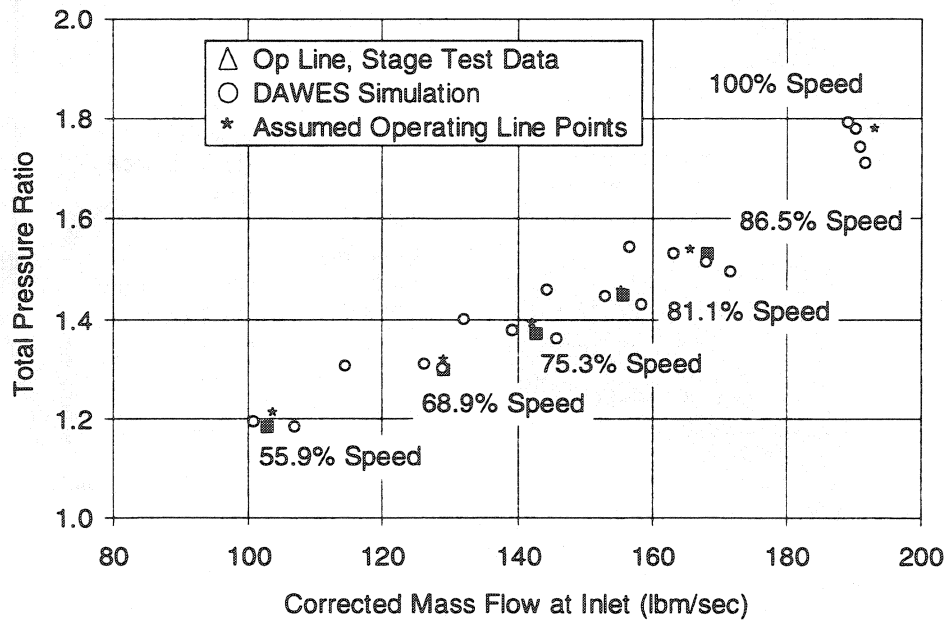
Figure 56. The DAWES Calculated Operating Conditions Agreed Well With the Measured Data for the TFE731-60.

5.4 Results

The relation between fan rotor inlet shock position and the presence of MPT noise may be explored graphically by examining contour plots of relative Mach number on blade-to-blade cuts across the flowpath near the blade tip. Shock position is also evident in relative Mach number contour plots on meridional cuts through the flowpath.

The range of wheel speeds analyzed in this study covered the complete variation in inlet shock position. At 100 percent speed, as may be seen in Figure 57, the shock is completely contained within the passage, just downstream of the leading edge of the rotor. Because the shock is completely inside the passage, the pressure disturbance cannot migrate upstream, and therefore MPT noise is not generated. As the wheel speed is reduced to 86.5 percent, the shock moves upstream, outside of the passage (Figure 58). Under these conditions, MPT noise is present. This is confirmed by the narrow band frequency plot in Figure 58, which shows the spikes across all frequencies, characteristic of MPT noise. The shock continues moving upstream and its intensity weakens, as the wheel speed is reduced to 81.1 and 75.3 percent (Figures 59 and 60). The corresponding narrow band frequency plots, shown in Figures 59 and 60, display an obvious reduction in Sound Pressure Level (SPL) amplitude of the MPT noise. Finally, at 68.9 percent speed, as seen in Figure 61, the shock is no longer present, and the narrow band acoustic data confirms that the MPT noise is not detected.

The DAWES predictions of inlet shock location and strength correspond to the narrow band acoustic data available for MPT noise generation; however, the precise speed for MPT onset was not measured. Nevertheless, it should be possible to more accurately bracket the predicted MPT onset fan speed by running additional DAWES cases at speeds between 68.9 and 75.3 percent. The speed at which the inlet shock forms upstream of the rotor would be indicative of MPT noise onset. Similarly, in the range between 86.5 and 100 percent speed, the speed at which the shock moves into the passage would represent the cessation of MPT noise.

Although the upstream boundary of the computational grid was intentionally positioned well upstream of the rotor leading edge, its proximity to the inlet shock structure may somewhat still be influencing the shock behavior. Inspection of contours of relative Mach number in the complete upstream region of the flowpath (Figure 62) indicates that the shock structure remains well downstream of the inlet, where boundary conditions of tangentially-uniform total pressure, temperature, and tangential velocity are imposed. However, to determine if the formation of the upstream shock structure is truly unrestricted, the inlet boundary should be positioned further upstream and selected analyses should be rerun to determine if the shock structure moves further upstream, or is altered in any way.
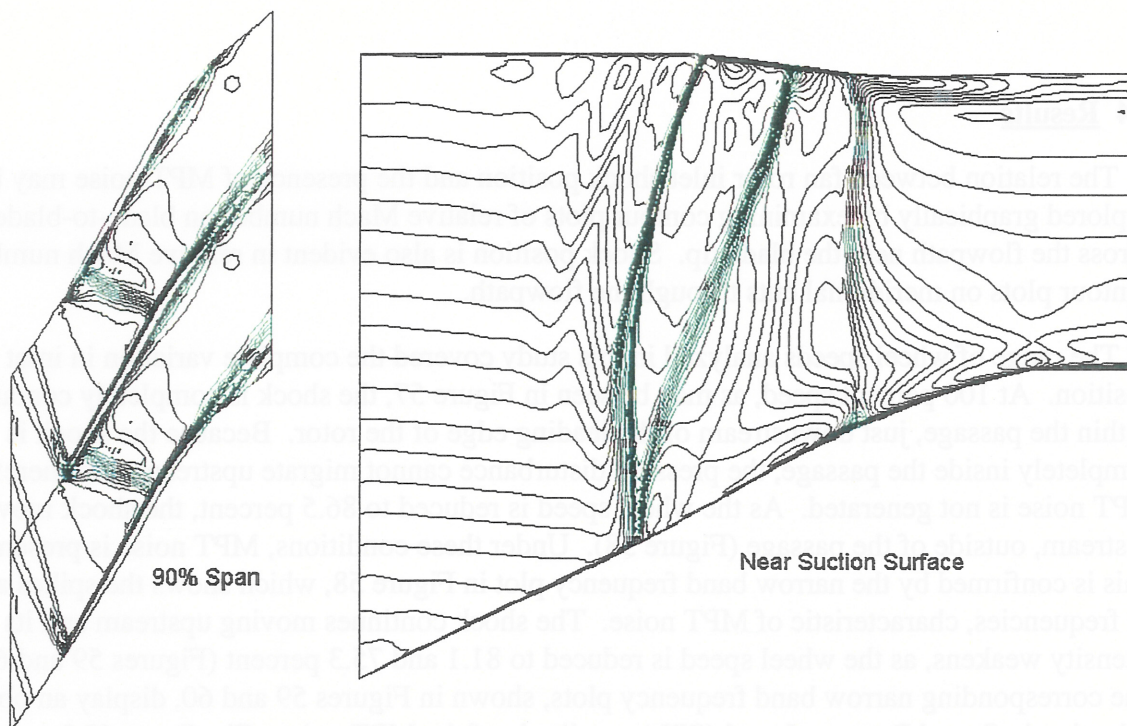
90% Span

Near Suction Surface

(a) Mach number contour lines in the circumferential and meridional planes

1.6
1.4
1.2
1.0
0.8
0.6
0.4

Relative Mach Number Contours
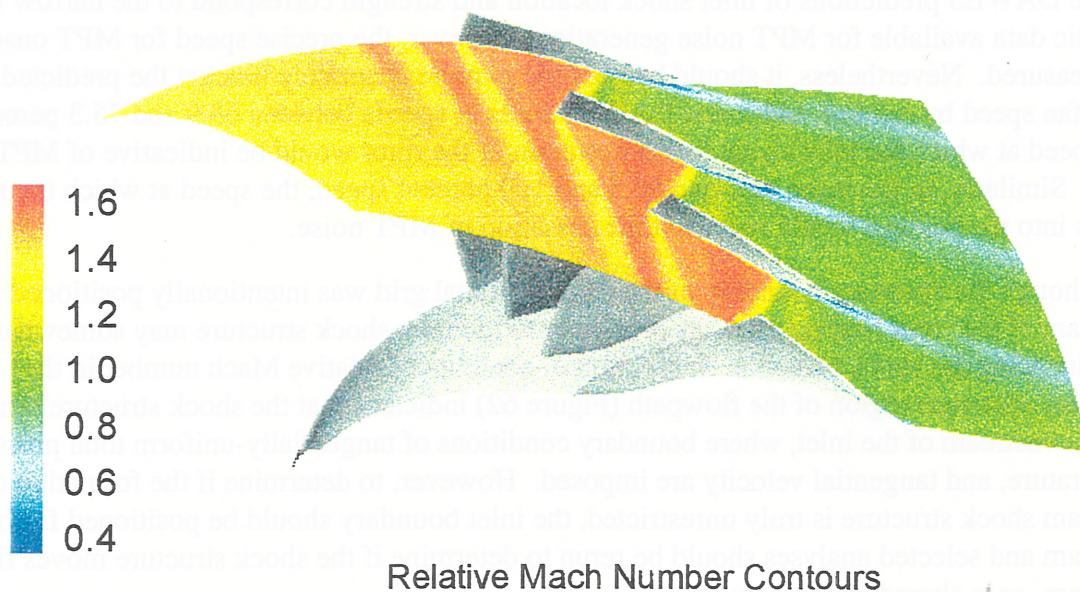
(b) Mach number color contours in a circumferential plane at 90% span

Figure 57.   DAWES Calculations Show a Strong Shock in the Blade Passage at 100 Percent Speed.
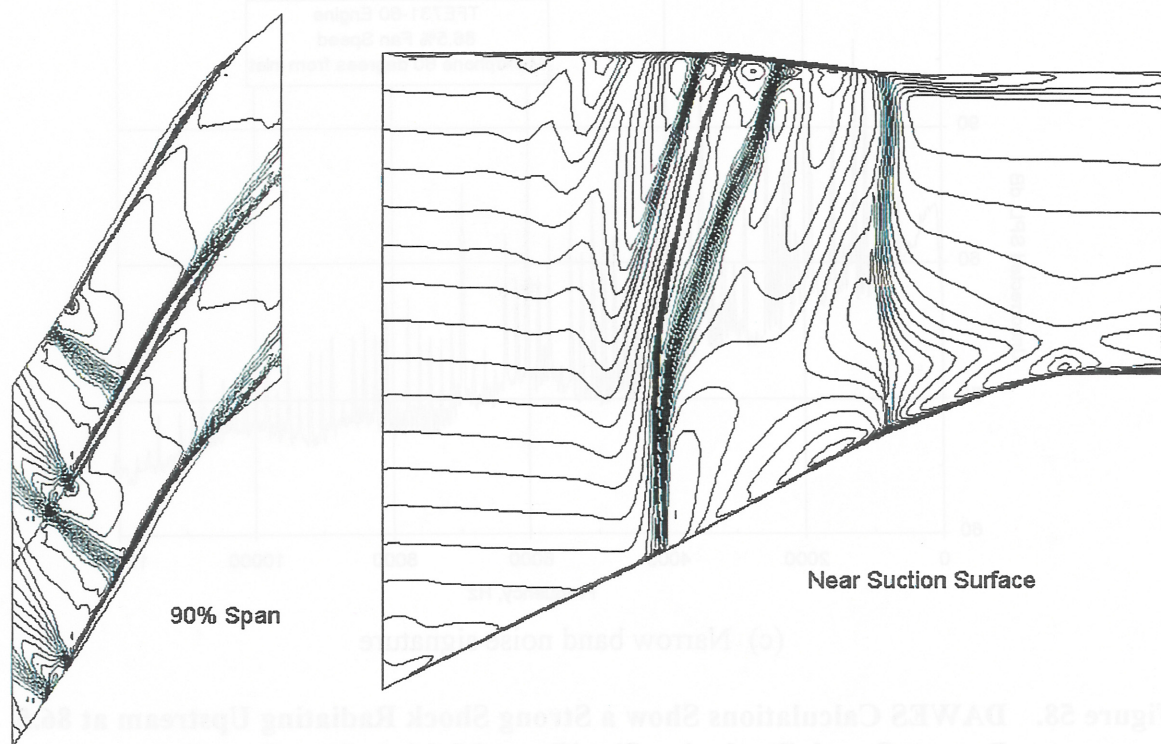
(a) Mach number contour lines in the circumferential and meridional planes

Relative Mach Number Contours
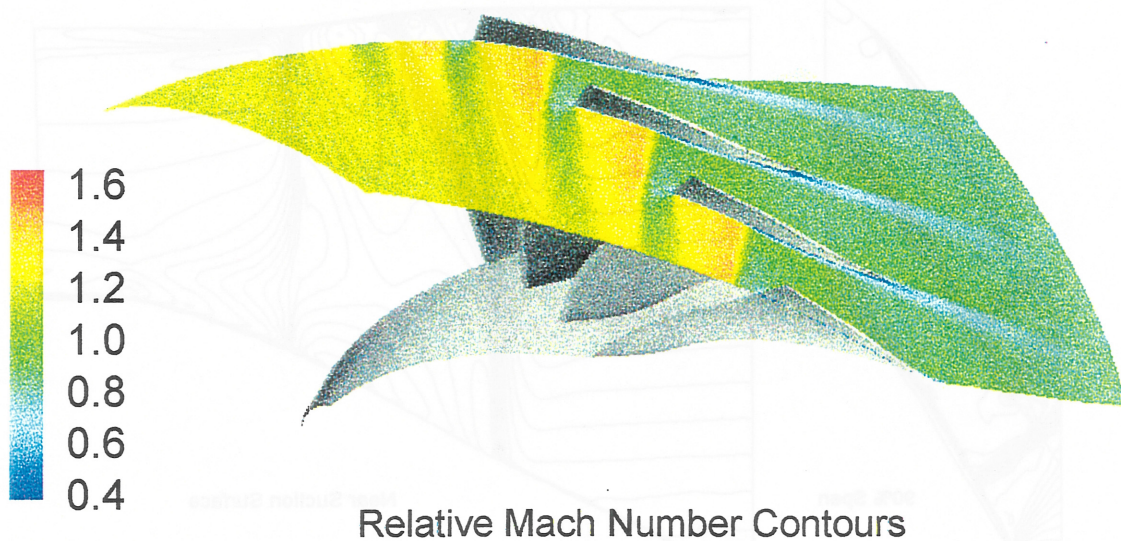
(b) Mach number color contours in a circumferential plane at 90% span

Figure 58.   DAWES Calculations Show a Strong Shock Radiating Upstream at 86.5 Percent Speed, Producing Significant Multiple Pure Tone Noise.
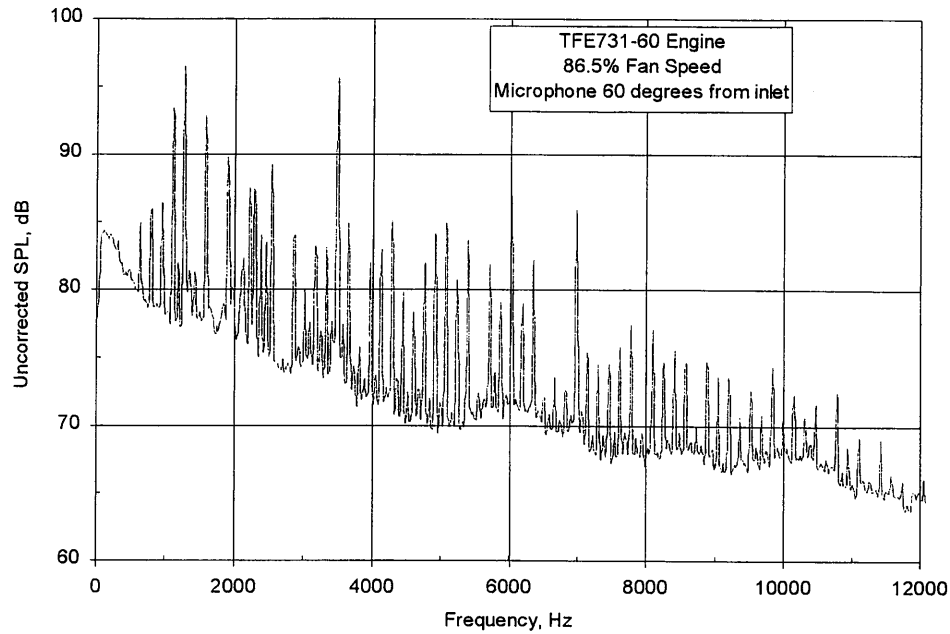
(c) Narrow band noise signature

Figure 58. DAWES Calculations Show a Strong Shock Radiating Upstream at 86.5 Percent Speed, Producing Significant Multiple Pure Tone Noise (Concluded).
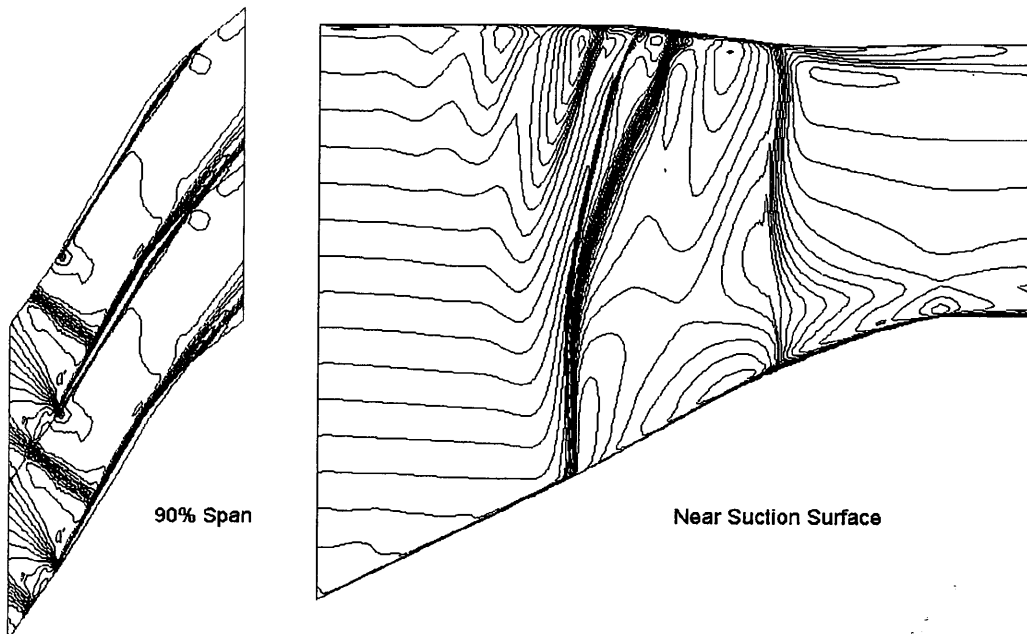
(a) Mach number contour lines in the circumferential and meridional planes

Figure 59. DAWES Calculations Show a Weaker Shock Radiating Upstream at 81.1 Percent Speed.

58

Relative Mach Number Contours
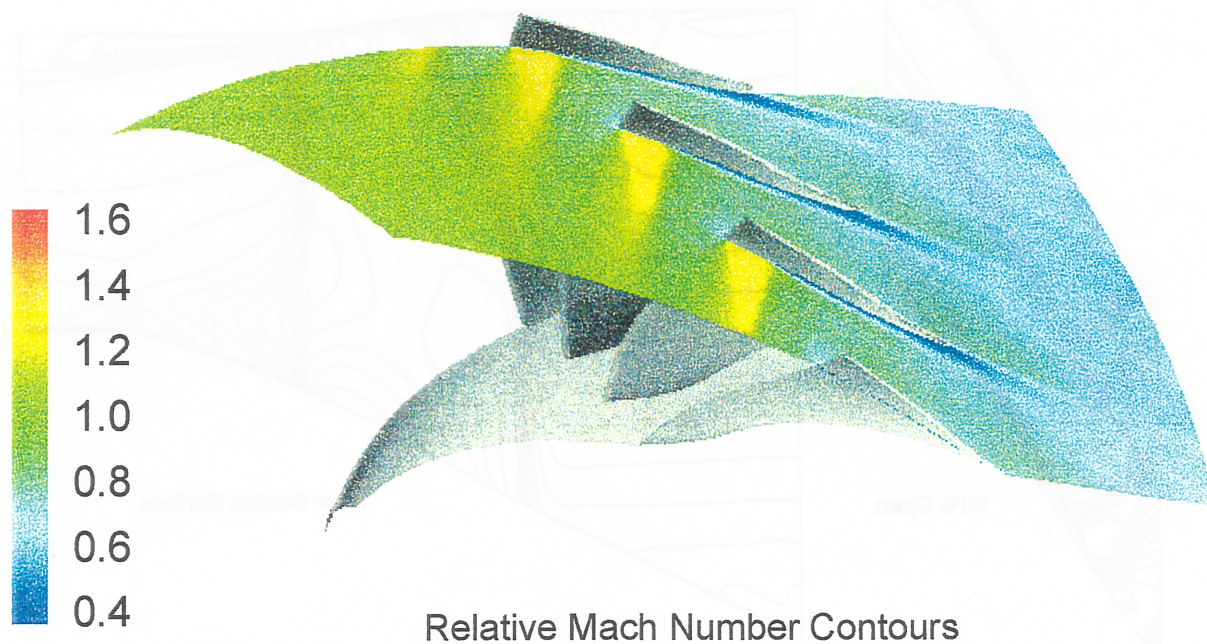
(b) Mach number color contours in a circumferential plane at 90% span
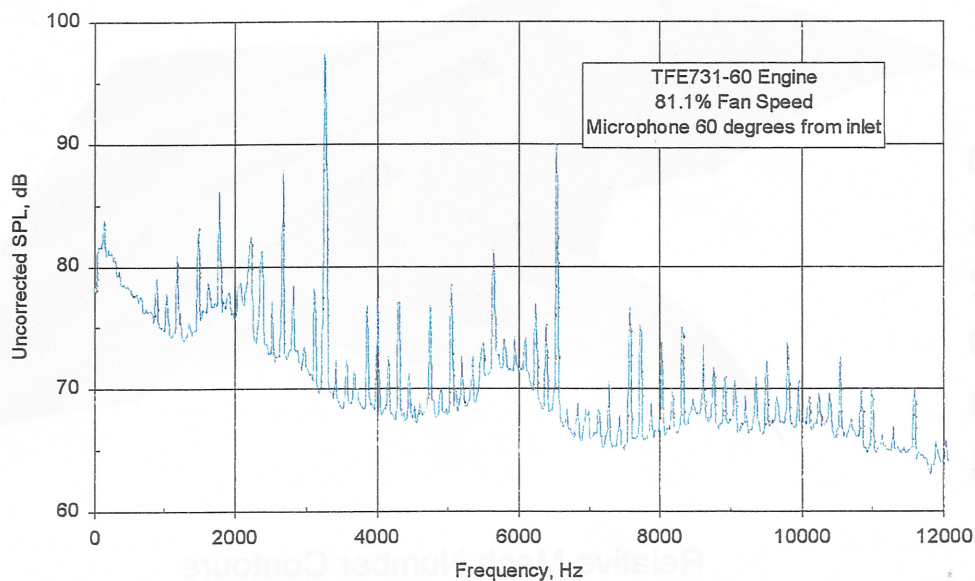
(c) Narrow band noise signature

Figure 59. DAWES Calculations Show a Weaker Shock Radiating Upstream at 81.1 Percent Speed (Concluded).
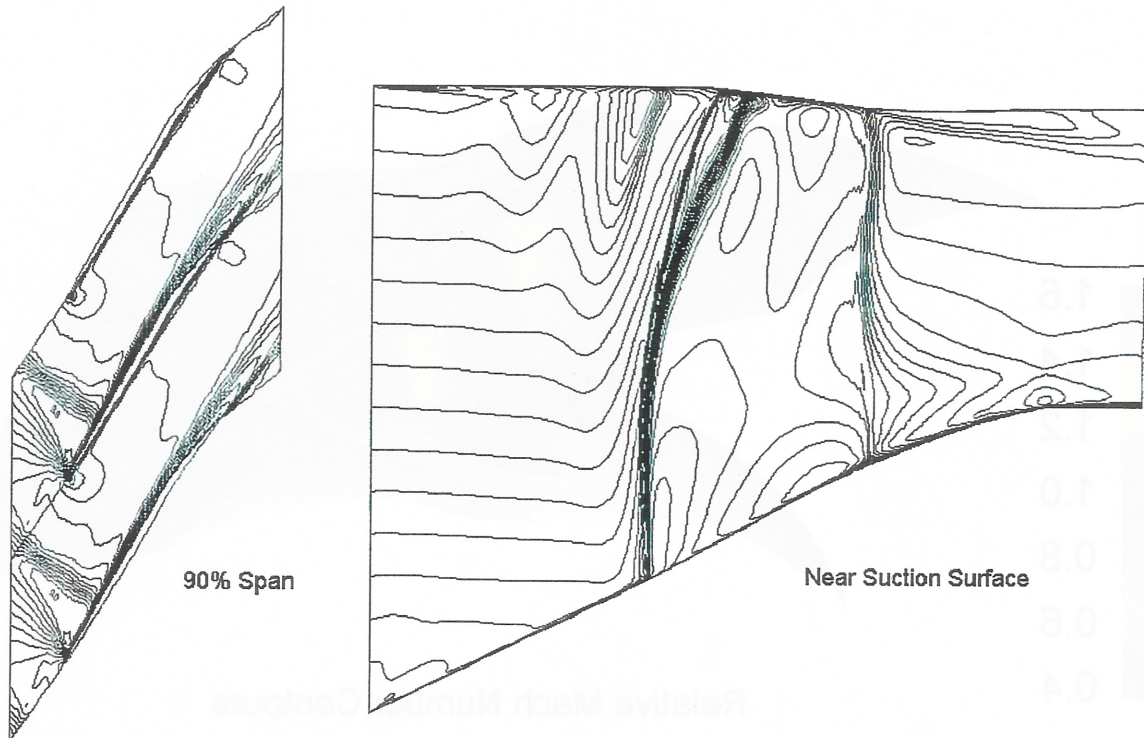
(a) Mach number contour lines in the circumferential and meridional planes

Relative Mach Number Contours
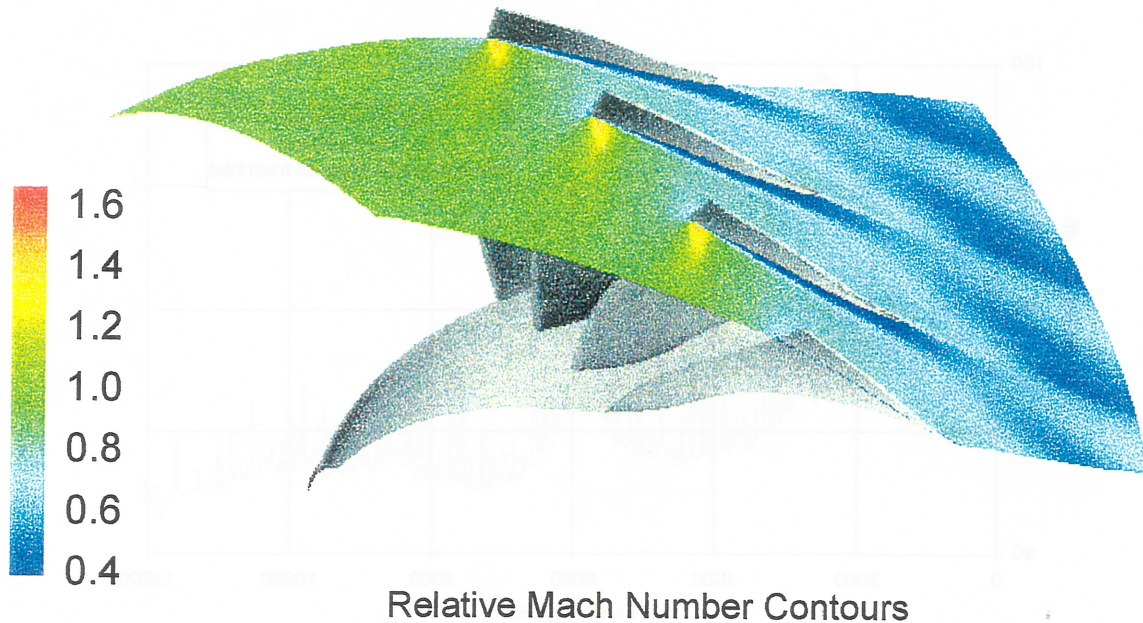
(b) Mach number color contours in a circumferential plane at 90% span

Figure 60. DAWES Calculations Show a Weaker Shock Radiating Upstream at 75.3 Percent Speed.
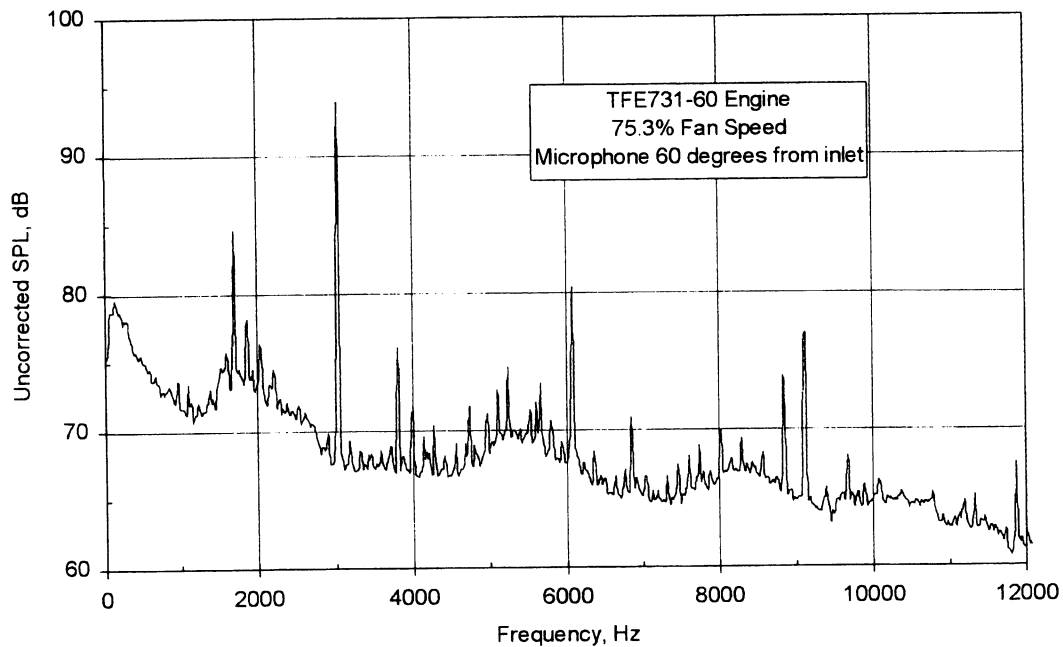
(c) Narrow band noise signature

Figure 60. DAWES Calculations Show a Weaker Shock Radiating Upstream at 75.3 Percent Speed (Concluded).
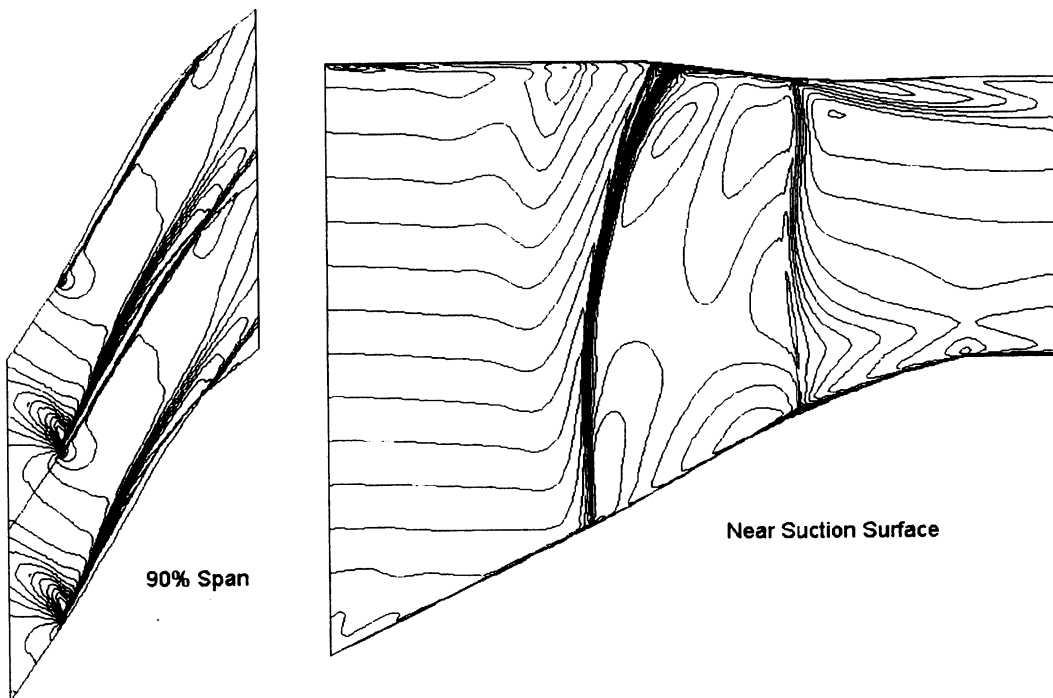
(a) Mach number contour lines in the circumferential and meridional planes

Figure 61. DAWES Calculations Show No Shock Is Present at 68.9 Percent Speed.

61
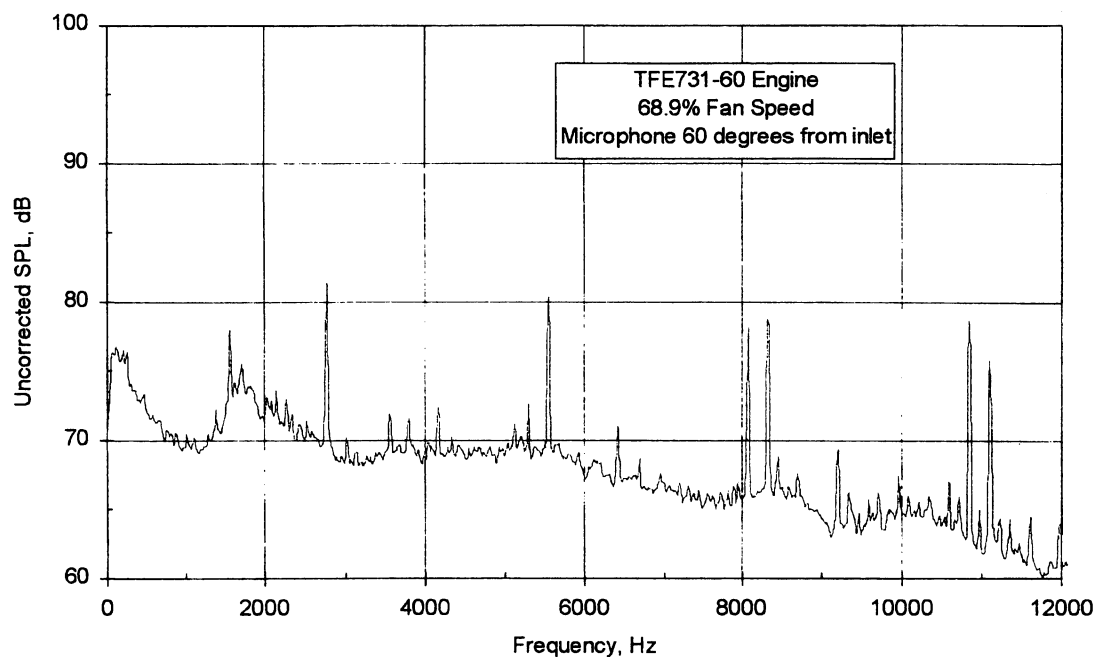
(b) Narrow band noise signature

Figure 61. DAWES Calculations Show No Shock Is Present at 68.9 Percent Speed (Concluded).
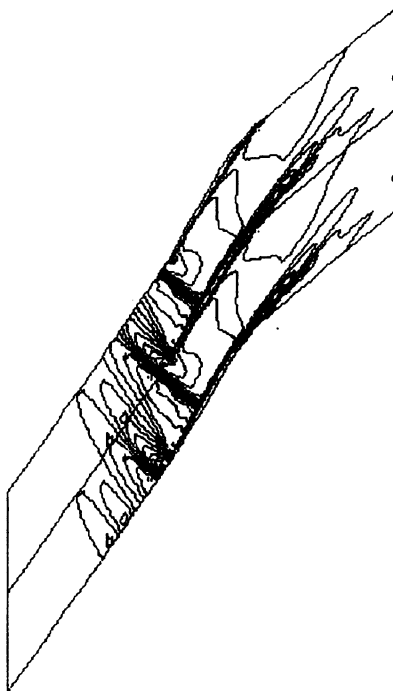
Figure 62. The Uniform Upstream Boundary Condition Did Not Apparently Affect Shock Formation Near the Blade.

5.5 Grid Resolution Study

The issue of shock resolution was investigated, in order to determine if higher computational grid densities would be required to adequately resolve the shock structure, for purposes of accurately predicting MPT noise onset.

The initial DAWES analyses of the TFE731-60 fan rotor at 100 percent speed were performed with a typical "design-resolution" grid, consisting of 33 nodes in the pitchwise direction, 71 nodes spanwise, and 131 nodes streamwise, for a total of 306,933 nodes. There were six equally-spaced cells in the tip clearance region. The nodes adjacent to the blade surfaces were positioned at approximately 0.5 percent pitch, and the nodal spacing was expanded using a hyperbolic-tangent-based algorithm.

In addition, selected points at 100 percent speed were also analyzed using a "high-resolution" grid, consisting of 41 nodes pitchwise, 81 nodes spanwise, and 256 nodes streamwise (850,176 nodes total). Again, six equally-spaced cells were placed in the tip clearance, and essentially the same pitchwise spacing was maintained for the nodes nearest the blade surfaces.

As may be seen in Figure 63, the analyses performed at 100 percent speed with the high-resolution grid were shifted slightly higher in pressure ratio, compared to the speed line of the original design-resolution grid. In addition, when details of shock structure were examined using contour plots of relative Mach number (Figure 63), the high-resolution grid produced more crisply-defined shocks, as would be expected. However, the shock positions did not appear to change significantly with increased grid resolution. Therefore, for the purposes of the Rotor Inlet Shock Study, the higher grid density did not appear to be critical.

For this reason, and because the very dense grid carries the penalty of significantly increased computation time, it was decided to perform all of the analyses with a grid only slightly denser than the design-resolution grid. The final grid used for the complete shock study consisted of 41 nodes pitchwise, 81 nodes spanwise, and 145 nodes streamwise (481,545 nodes total), with eight equally-spaced cells in the clearance region. In addition, the pitchwise spacing for the nodes nearest the blade surfaces was compressed, such that they were approximately 0.15 percent pitch from the blade in order to improve boundary layer resolution. This grid compression in the boundary layer has been found to be desirable for the AE version of DAWES, with its recent improvement in viscous stress discretization. Calibrations indicate that more accurate loss predictions are achieved when nodes are positioned deeper in the boundary layer. With this final computational grid, the speed lines shifted higher in pressure ratio, moving toward the acoustic test points, as shown in Figure 64, for the 86.5 percent speed line.

63

(a) speed line shift
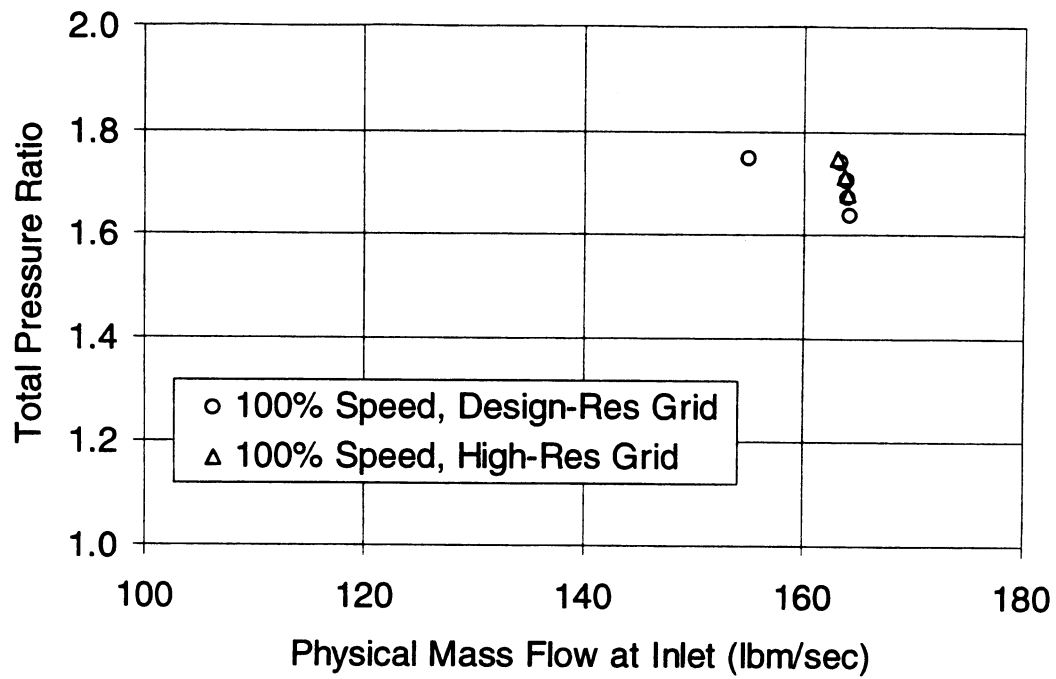
Design Resolution   High Resolution
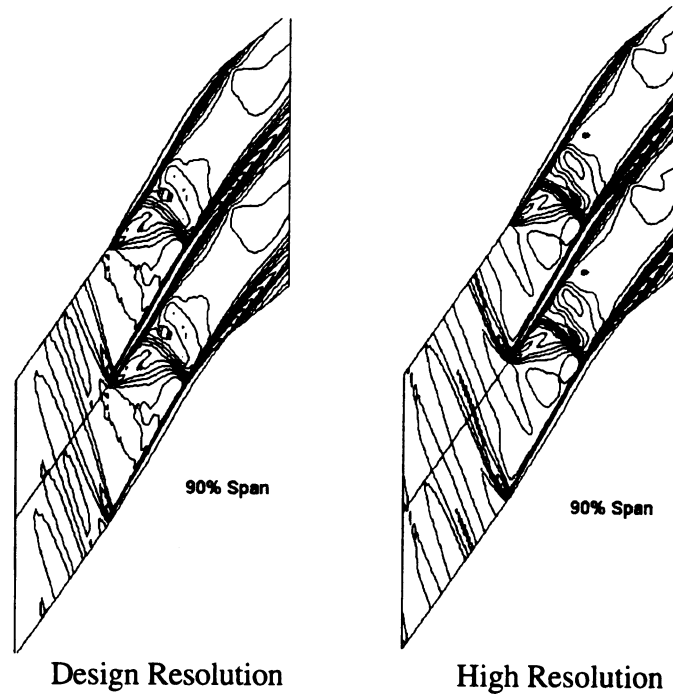
(b) Tangential view of shocks

Figure 63.   High-Resolution Computational Grid Resulted in a Small Impact on the Analysis Results.

Design Resolution   High Resolution

(c) Meridional view of shocks

Figure 63. High-Resolution Computational Grid Resulted in a Small Impact on the Analysis Results (Concluded).

Figure 64. The Final Computational Grid With High Resolution Near the Walls Shifts the Speed Lines Slightly Higher.

6.0 ROTOR WAKE/STATOR INTERACTION STUDY

6.1 Background

Interaction of the fan rotor wake with the leading edge of the fan stator represents a significant source of noise at certain fan speeds. The noise associated with this interaction is most noticeable at approach conditions, when other noise sources ar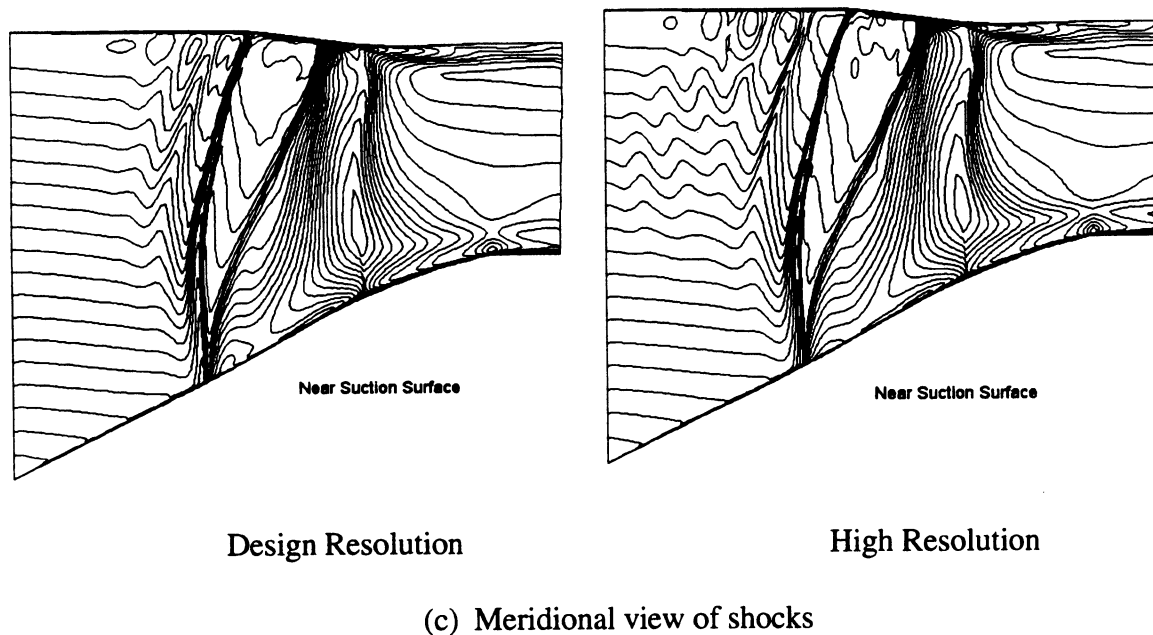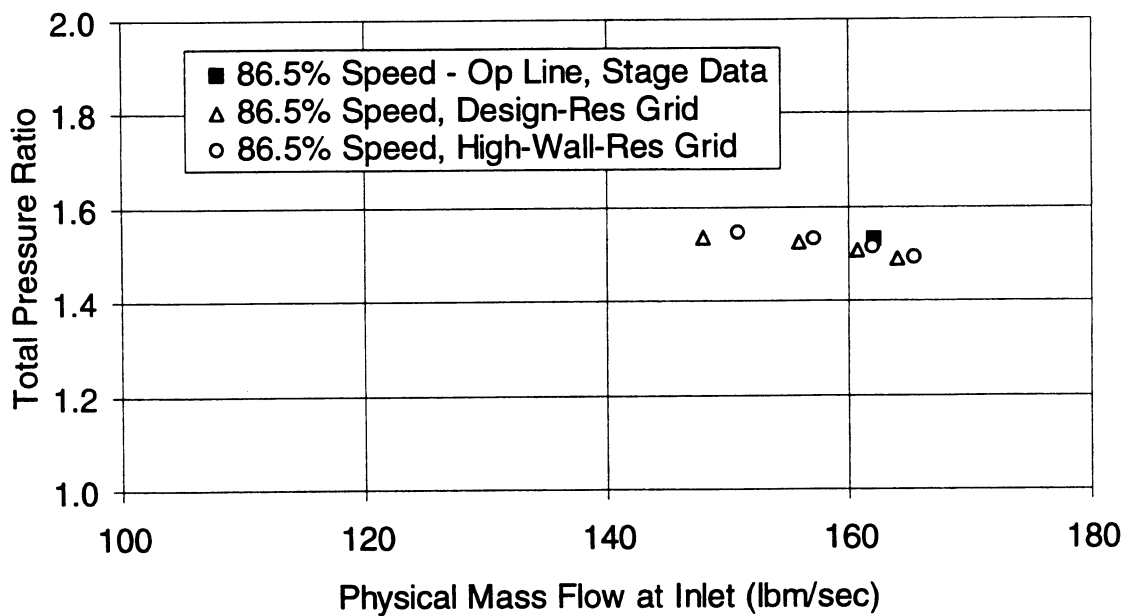e not dominant. Rotor-stator interaction tones are caused as the rotor wake impinges on the vane leading edge. The wakes emanating from the rotor are skewed and rotate circumferentially as they move downstream. Based on theory, the rotor wake/stator interaction noise occurs when the wake trace speed over the stator leading edge is supersonic. Thus, to minimize the interaction noise, the wake trace speed should be subsonic.

If the shape of the rotor wake is known, then the wake trace speed may be controlled during the design of the stator. This can be accomplished through vane axial and/or tangential lean. Increased axial lean (or sweep) increases the distance between the stator and rotor, causing a longer time increment for the circumferential wake pattern to impact the leading edge tip relative to the hub. Increased tangential lean (pressure side down) increases the delta in slope between the vane leading edge and wake trace, thereby reducing the amount of simultaneous impingement.

6.2 Objective

The objective of this subtask was to use the TFE731-60 fan rotor wake structure predicted by the DAWES program to define a redesigned stator with the leading edge configured to minimize the acoustic effects of rotor wake/stator interaction, without appreciably degrading performance. The V072 acoustic prediction program was used to confirm the effect of the redesign on the interaction noise, and the stator redesign is evaluated with the DAWES program to determine the overall performance benefit or penalty relative to the original stator.

6.3 Approach

Interaction of the fan rotor wake with the stator leading edge was assessed using a graphical technique. A contour plot of the rotor wake was produced on a surface formed by tangentially sweeping the stator leading edge curve. By superimposing the stator leading edge curve on the rotor wake plot, the time required for the wake to traverse a given distance along the leading edge was computed, thereby obtaining the wake trace speed. This process was applied to obtain an acoustic redesign of the existing TFE731-60 fan stator.

6.4 Rotor Wake Trace Speed Calculation

The first step in the process was to identify the location of the stator leading edge on the DAWES computational grid of the rotor analysis, as shown in Figure 65. The intersection of the stator leading edge curve and the rotor grid was then discretized, such that small annular sections approximating the surface swept by the leading edge are defined in terms of a streamwise grid station and bounding spanwise grid lines on the rotor computational grid, as illustrated in Figure 66. By generating contour plots of total pressure on each of these annular segments, a "mosaic"
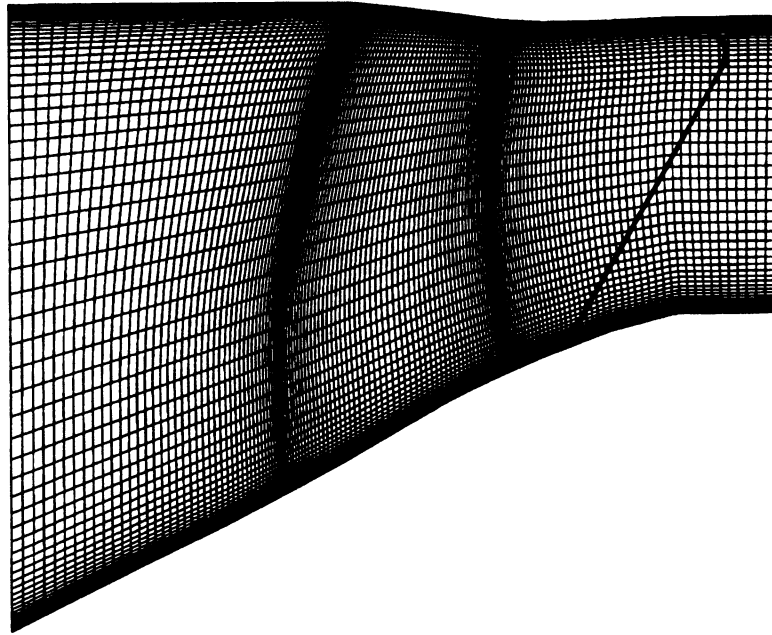
Figure 65. The Stator Leading Edge Is Superimposed on the Computational Grid of the Fan Rotor.
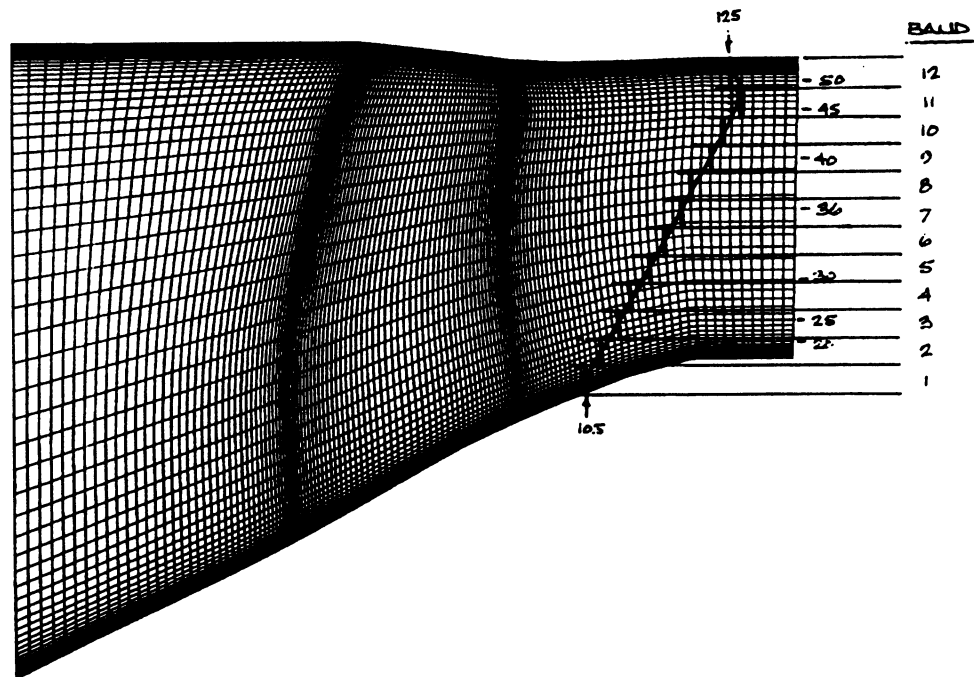
Figure 66. Annular Sections Are Defined Which Approximate the Curve of the Leading Edge.

67

was formed of the wake shape on the surface tangent to the stator leading edges. Such a wake contour plot is shown in Figure 67 for the TFE731-60 Fan rotor at approach speed.

The position of the wake centerline was then located on the wake plot and the stator leading edge curve was superimposed at some arbitrary angular position. Once the positions of the rotor wake centerline and the stator leading edge were established on the swept surface, the wake trace speed was be determined for each discrete annular section of the stator leading edge.

Referring to Figure 68, the local trace speed, V_T, at a spanwise location $k+1/2$ is given by:

$$V_T = \Delta\lambda_{SLE} / \Delta t$$

where the distance, $\Delta\lambda$, traversed by the rotor wake along the stator leading edge is given by:

$$\Delta\lambda_{SLE} = \left[(\Delta r)^2 + (r\Delta\theta)^2 + (\Delta x)^2\right]^{1/2}$$

and where, as shown in Figure 69,

$$\Delta r = r_{k+1} - r_k$$
$$r\Delta\theta = (r_{k+1} + r_k)(\theta_{k+1} - \theta_k) / 2$$
$$\Delta x = x_{k+1} - x_k$$

The time required for the wake to traverse the discrete annular section of the stator leading edge is given by:

$$\Delta t = \Delta\theta_T / \omega$$

where:

$$\omega = \text{Wheel Speed (rad / sec)}$$

and the traversed arc, $\Delta\theta_T$, as shown in Figure 70, is given by:

$$\Delta\theta_T = \Delta\theta_{k+1} - \Delta\theta_k$$

where:

$$\Delta\theta_{k+1} = \theta_{RW,k+1} - \theta_{SLE,k+1}$$
$$\Delta\theta_k = \theta_{RW,k} - \theta_{SLE,k}$$

68
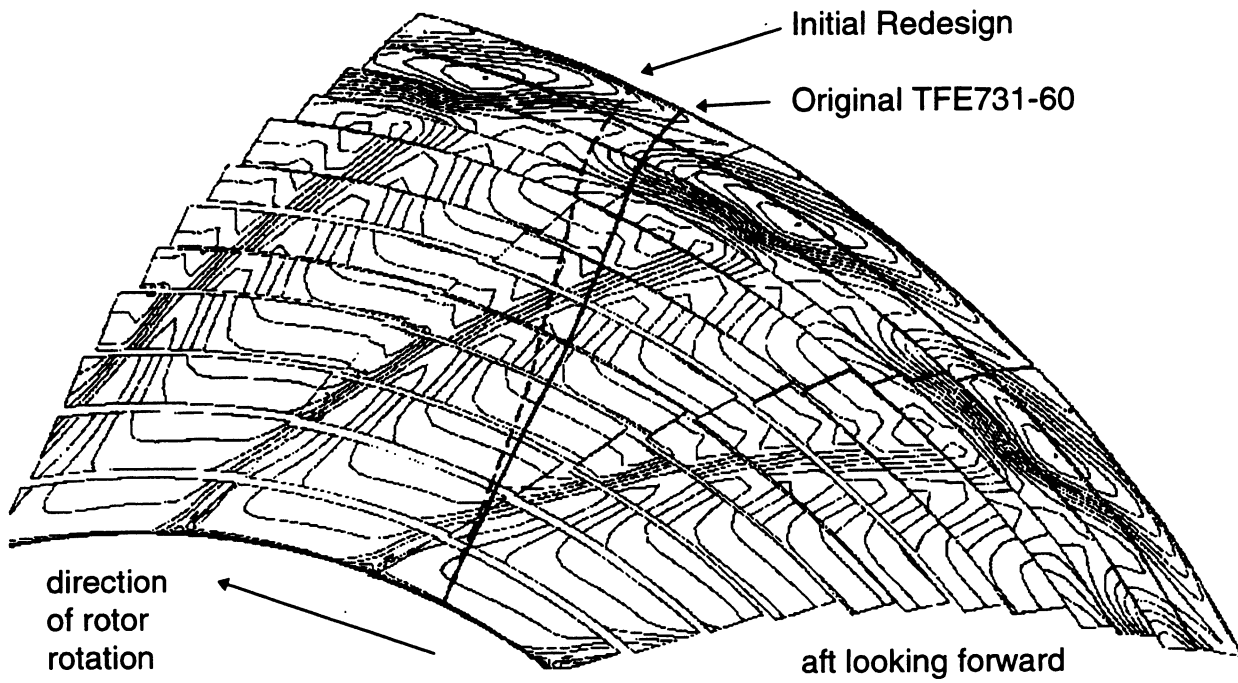
Figure 67. Wake Contour Plot at the Stator Leading Edge Surface for the TFE731-60 Fan at Approach Speed.
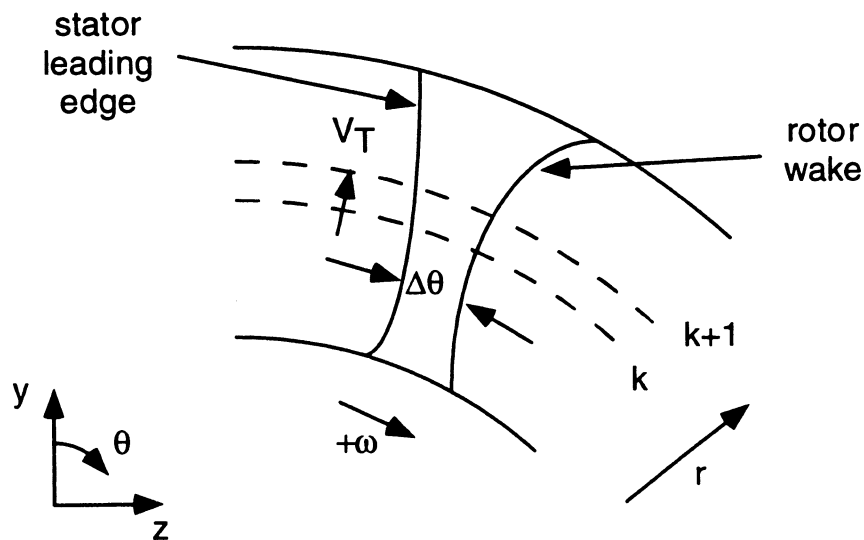
Figure 68. The Local Wake Trace Speed, V_T, Is Computed Along the Stator Leading Edge.
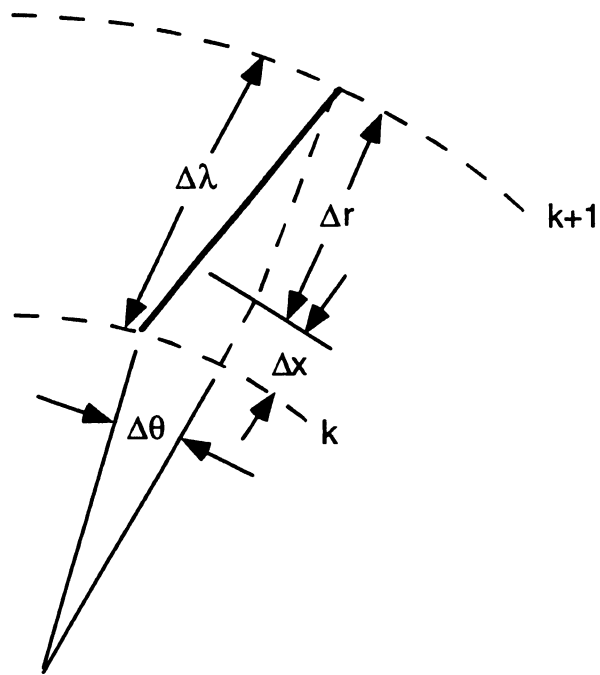
Figure 69. The Distance , $\Delta\lambda$, Is Defined Between Annular Section End Points of the Stator Leading Edge.
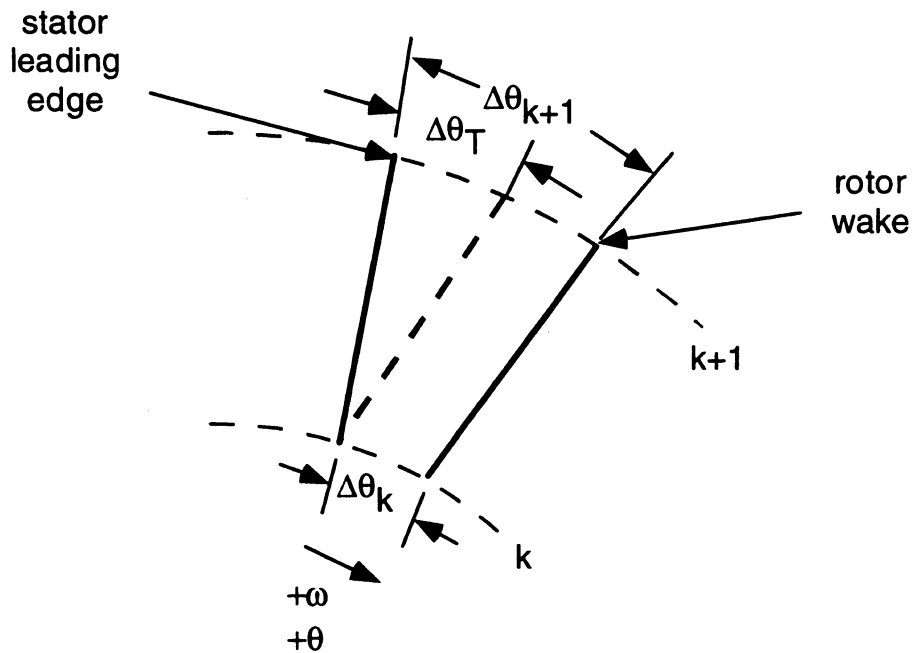
Figure 70. The arc, $\Delta\theta_T$, Is Traversed by an Annular Section of the Wake as it Moves Across the Stator Leading Edge.

70

6.5 TFE731-60 Fan Stator Redesign

Because of limited time available for the stator redesign effort, the modifications considered were limited to lean changes relative to the original stator, with the constraint of maintaining the performance as close as possible to the original component. Rather than computing wake trace speeds, the plot of rotor wake shape at approach conditions (Figure 67) was employed to qualitatively determine a new stator lean which would increase the time required for the wake to traverse the stator leading edge.

The design approach used was to modify the tangential lean from the TFE731-60 stator without modifying axial lean. (The baseline stator had a relatively large amount of axial lean.) Because tangential lean is input into the radial equilibrium flow solver/geometry generator program (AXCAPS) at mid-chord, a separate program was written to quickly plot the vane leading edge coordinates. Four iterations were completed with varying amounts of tangential lean and bow. A DENTON 3-D inviscid analysis was initially used to quickly compare airfoil section loadings against the baseline. The best iteration was then analyzed, along with the baseline, using the DAWES 3-D viscous analysis program. An acoustics analysis was also performed for the airfoil geometry to assess the reduction in rotor-stator interaction tones.

A comparison of the vane leading edge geometry for the baseline and redesign is shown in Figure 71. The figure clearly shows the increased lean. The circumferential offset at the tip was 0.60 inch. Airfoil section loadings analyzed using the DENTON program were compared at the hub, midspan, and tip, and are shown in Figures 72 to 74, respectively. The figures show similar loadings with differences believed to have no significant effect on the aerodynamic performance. Other iterations with increased tangential lean resulted in unacceptable airfoil loadings at the tip, with larger peak Mach numbers and greater suction surface diffusion rates.

6.6 DAWES Analyses

The blade and flowpath geometry descriptions for both the original and redesigned TFE731-60 fan stators were obtained from AE's axisymmetric streamline curvature program, AXCAPS. This program provides a discrete-point definition of the blade geometry along specified stream surfaces intersected with the blade surface. Endwall definition is also provided in terms of radial and axial coordinates at discrete points. The AXCAPS model of the flowpath was identical for both stators, and is shown in Figure 75.
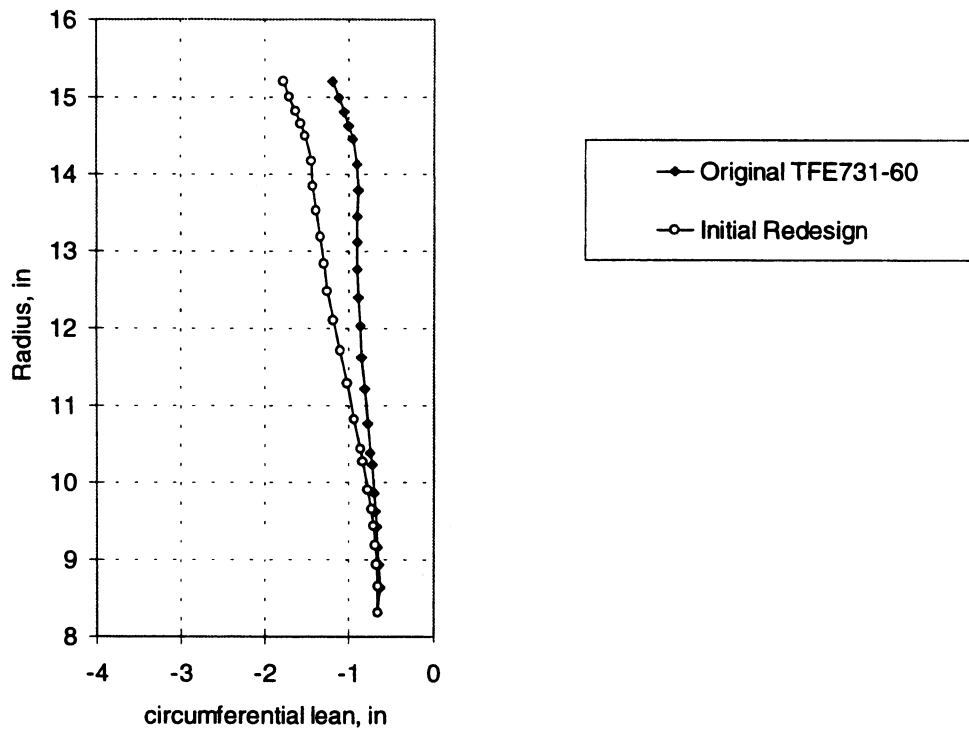
Figure 71. Differences in Stator Leading Edge Geometry Show the Additional Tangential Lean of the Acoustically Redesigned Stator.
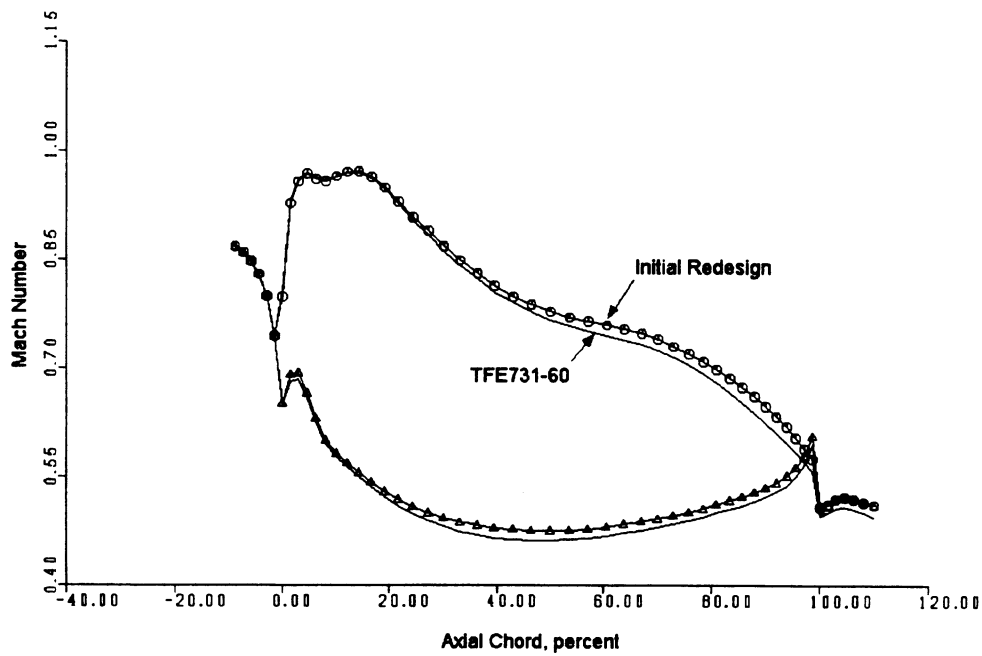
Figure 72. Inviscid Predictions of the Airfoil Section Loadings at the Hub Show Only Small Differences Between the Original and Redesigned Stators.
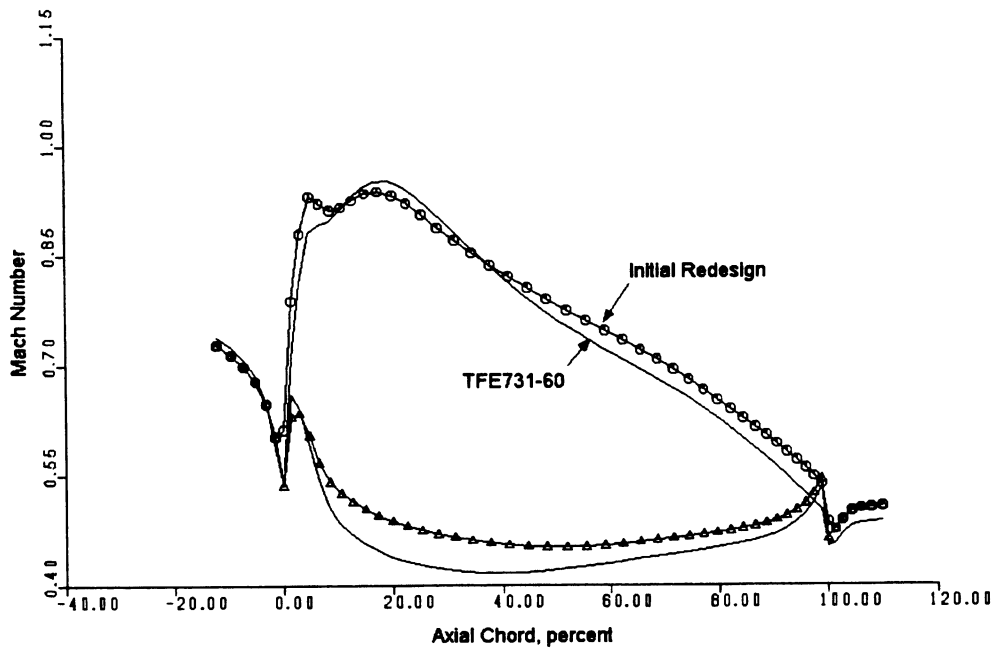
Figure 73. Inviscid Predictions of Airfoil Section Loadings at Midspan Show Only a
Small Difference Between the Original and Redesigned Stators.
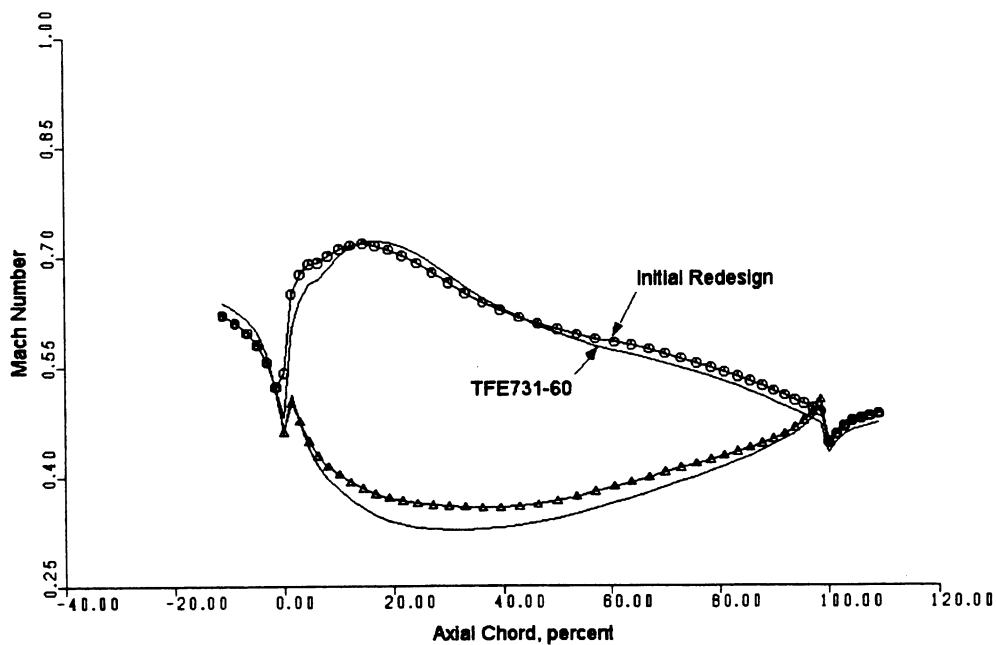
Figure 74. Inviscid Predictions of Airfoil Section Loadings at Shroud Show Only a
Small Difference Between the Original and Redesigned Stators.

73
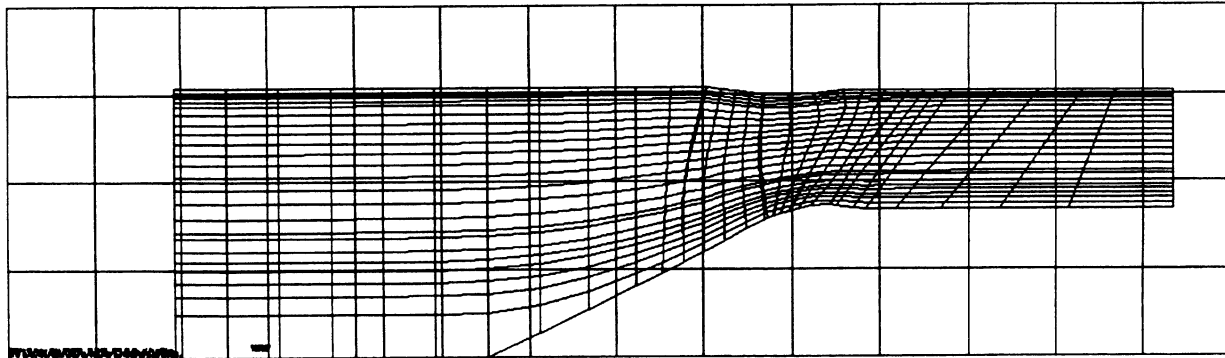
Figure 75. **The AXCAPS Model of the Flowpath for the TFE731-60 Fan Is Identical for the Original and Acoustically Redesigned Fan.**

The computational domain for the CFD analysis consisted of a single stator blade passage, with the suction surface of one blade forming one pitchwise boundary, and the pressure surface of the adjacent blade forming the other pitchwise boundary. The inlet to the computational domain was positioned approximately 1.3 axial chord lengths upstream, and the exit was located approximately 1.0 axial chord lengths downstream.

The computational grid for the DAWES program is a structured single-block skewed H-grid. The grid size employed for both stator analyses was specified as:

Pitchwise:	41 Nodes
Spanwise:	81 Nodes
Streamwise:	145 Nodes (56 nodes on blade)

The total grid size was 481,545 nodes. Grid spacing was nonlinearly expanded from the walls using a hyperbolic tangent-based algorithm, with the grid node closest to the blade surface located at approximately 0.15 percent pitch away from the surface.

Typical sections of the computational grid are presented in Figures 76 to 78. The meridional flowpath is identical for the original and acoustically-redesigned stators. The blade sections are also unchanged. Only the blade lean has been altered, as shown in the flowpath cross sections of Figure 78.
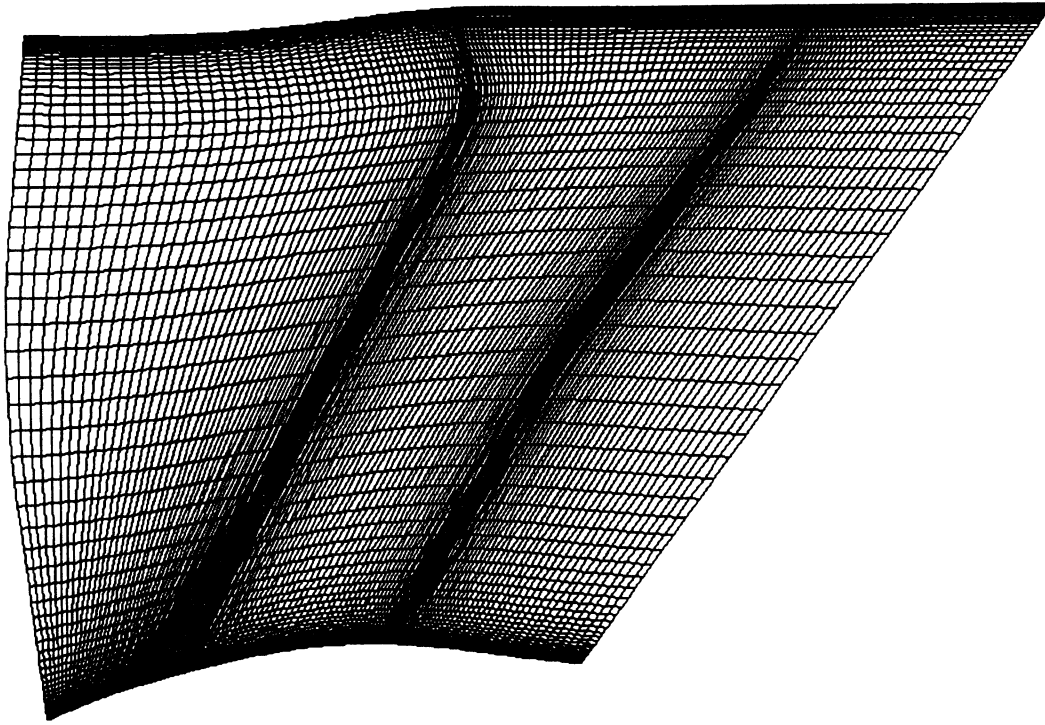
Figure 76. Meridional View of the TFE731-60 Fan Stator Shows the Axial Sweep Common to Both the Baseline and Acoustically Redesigned Stators.
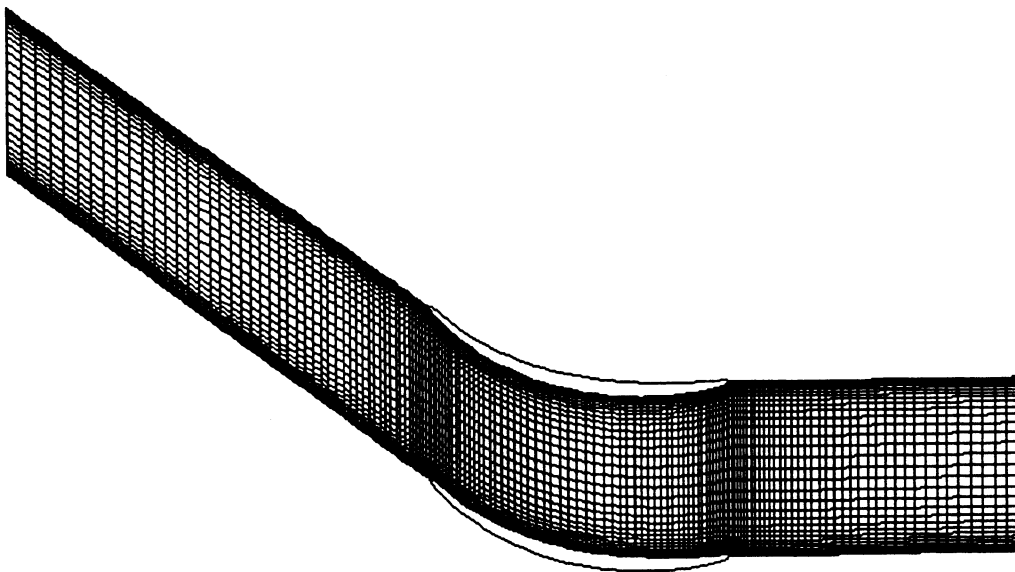
Figure 77. Midspan Section of the TFE731-60 Fan Stator Is Identical for Both the Original and Redesigned Stators.

leading edge   midchord   trailing edge
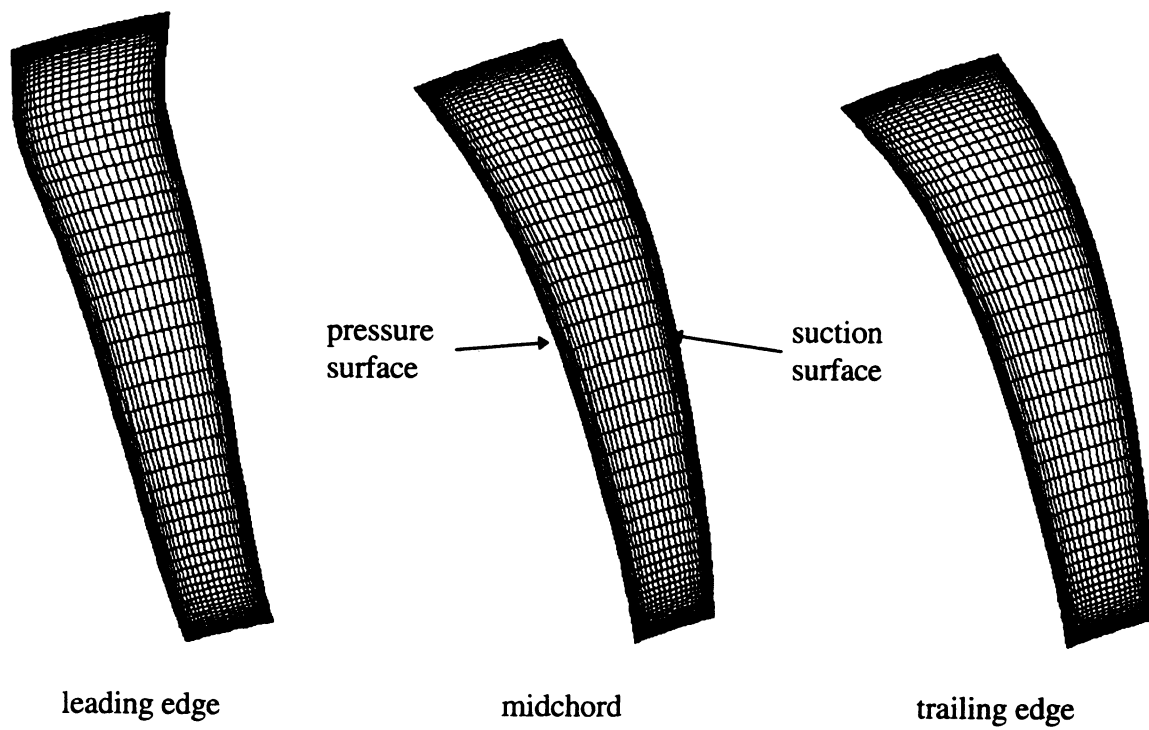
(a) original TFE731-60 design

leading edge   midchord   trailing edge
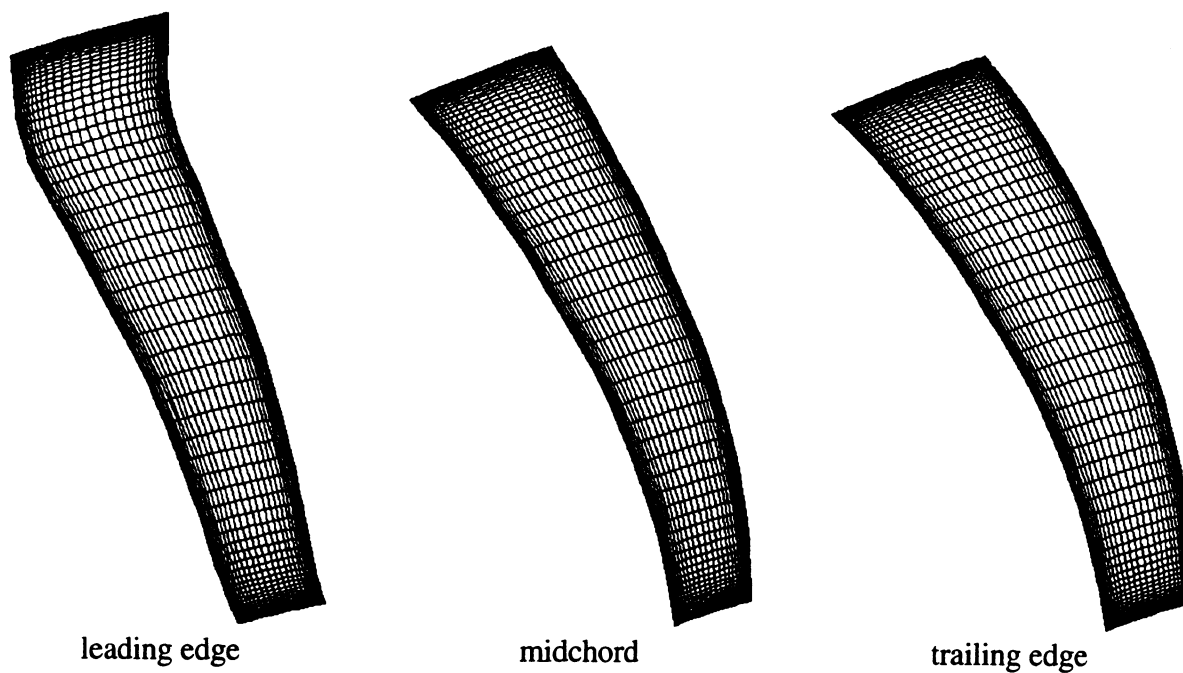
(b) acoustic redesign

Figure 78. Passage Cross Sections at the Stator Leading Edge, Midchord, and Trailing Edge Show the Tangential Lean of the Redesigned Stator.

76

DAWES flow analyses were performed for both the original and redesigned TFE731-60 Fan stators. The same design point flow conditions were analyzed for both blade rows; i.e., inlet conditions and back pressures were identical for both stators.

6.7 Aerodynamic Results

Comparison of the predicted 1-D aerodynamic performance values for the two stators indicates that the performance is essentially unchanged for the acoustic redesign, as shown in the following table.

	Original Stator Design	Acoustic Redesign
Mass Flow, lbm/sec	94.09	94.22
Total Pressure Ratio	0.9847	0.9840

Contour plots of total pressure across the passage at the stator trailing edge are shown in Figure 79 for both stator designs. The total pressure contours of the redesigned stator are essentially unchanged from the original stator. Loading plots for the two stators, at selected spanwise locations, are compared in Figure 80. The loadings do not change significantly when the stator is modified. Therefore, it may be concluded that the redesigned stator, in order to reduce interaction noise, had essentially no impact on aerodynamic performance.

(a) original stator   (b) redesigned stator
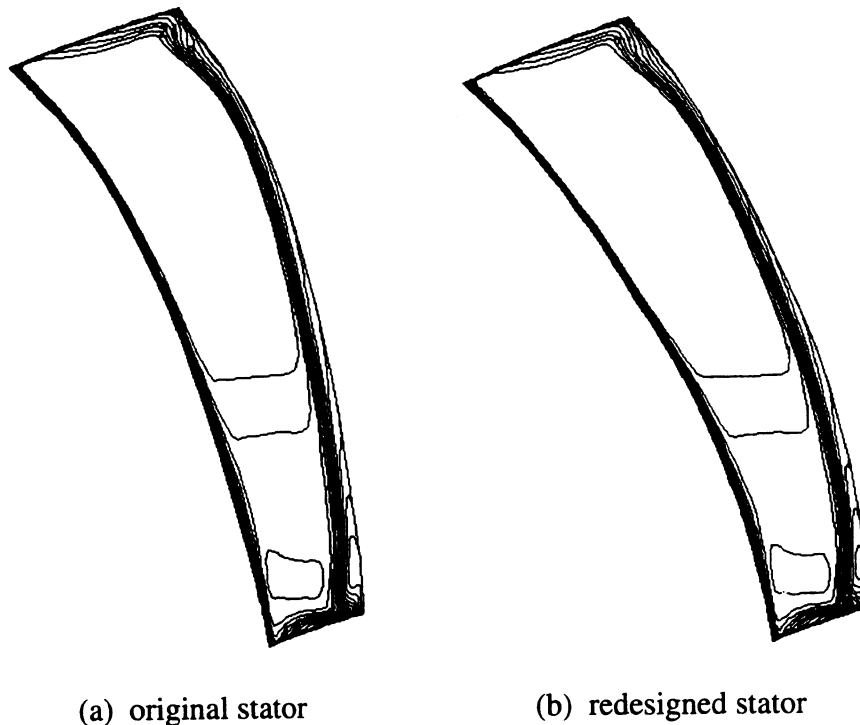
Figure 79. **Contours of Total Pressure Across the Vane Passage at the Trailing Edge Show Similar Characteristics for the Two Stators.**
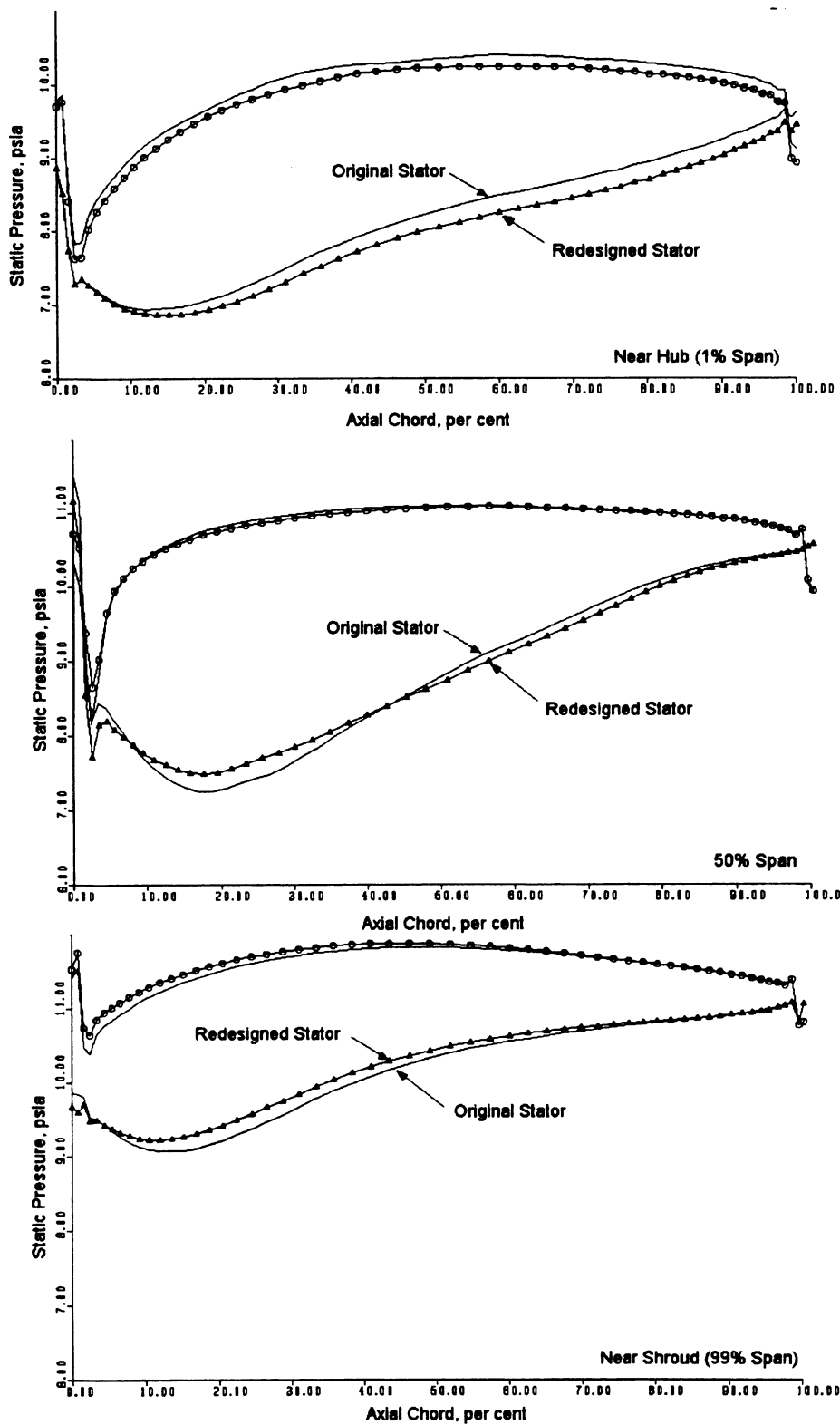
Figure 80. **DAWES Predictions of Airfoil Section Loadings Show Small Differences Between Original and Redesigned Stators.**

78

6.8 Acoustic Analysis and Results

An acoustic analysis of the redesigned stator was performed using the V072 program. The operating procedures and input data used were identical to those used in Section 4.0. The following table shows that a significant noise reduction was not achieved with the design. The current design has a very conservative lean to maintain performance with the same platform and airfoil, and the change in design was not sufficient to produce the desired noise reduction effect. Analysis of the V072 output with the ARC code showed no difference in the acoustic radiation pattern in the farfield. Further work is needed to design a stator with more aggressive lean that will meet the performance objectives.

	Acoustically redesigned stator		Baseline TFE731-60 stator	
	BPF	2xBPF	BPF	2xBPF
75.3% Speed	134.4	113.9	134.9	114.0

7.0 CONCLUSIONS

The results of the QF-12 Swept Rotor Fan Analysis show that:

- The use of CFD flow simulations to predict MPT noise, based on the presence of a rotor inlet shock structure, was not conclusive for the QF-12 fan. Further investigation of the differences between the actual and modeled rotor blade geometry, including any blade deflections, would be necessary to determine more fully the reasons for the high level of measured MPT noise, despite the apparent lack of a strong rotor inlet shock structure in the flow simulations.

- More accurate modeling of the 3-D geometry of the midspan damper would be required to conclusively identify the damper shock-induced flow separation as the cause of the aerodynamic performance deficiency. The present modeling of the damper, without sweep or fillets, may not be sufficiently accurate to properly simulate the true flow conditions near the pressure surface of the rotor.

The results of the Acoustic Code Calibration show that:

- The noise power levels for the various propagating modes appear to be underpredicted but the reason behind this is undetermined.

- The Acoustic Radiation (Eversman) Code is a relatively easy-to-use, well documented finite-element code that, although it is very memory intensive, generates inlet radiation solutions fairly quickly.

- More detailed acoustic data for the TFE731-60 is needed to adequately assess the predictive quality of the Eversman code results. Also, it would be useful to modify the code so that absolute rather than relative sound pressure levels are output.

- There has been difficulty in approaching the dimensioned limits for the number of elements on the fan face and on the upper nacelle surface. The source of this difficulty needs to be identified and corrected.

The results of the Rotor Inlet Shock Study show that:

- The DAWES program may be used as a tool to predict the existence of MPT noise for fan rotors by examining predictions of rotor inlet shock structure at selected fan speeds.

- By refining the speed range over which the fan rotor is analyzed, it should be possible to predict the onset speed for MPT noise. However, acoustic data for the TFE731-60 Fan was not detailed enough to assess the accuracy of the DAWES program for such predictions.

- With the ability to accurately predict MPT noise onset using a CFD flow simulation tool, it should be possible to acoustically tailor the design of a fan rotor, during the component design phase, in order to minimize MPT noise.

Recommendations for further study would include the following activities:

- Assess the impact of the computational grid inlet boundary proximity, as it affects the upstream structure of the inlet shock.

- Assess the accuracy of the numerical predictions of MPT noise onset.

- Demonstrate the ability to design a fan rotor to minimize MPT noise by using advanced design concepts in conjunction with CFD predictions of inlet shock behavior.

The results of the Rotor Wake/Stator Interaction Study show that:

- The TFE731-60 fan stator was redesigned to reduce the rotor-stator interaction tones generated by the upstream rotor wakes impacting the vane leading edge. The vane tangential lean was increased and the transition (bow) was shifted radially outward. There was no change to axial lean. Based on 3-D inviscid and viscous analyses, the redesign showed no performance difference.

- The graphical technique, using CFD predictions of rotor wake shape, appears to serve adequately to determine the requirements for a stator leading edge design, which will minimize wake interaction noise.

- The stator redesign activity described here serves to demonstrate this graphical technique for acoustically tailoring a stator to minimize noise from rotor wake/stator leading edge interaction. To better determine the acoustic benefit of stator design accounting for wake trace speed, a more aggressive redesign activity needs to be performed.

- The conservative lean selected for the stator design was not sufficient to produce a significant noise benefit as computed with the V072 code. Further work is needed to design a more aggressive lean that may produce a noise benefit while maintaining performance.

8. REFERENCES

1. R.E. Hayden, D.B. Bliss, B.S. Murray, K.L. Chandiramani, J.I. Smullin, P.G. Schwaar, "Analysis and Design of a High Speed, Low Noise Aircraft Fan Incorporating Swept Leading Edge Rotor and Stator Blades," NASA CR-135092, December 1977.

2. J.G. Lucas, R.P. Woodward, M.J. MacKinnon, "Acoustic Evaluation of a Novel Swept-Rotor Fan," AIAA Paper 78-1121, AIAA 11th Fluid and Plasma Dynamics Conference, 10-12 July 1978.

3. D. A. Topol and D. A. Philbrick, "Fan Noise Prediction System Development: Wake Model Improvements and Code Evaluations," NASA Report on Contract NAS3-25952 (Task 10), April 1993.

4. D. A. Topol and D. C. Mathews, "Rotor Wake/Stator Interaction Noise Prediction Code, Technical Documentation and User's Manual," NASA Report on Contract NAS3-25952 (Task 10), April 1993.

5. Measurement of Far Field Noise from Gas Turbine Engines During Static Operations, Society of Automotive Engineers Aerospace Recommended Practice 1846, February 1990.

6. H. D. Meyer, "Fan Noise Prediction System Development: Source/Radiation Field Coupling and Workstation Conversion for the Acoustic Radiation Code," NASA Report on Contract NAS3-25952 (Task 10), April 1993.

7. I. D. Roy, W. Eversman, and H. D. Meyer, "Improved Finite Element Modeling of the Turbofan Engine Inlet Radiation Problem," NASA Report on Contract NAS3-25952 (Task 10), April 1993.

8. P. H. Bent, "Fan Noise Prediction Assessment", NASA Report on Contract NAS1-20103, May 1995.

REPORT DOCUMENTATION PAGE

Form Approved
OMB No. 0704-0188

1. AGENCY USE ONLY (*Leave blank*)	2. REPORT DATE	3. REPORT TYPE AND DATES COVERED
	November 1996	Final Contractor Report

4. TITLE AND SUBTITLE

Quiet High-Speed Fan

5. FUNDING NUMBERS

WU–538–03–11
C–NAS3–27483

6. AUTHOR(S)

Lysbeth Lieber, Russ Repp, and Donald S. Weir

7. PERFORMING ORGANIZATION NAME(S) AND ADDRESS(ES)

AlliedSignal Engines
111 South 34th Street
P.O. Box 52181
Phoenix, Arizona 85072–2181

8. PERFORMING ORGANIZATION REPORT NUMBER

E–10398

9. SPONSORING/MONITORING AGENCY NAME(S) AND ADDRESS(ES)

National Aeronautics and Space Administration
Lewis Research Center
Cleveland, Ohio 44135–3191

10. SPONSORING/MONITORING AGENCY REPORT NUMBER

NASA CR–198518

11. SUPPLEMENTARY NOTES

Project Manager, Carlos R. Morrison, Propulsion Systems Division, NASA Lewis Research Center, organization code 2770, (216) 433–8447.

12a. DISTRIBUTION/AVAILABILITY STATEMENT

Unclassified - Unlimited
Subject Category 03

This publication is available from the NASA Center for AeroSpace Information, (301) 621–0390.

12b. DISTRIBUTION CODE

13. ABSTRACT *(Maximum 200 words)*

A calibration of the acoustic and aerodynamic prediction methods was performed and a baseline fan definition was established and evaluated to support the quiet high speed fan program. A computational fluid dynamic analysis of the NASA QF–12 Fan rotor, using the DAWES flow simulation program was performed to demonstrate and verify the causes of the relatively poor aerodynamic performance observed during the fan test. In addition, the rotor flowfield characteristics were qualitatively compared to the acoustic measurements to identify the key acoustic characteristics of the flow. The V072 turbofan source noise prediction code was used to generate noise predictions for the TFE731-60 fan at three operating conditions and compared to experimental data. V072 results were also used in the Acoustic Radiation Code to generate far field noise for the TFE731-60 nacelle at three speed points for the blade passage tone. A full 3-D viscous flow simulation of the current production TFE731-60 fan rotor was performed with the DAWES flow analysis program. The DAWES analyses was used to estimate the onset of multiple pure tone noise, based on predictions of inlet shock position as a function of the rotor tip speed. Finally, the TFE731-60 fan rotor wake structure predicted by the DAWES program was used to define a redesigned stator with the leading edge configured to minimize the acoustic effects of rotor wake/stator interaction, without appreciably degrading performance.

14. SUBJECT TERMS

Aeroacoustics; Turbofans; Fan aerodynamics

15. NUMBER OF PAGES
93

16. PRICE CODE
A05

17. SECURITY CLASSIFICATION OF REPORT	18. SECURITY CLASSIFICATION OF THIS PAGE	19. SECURITY CLASSIFICATION OF ABSTRACT	20. LIMITATION OF ABSTRACT
Unclassified	Unclassified	Unclassified	